The role of BDNF and Nogo-A signalling in modulating the architecture of mature hippocampal neurons

Von der Fakultät für Lebenswissenschaften
der Technischen Universität Carolo-Wilhelmina zu Braunschweig
zur Erlangung des Grades
eines Doktors der Naturwissenschaften
(Dr. rer. nat.)
genehmigte
Dissertation

von Yves Philip Kellner
aus Hamburg

1. Referent: Prof. Dr. Martin Korte
2. Referent: Prof. Dr. Reinhard Köster
3. Referent: Prof. Dr. Mark Hübener

eingereicht am: 02.06.2014
mündliche Prüfung (Disputation) am: 15.10.2014

Druckjahr 2014

Vorveröffentlichungen der Dissertation:

Teilergebnisse aus dieser Arbeit wurden mit Genehmigung der Fakultät für Lebenswissenschaften, vertreten durch den Mentor der Arbeit, in folgenden Beiträgen vorab veröffentlicht:

Publikationen:

Y. Kellner, N.Gödecke, T. Dierkes, N. Thieme, M. Zagrebelsky and M. Korte

The BDNF effects on dendritic spines of mature hippocampal neurons depend on neuronal activity; Front. Synaptic Neurosci. (2014).

K. Michaelsen-Preusse*, Y. Kellner*, M. Korte and M. Zagrebelsky (*equal contribution)

Analysis of Actin Turnover and Spine Dynamics in Hippocampal Slice Cultures; Laser Scanning Microscopy and Quantitative Image Analysis of Neuronal Tissue; New York, NY: Springer New York (2014).

A. Zemmar, O. Weinmann, Y. Kellner, X. Yu, R. Vicente, M. Gullo, H. Kasper, K. Lussi, Z. Ristic, A. Luft, M. Rioult-Pedotti, Y. Zuo, M. Zagrebelsky, and M.E. Schwab

'Neutralization of Nogo-A enhances synaptic plasticity in the rodent motor cortex and improves motor learning *in vivo*'; Journal of Neuroscience (2014).

Publikationen eingereicht:

Y. Kellner, S. Kramer, S. Fricke, N. Lonnemann, M.E. Schwab, M. Korte and M. Zagrebelsky

'Nogo-A acutely modulates the actin cytoskeleton to control structural plasticity at single dendritic spines'.

J. H. Chen*, Y. Kellner*, M. Zagrebelsky, M. Grunwald, M. Korte and P. J. Walla; (*equal contribution)

'Two-photon correlation spectroscopy in single dendritic spines reveals fast actin filament splitting and reorganization mechanism of activity-dependent growth'.

Tagungsbeiträge:

Y. Kellner, M. Zagrebelsky and M. Korte; Molecular mechanisms of BDNF-TrkB signalling in dendritic spine plasticity at hippocampal neurons; 9th Göttingen Meeting of the German Neuroscience Society 2011.

Y. Kellner, M. E. Schwab, M. Korte and M. Zagrebelsky; Nogo-A acutely modulates actin dynamics within dendritic spine of mature hippocampal neurons; 8th FENS Forum of European Neuroscience 2012.

Y. Kellner, M. E. Schwab, M. Korte and M. Zagrebelsky; Nogo-A orchestrate actin dynamics within dendritic spine of mature hippocampal neurons; 10th Göttingen Meeting of the German Neuroscience Society 2013.

Y. Kellner, M. E. Schwab, M. Korte and M. Zagrebelsky; Nogo-A signalling controls actin turnover and modulates dendritic spine dynamics in CA3 hippocampal neurons; Society for Neuroscience 43rd Annual Meeting 2013.

‘Somehow the unstable stuff of which we are composed has learned the trick of maintaining stability.’

Walter Cannon - The Wisdom of the Body, 1932

für Anne & Josef Kellner

Table of contents

1 Abstract

The functions of neural circuits underlying learning and memory processes in the adult brain are determined by the interplay between the activity and the structure of the neurons forming them. Moreover, learning and memory processes rely upon a tight balance between the ability of synaptic connections to undergo adaptive changes and their stabilization. Particularly, the overall neuronal architecture of the mature brain is remarkably stable, implying that a set of molecules is regulating the balance between stability and plasticity of mature neuronal networks. In my work I investigated the role in regulating structural plasticity at dendritic spines of two molecules known to either restrict (Nogo-A) or promote (BDNF) synaptic plasticity. The myelin associated protein Nogo-A has been shown to limit functional and structural recovery after an injury in the adult central nervous system (CNS) and has recently been implicated as a suppressor of activity-dependent synaptic plasticity. I analysed whether Nogo-A signalling modulates the spine actin cytoskeleton to control structural plasticity at dendritic spines of CA3 hippocampal pyramidal cells. Interfering with Nogo-A signalling by loss-of-function experiments rapidly and transiently increased F-actin stability and resulted in an increase in dendritic spine length. In contrast, a gain-of-function experiment by applying an inhibitory Nogo-A peptide (Nogo-A-Δ20) resulted in a transient increase in dynamic F-actin. To understand the physiological relevance of Nogo-A in regulating structural plasticity, spatial learning and memory were analysed by comparing the performance of wild type *versus nogo-a* knockout (KO) mice in the Morris water maze. *Nogo-a* KO mice showed a behavioural advantage in forming a spatial reference memory in the early acquisition phase together with a transitory increase in dendritic spine density. These results indicate that Nogo-A functions as a molecular regulator of learning and memory processes by restricting structural plasticity in the hippocampus upon learning. Remarkably, these data may provide a mechanism for the action of Nogo-A in regulating spatial and temporal specificity of structural plasticity in maintaining the balance between plasticity and stability for the proper functions of the mature CNS network. As an example of a positive regulator and mediator of activity-dependent synaptic plasticity, I investigated the neurotrophin Brain-derived neurotrophic factor (BDNF). Here I specifically addressed the role of BDNF signalling in modulating the architecture of primary hippocampal neurons and their dendritic spines using a series of gain- and loss-of-function approaches in hippocampal cultures. I showed that the effects exerted by BDNF on the dendritic architecture of hippocampal neurons are dependent on the neuron's maturation stage. Moreover, BDNF is specifically required for the activity-dependent maintenance of dendritic spine density as well as their mature spine morphology in excitatory hippocampal neurons.

Zusammenfassung

Die Funktion neuronaler Netzwerke im adulten Gehirn wird bestimmt durch das Wechselspiel von Aktivität und Struktur und ihrer Fähigkeit zur funktionellen und strukturellen Plastizität, was als Grundlage für Lern- und Erinnerungsvorgänge gilt. Grundsätzlich kann angenommen werden, dass die Morphologie bei der Mehrheit der Synapsen im adulten Gehirn sehr stabil ist, so dass Moleküle, welche die Stabilität (Nogo-A) und Plastizität (BDNF) von Neuronen in einem Gleichgewicht halten, hier eine besonders wichtige Rolle erfüllen. Das Myelin assoziierte Protein Nogo-A schränkt sowohl funktionelle als auch strukturelle Plastizität im adulten zentralen Nervensystem (ZNS) ein. In dieser Studie wurde untersucht, ob der Nogo-A Signalweg das Aktincytoskelett reguliert und somit einen Einfluss auf die strukturelle Plastizität von dendritischen *spines* hippocampaler CA3 Neurone nimmt. Die Inhibition des Nogo-A Signalweges führte zu einer schnellen und transienten Stabilisierung des Aktinzytoskelettes und zu einem Anstieg der Länge der *spines*. Bei einer Aktivierung durch Zugabe des Nogo-A-Δ20 Peptides hingegen, kam es zu einem Anstieg der Aktin-dynamik. Um die physiologische Bedeutung von Nogo-A in der Regulierung von struktureller Plastizität bei Lern- und Gedächtnisvorgängen zu untersuchen, wurden *Wild type* mit *nogo-a knockout* (KO) Mäusen im *Morris water maze test* verglichen. *Nogo-a* KO Mäuse wiesen eine schnellere Bildung des räumlichen Referenzgedächtnisses auf, was mit einem transienten Anstieg der *spine*-Dichte pyramidaler CA3 Neurone einherging. Es zeigte sich demnach, dass Nogo-A als molekularer Regulator von Lern- und Gedächtnisvorgängen agieren könnte, indem es strukturelle Plastizität im Hippocampus einschränkt. Bemerkenswerterweise zeigen diese Ergebnisse einen Mechanismus auf, wie Nogo-A ein Gleichgewicht zwischen Stabilität und Plastizität aufrechterhalten könnte, um die Funktionalität des adulten ZNS zu gewährleisten. Im zweiten Teil meiner Arbeit wurde am Beispiel eines positiven Regulators und Mediators synaptischer Plastizität das Neurotrophin *Brain-derived neurotrophic factor* (BDNF) untersucht. Im Mittelpunkt meiner Versuche standen die Auswirkungen der Aktivierung bzw. die Inhibierung des BDNF-TrkB Signalweges in adulten hippocampalen Pyramidenneuronen auf die Dichte, Morphologie und das Aktinzytoskelett dendritischer *spines*. Die Ergebnisse zeigten, dass die Regulation der dendritischen Komplexität durch BDNF vom Entwicklungszustand der Neurone abhängig ist. Des Weiteren zeigte sich, dass BDNF in hippocampalen Neuronen für die aktivitätsabhängige Aufrechterhaltung sowohl der Anzahl als auch der Form dendritischer *spines* nötig ist. Damit sind die Effekte von BDNF hochspezifisch und beeinflussen nur wenige Parameter neuronaler Funktion und Struktur.

2 Introduction

Since the first drawings of neuronal cells made by Santiago Ramón y Cajal at the end of the 19th century, scientist have been interested in understanding whether and how the diverse and highly complex architecture of neurons is connected to their function as well as to higher cognitive processes performed by the central nervous system (CNS). Already at that historically early time point the analysis of the morphology of dendritic and axonal processes resulted in the initial understanding about the functional organisation of the different brain areas leading to some fundamental hypothesis about how advanced cognitive processes are working. In the 1950s, the development of new electrophysiological and electron microscopy methods resulted in the identification of the synapses as the site at which neurons communicate. Synapses are highly dynamic structures shown to change their function and their morphology in response to alterations in neuronal activity in a process known as synaptic plasticity. Both functional and structural plasticity have been strongly correlated to learning and memory processes in the brain. On the other hand time-series experiments have revealed that the mature CNS network is remarkably stable. These observations raise the following question: what are the molecular mechanisms regulating the tight balance between stability and plasticity of the neuronal network in the adult CNS? In this context I analysed the role of the brain-derived neurotrophic factor (BDNF), a well-known plasticity promoting molecule and of the inhibitory protein Nogo-A in modulating structural plasticity at dendritic spines.

2.1 Structural and functional synaptic plasticity

The correct function of neural circuits depends upon both function and structure of neurons. Already Spencer (1862), Tanzi (1893) and Cajal (1893) speculated that memory storage requires changes of existing neuronal processes, rather than the addition of new neuronal cells. Later, Donald O. Hebb further developed this idea by postulating that alterations in synaptic strength, as well as formation of new synapses may mediate memory storage (Hebb, 1949). He suggested that synapses get strengthened whenever correlated neuronal activity occurring a pre- and a postsynaptic neuron leads to biochemical and / or structural modifications altering the communication between connected neurons. These activity-dependent functional and structural changes at synapses are called synaptic plasticity and are correlated to learning and memory processes (Bliss and Collingridge, 1993; Holtmaat and Svoboda, 2009; Kandel, 2001; Xu et al., 2009; Yang et al., 2009a). The best described form of functional synaptic plasticity - long-term potentiation (LTP) was discovered in the hippocampus by Bliss and

Lømo in 1973 (Bliss and Lomo, 1973) and reflects an activity-dependent long lasting increase in synaptic strength. Synaptic plasticity is involved in encoding and storage, distinct patterns of neural activity, where LTP together with long-term depression (LTD, weakening of synaptic contacts) might be a cellular model of learning and memory processes (Bliss and Collingridge, 1993; Kandel, 2001; Martin et al., 2000). The molecular mechanisms mediating the strengthening of glutamatergic synapses involve two receptors: the alpha-amino-3-hydroxy-5-methyl-4-isoxazolepropionic acid receptor (AMPAR) and the N-methyl-D-aspartate receptor (NMDAR). A strong stimulus leads, via Na^+ influx through AMPARs into the post synapse and its depolarization to an activation of the NMDARs (Mg^{2+} ion is expelled) and consequently to a strong influx of Ca^{2+} ions. The following activation of protein kinases and second messengers results in a higher efficiency of ionic conductance by AMPAR phosphorylation, followed by the insertion of new AMPARs at the membrane and local protein synthesis (for review see: Derkach et al., 2007). Moreover, a long lasting increase in synaptic strength is achieved by alterations in the expression of specific genes leading to the accumulation of mRNAs and proteins at active synapses supporting functional and structural plasticity (for review see: Citri and Malenka, 2008; Malenka and Bear, 2004). The description of the structural composition of synapses was a further step towards understanding the basis of structural synaptic plasticity. Most excitatory synapses consist of a presynaptic axonal bouton and postsynaptic protrusion, known as a dendritic spine (Figure 1).

The idea that dendritic spines are stable structures was questioned by Crick when he proposed that spines change their morphology in response to synaptic stimulation (Crick, 1982). These anatomical changes of dendritic spines are supposed to be correlated to a more efficient transmission of electrical current between neurons. Indeed, the volume of the spine head is directly proportional to the size of the post synaptic density (PSD) which in turn correlates to the number of postsynaptic receptors (Nusser et al., 1998) and to the number of docked vesicles at the presynapse (Schikorski and Stevens, 1999; for review see: Holtmaat and Svoboda, 2009). Furthermore, a series of ultrastructure studies showed that actin is highly abundant in spines, suggesting that it may contribute to their anatomical changes (Fifková and Delay, 1982; Matus et al., 1982).

Dendritic spines

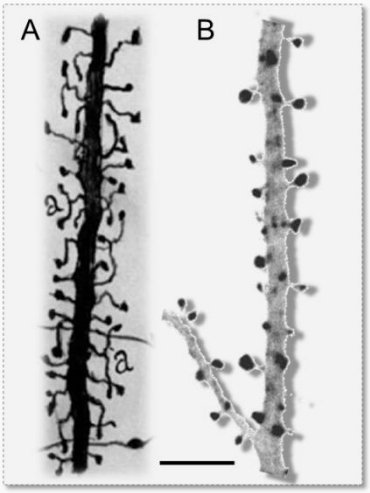

Figure 1: Dendritic spines
A Cajal's hand drawings of dendritic spines. Adapted from Yuste, 2011.
B Micrograph showing hippocampal dendrite covered with spines. Scale bar 5 µm.

Dendritic spines are small protrusions that emerge from the dendritic shaft of most principal neurons in the brain and are characterized by a large diversity in size and shape (Figure 1A and B). They consist of a small cub-like had (~ 1 µm in diameter), connected by a thin neck (~0.2 µm) to the underlying dendrite and are up to 3 micrometres in length. Spines can be morphologically categorized into three types: stubby, mushroom and thin spines (Peters and Kaiserman-Abramof, 1970). Spines are found in many species and are particular abundant in the CNS of vertebrates. The high conservation of dendritic spines throughout the species and the different brain regions suggests that they must be essential for brain functions. Most excitatory neurons carry spines whereas inhibitory interneurons don't or these are present at a much lower density. This raises the question of what is the function of spines? Already Cajal speculated that spines increase the surface area of dendrites (Ramón y Cajal, 1899). Indeed, it was shown that spines serve to enhance synaptic connectivity (Peters and Kaiserman-Abramof, 1969; Shepherd, 1996; Yuste, 2013). Moreover, spines form electrical compartments that modify synaptic potentials and biochemical compartments that implement input-specific synaptic plasticity (for review see: Yuste, 2011). Interestingly, the spine neck controls calcium diffusion and electrically filters synaptic potentiation (Araya et al., 2006; Tønnesen et al., 2014; Yuste et al., 2000).

More recently time-lapse imaging techniques combined with electrophysiological stimulation showed that the alterations in spine morphology are correlated to changes in neuronal activity in primary cultures (Boyer et al., 1998; Papa et al., 1995; Segal, 1996). Nevertheless, this observation was questioned because spines might easily change their shape due to the lack of the neuropil in the primary culture (Edwards, 1998). A series of studies revealed that the induction of LTP in hippocampal slices leads to the appearance of new spines at the apical dendrites of CA1 pyramidal neurons (Engert and Bonhoeffer, 1999; Maletic-Savatic et al., 1999), whereas induction of LTD is followed by the disappearance or shrinkage of existing spines (Nägerl et al., 2004; Zhou et al., 2004). The changes in spine numbers occurs within 30 minutes from the stimulation and cannot

cause the initial strengthening of synapses arising within minutes. Finally, two-photon imaging together with glutamate uncaging helped to examine the relationship between spine plasticity and LTP. Kasai and colleagues reported that synaptic enhancement is correlated with an increased spine head volume (Matsuzaki et al., 2004a) and in the appearance of new dendritic spines (Kwon and Sabatini, 2011). Overall, the strengthening of synaptic contacts involves structural plasticity of dendritic spines and axonal boutons and has been correlated to functional changes at synapses (Bourne et al., 2013; Engert and Bonhoeffer, 1999; Maletic-Savatic, 1999; Toni et al., 1999). Interestingly, they are supposed to underlie learning and memory processes (Hofer et al., 2009; Holtmaat et al., 2006; Xu et al., 2009; Yang et al., 2009). To monitor easily functional and structural changes in neuronal networks *in vitro* model systems have been developed like hippocampal or cortical cultures. Particularly useful in this context are for example cultivated brain slices which preserve the neuronal circuitry and are comparable to the *in vivo* conditions.

2.2 The hippocampus

The neuroanatomists Camillo Golgi (1886), Ramón y Cajal (1911) and Lorente de Nó (1934) were the first to describe a unique group of millions of neurons highly organized into laminar and circuits deep within the medial temporal lobe – the hippocampus. The Hippocampus is a bilateral bulb-like shaped brain region, deep underneath the neocortex. It is one of the most intensively studied brain regions used to investigate how neuronal circuits operate in the CNS. Anatomically, the hippocampal can be divided into two main sub regions: the dentate gyrus (DG) and the cornu ammonis (Amun's horns; CA) consisting of CA1, CA2, CA3 and CA4. The hippocampal formation has been shown to mediate the transition from short to long-term memory (Alvarez et al., 1994). Indeed, patients who underwent a bilateral hippocampal resection (previously performed to treat medication-resistant generalized seizures) suffer from anterograde amnesia (Scoville and Milner, 1957, 2000). In particular the hippocampus is crucial for the formation and recall of spatial, contextual, and episodic memory (Burgess et al., 2002; Eichenbaum, 2004; Squire et al., 2004) by integrating sensory and spatial information from the entorhinal cortex (EC) to create context-specific representations (Knierim et al., 2006; Manns and Eichenbaum, 2006; Suzuki et al., 1997). The formation and recall of these memories is supposed to be processed by a tri-synaptic circuit reciprocally connecting the EC to the hippocampal network (Andersen et al., 1971). The EC layer II (ECII) project via the perforant path to the dentate gyrus (DG). In turn, the granule cells of the DG send their axonal projections, the mossy fibres to the proximal part of the CA3 neuron dendrites. Finally the axonal

projections from CA3, the Schaffer collaterals terminate primarily onto the apical and in part onto the basal dendrites of CA1 cells (Ishizuka et al., 1990; Li et al., 1994). The simple and unique projection pattern as well as the laminar organisation of the hippocampus (stratum oriens (so), stratum pyramidale (sp), stratum radiatum (sr), stratum lacunosum-moleculare (sl-m)), allow using transversal slices (where the main circuitry is preserved) to study *in vitro* the hippocampal function and morphology. The hippocampus contains two major cell types: small granule neurons in the DG and pyramidal neurons in the CA region. Pyramidal neurons are characterized by their characteristic pyramidal-shaped soma and their distinct dendritic tree: several short and complex basal dendrites emerge from the base and one large apical dendritic tree grows from the apex of the soma. Particularly of interest in this study is the CA3 region of the hippocampus, which is characterized by pyramidal neurons which are quite variable in their dendritic length: small neurons have a total dendritic length of 8-10 mm whereas large cells (located distal in the CA3 region) display a total length of 16-18 mm (Ishizuka et al., 1995). Their proximal dendritic compartment carries special synapses - the mossy fibre-CA3 synapses are characterized by large pre-synaptic boutons (mossy fibre terminals) and large dendritic spines (thorny excrescences) providing a powerful excitation to CA3 neurons (Gonzales et al., 2001). Interestingly, the anatomical and physiological characteristic of the CA3 region are essential in the encoding of novel information involving associations between cues and spatial locations (for review see Kesner, 2007). Of particular interest in my study are molecules mediating and regulating functional and structural plasticity at dendritic spines of CA3 pyramidal neurons. The investigation of these molecules in relation to learning processes is still a central question in neuroscience.

2.3 Extra and intercellular modulators of functional and structural plasticity

2.3.1 BDNF and its role in regulating neuronal morphology

Neurotrophins belong to the group of neurotrophic factors and with the discovery of the first neurotrophin the Nerve growth factor (NGF) Levi-Montalcini revolutionized our current understanding of the role of molecular guidance cues during neuronal development (Cohen et al., 1954; Levi-Montalcini, 1987). Hans Thoenen set a further landmark in our understanding on neurotrophins function by postulating that neurotrophins play a role in activity-dependent synaptic plasticity (Thoenen, 1991; Zafra et al., 1990). Indeed, further studies confirmed that neurotrophins are essential for multiple aspects of structural and functional plasticity (reviews (Chao, 2003; Huang and Reichardt, 2001; McAllister et al., 1999). Three further neurotrophins have been described: the Brain-derived Neurotrophic Factor (BDNF) and neurotrophin 3 and 4 (NT-3, NT-4). Next, I highlight BDNF and its signalling pathway in the CNS (Figure 2). The effects exerted by BDNF result from its binding to two different receptors: TrkB receptor tyrosine kinase B (TrkB) and pan neurotrophin receptor $p75^{NTR}$. BDNF is initially synthesized as precursor proBDNF, the pro-domain is then proteolytically cleaved and the mature BDNF is secreted to promote neuronal survival and enhance synaptic plasticity by activating the receptor tyrosine kinase B (TrkB; Klein et al., 1990). Whether proBDNF is released from neurons and what is its physiological function is still controversial (Dieni et al., 2012; Matsumoto et al., 2008; Yang et al., 2009b), nevertheless, proBDNF has been shown to bind with a high affinity to the $p75^{NTR}$ thereby negatively regulating synaptic plasticity and inducing apoptosis (Lu et al., 2005; Teng et al., 2005).

The binding of BDNF dimers to TrkB receptors triggers ligand-induced receptor dimerization and transphosphorylation of specific tyrosine residues of intracellular kinase domains resulting in diverse cellular responses (Figure 2). Three main intracellular pathways are activated resulting in neuronal survival and differentiation via the phosphatidylinositol- 3 kinase (PI3K) pathway; in differentiation and neurite growth via the mitogen-activated kinase (MAPK) pathway; and in activity-dependent synaptic plasticity via the PLCɣ pathway (Figure 2; Bibel, 2000; Blum and Konnerth, 2005; Minichiello, 2009). The BDNF-TrkB signalling (Figure 2) has been implicated in numerous processes of functional and structural synaptic plasticity by regulating protein synthesis via the transcription factor cAMP response element binding protein (CREB; for reviews see: Gottmann et al., 2009; Park and Poo, 2012; Zagrebelsky and Korte, 2013).

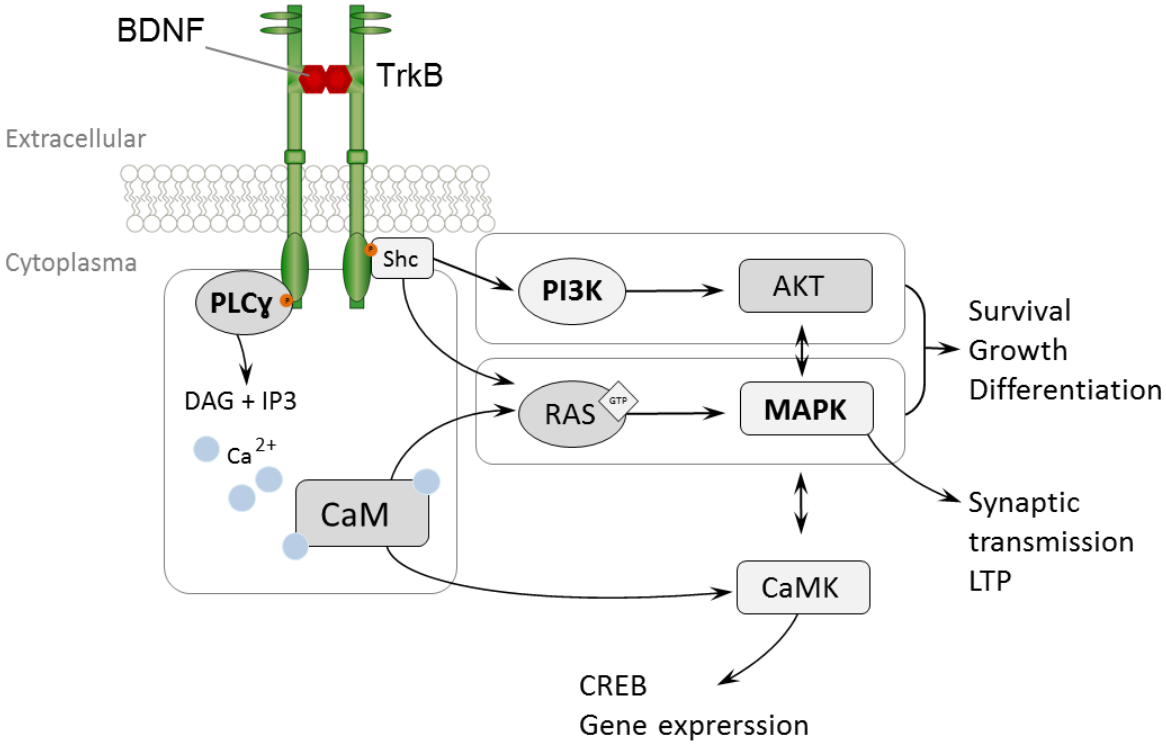

Figure 2: BDNF-TrkB receptor downstream signalling pathways.

Homodimeric BDNF induces the dimerization of the TrkB receptors and a phosphorylation of the tyrosine (Y^{515}) creates the binding site for Shc (Src homology 2/α-collagen-related protein), whereas tyrosin (Y^{816}) forms the adaptor site for PLC-ɣ. The activated signalling pathways (1) PI3K-, (2) MAPK-,(3) PLC-ɣ-pathways mediate the effects of BDNF on neuronal survival, growth, differentiation and, synaptic transmission and LTP as well as gene expression. P, phosphorylation; PI3K, phosphatidylinositol 3-kinase; Akt, Akt kinase; Ras, small GTP-binding protein Ras; CaM, calmodulin; CaMK (Ca^{2+}-CaM-dependent kinase II and IV); DAG, diacylglycerol; IP3, inositol 1,4,5-trisphosphate; Ca^{2+}, intracellular Calcium , CREB, cAMP response element-binding protein. (Adapted from: Blum and Konnerth, 2005).

The role of BDNF has been extensively analysed *in vitro* upon the application of exogenous BDNF. The data obtained support the notion that BDNF is involved in regulating the fine-tuning of the cortical network during development by selectively enhancing dendritic growth in an activity-dependent manner (Horch et al., 1999; Mcallister, 1995; McAllister et al., 1996). Application of exogenous BDNF to developing primary hippocampal neurons has been results in a significant increase in the number of primary neurites as well as an increase in neurite complexity and length (Ji et al., 2005; Kwon and Sabatini, 2011). Likewise, dendritic spine density and morphology of mature primary hippocampal neurons are significantly altered via BDNF application (Ji et al., 2005, 2010). Interestingly, an acute and fast delivery of BDNF increases the number of mushroom like spines, whereas a gradual and slow BDNF application induces more thin-like spines (Ji et al., 2010). This is supposed to be due to the consolidation of existing synapses and the formation of new synapses, respectively (Lu et al., 2013).

Similarly, mature organotypic hippocampal neurons treated with BDNF show a significant increase in dendritic spine density and in the number of synapses (Tyler and Pozzo-miller, 2003, 2001). Also a long lasting BDNF overexpression increases the spine turnover in layer 2/3 pyramidal neurons of the visual cortex (Horch et al., 1999), as well as the recruitment of PSD-95 to synapses, possibly leading to an increase in spine number and size (Yoshii and Constantine-paton, 2007). Functional changes at synapses have been correlated to structural alteration at dendritic spines. Among the molecular candidates, supposed to link functional and structural changes the activity-dependently secreted BDNF has a prominent position. A study performed in hippocampal slice cultures pairing postsynaptic spikes and two-photon glutamate uncaging at single spines resulted both in LTP induction and in an increase of the spine head volume (Tanaka et al., 2008). The spine head enlargement is prevented by the blockade of the BDNF-TrkB signalling. Moreover, presynaptic stimulation (glutamate uncaging) plus the addition of exogenous BDNF has been shown to induce an increase in the spine head in the absence of postsynaptic spikes (Tanaka et al., 2008). This suggests that activity-dependent BDNF secretion mediates both LTP and spine growth. Taken together, the *in vitro* studies described above strongly support the notion that, in the hippocampus exogenous BDNF promotes dendritic formation and growth during development and regulates functional as well as structural plasticity at spines of mature neurons.

But as strong as the evidence for a role of BDNF in modulating dendritic architecture might appear, the preparation techniques (Danzer et al., 2004) and the culture conditions (Chapleau et al., 2008) have been shown to influence the expression levels as well as the cellular response to BDNF, possibly confounding the analysis under these conditions. Suggestive for a role of BDNF *in vivo* is the correlation between the physiological variability in BDNF expression levels in the mouse dentate gyrus and the dendritic spine density in granule cells (Stranahan, 2011). Moreover, a reduction in BDNF serum levels is associated with a reduction in hippocampal volume in aging humans (Erickson et al., 2011) as well as in dendritic complexity and spine density in senescent rats (von Bohlen und Halbach, 2010). The *in vivo* role of BDNF has been very difficult to evaluate in the postnatal brain as *bdnf*−/− mouse mutants die too early for the role of BDNF to be assessed after its increased post-natal expression caused by neuronal activity (Hong et al., 2008; Zafra et al., 1990). The analysis of *bdnf*+/− mouse mutants, showing reduced BDNF levels, provided evidence that *in vivo* BDNF plays an important role in the induction of LTP in the hippocampus (Korte et al., 1995, 1996), the acquisition of extinction learning (Psotta et al., 2013) and in the structural rearrangement of adult cortical circuitry upon increased sensory input (Genoud et al., 2004; Korte et al., 1995). On the other hand, in *bdnf*+/− mice synapse density and spine morphology are indistinguishable from those in

WT mice (Genoud et al., 2004; Korte et al., 1996) and a compensatory increase in TrkB receptor expression occurs (Carretón et al., 2012), leaving open the question of whether BDNF modulates dendritic and spine architecture *in vivo*. Thus, a number of studies have been performed using different conditional gene targeted mouse lines and Cre-loxP mediated excision of *bdnf* (Rios et al., 2001; Gorski et al., 2003; Baquet et al., 2004; He et al., 2004; Chan et al., 2006; Monteggia et al., 2007; Unger et al., 2007; Rauskolb et al., 2010). Surprisingly, the effects on excitatory neurons in the hippocampus and cortex of a global BDNF deprivation throughout the CNS is extremely mild when compared to the effects observed upon a BDNF application *in vitro*. In a study from 2010 Rauskolb et al. showed that in a Tau-cre-loxP-BDNF-KO mouse (BDNF is deleted in all CNS neurons) the volume of the cortex is only slightly reduced and the one of the hippocampus unchanged. Accordingly, dendritic complexity of CA1 pyramidal cells is only mildly reduced and no changes could be observed in dendritic spine density. The spine type distribution in Tau-BDNF-KO neurons is significantly shifted towards a more immature phenotype pointing to a specific role of BDNF in the maintenance of mature dendritic spines in the adult hippocampus (Rauskolb et al., 2010). These results are consistent with the observation that the conditional deletion of TrkB in the hippocampus does not affect the gross dendritic morphology of CA1 pyramidal neurons (Luikart et al., 2005; Minichiello et al., 1999). It is noteworthy that while most of the published data supporting a role for BDNF in modulating dendrite and dendritic spine morphology derive from *in vitro* experiments applying exogenous BDNF, the role for endogenous BDNF in this context is still unclear. Moreover, *in vivo* the effects of endogenous BDNF in modulating the structure of neurons seem to be extremely specific, depending on the developmental stage, the brain area as well as the cell-type.

Overall, neurotrophins are essential for multiple aspects of structural and functional plasticity in the adult CNS. BDNF is a prime candidate in order to ensure that changes in synaptic function are followed by changes in structure of neurons as cellular correlates of learning and memory formation (Zagrebelsky and Korte, 2013). To ensure spatial and temporal specificity of plastic changes and preventing interference between different memories events a set of molecules are needed to regulate the balance between stability and plasticity of neuronal networks. Interestingly, recent studies indicate that a myelin associated protein restricting structural and functional plasticity in the adult CNS.

2.3.2 Nogo-A and its role in regulating neuronal morphology

The myelin associated neurite growth inhibitor Nogo-A is well known as an inhibitor of axonal sprouting and regeneration following injury in the adult CNS. In the adult brain, Nogo-A is mainly expressed in oligodendrocytes but also in neurons of highly plastic CNS regions such as the olfactory bulb, hippocampus or the cortex (Huber et al., 2002; Hunt et al., 2002; Meier et al., 2003; Mingorance et al., 2004; Richard et al., 2005; Zagrebelsky et al., 2010). The key question is: what are the physiological functions of Nogo-A proteins in the intact adult CNS? Recent studies have uncovered novel functions of Nogo-A and its receptors in the naïve CNS. A remarkable feature seems to be the stabilization of the CNS wiring by regulating structural and functional plasticity (synapse maturation, long-term synapse stability and activity-dependent synaptic plasticity). Nogo-A belongs to the reticulon family of proteins and is one splice variant of the *reticulon-4* gene (*rtn4*). By alternative splicing or different promoter usage the *rtn4* gene encode two further protein isoforms: Nogo-B and Nogo-C (Chen et al., 2000; GrandPré et al., 2000; Prinjha et al., 2000). All three isoforms share the same 180-200 amino acids (aa) long carboxyl terminus, the reticulon homology domain (RTN) consisting of two membrane-anchored hydrophobic regions linked by a hydrophilic-loop, the Nogo-66 domain (Figure 3A). The Nogo-66 domain represents one of the regions exhibiting inhibitory activity. However, no homology can be found between the NH2-terminal regions of the three RTN proteins (Kempf and Schwab, 2013; Oertle and Schwab, 2003). Nogo-A carries a long 800 aa NH2-terminal region containing a second inhibitory domain, Nogo-A-Δ20 specific for Nogo-A (Oertle et al., 2003). In the adult CNS Nogo proteins are localized predominantly (90%) in the endoplasmatic reticulum, however, Nogo-A was also found at the cell surface of oligodendrocytes and neurons (Oertle et al., 2003; Dodd et al., 2005).

2.3.3 Mechanisms of Nogo-A mediated signalling

The two major inhibitory domains Nogo-66 and Nogo-A-Δ20 were used to screen for potential Nogo receptors and up to now several interaction partners were characterized as summarised below (Figure 3B). For the Nogo-66 domain two receptors have been identified: the Nogo-66-receptor 1 (NgR1; Fournier et al., 2001) and the paired immunoglobulin-like receptor B (PirB; Atwal et al., 2008). NgR1 is anchored via *a* Glycosylphosphatidylinositol-(GPI) domain and lacks an own intracellular signalling domain (Venkatesh et al., 2005).

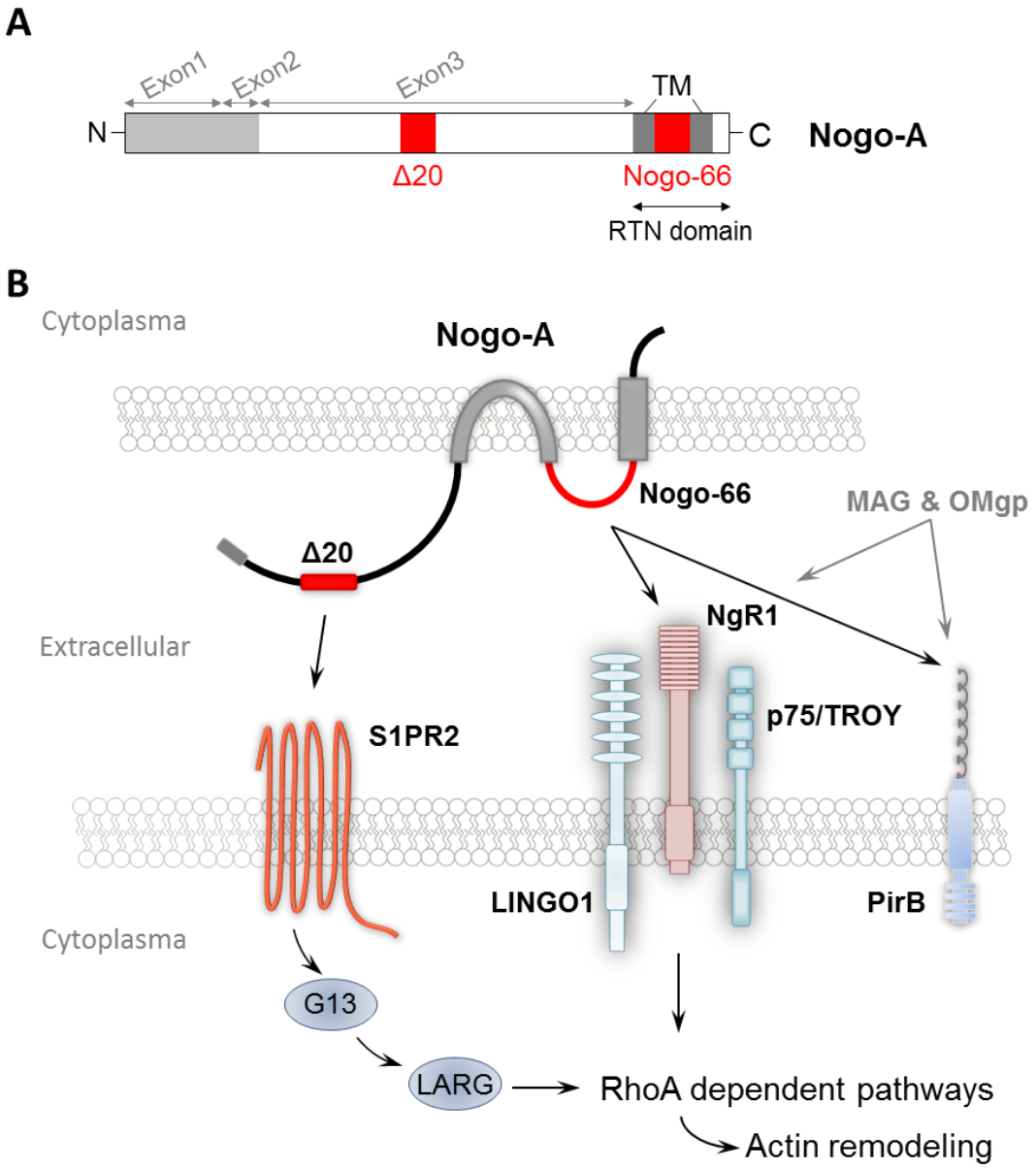

Figure 3: Molecular mechanisms related to Nogo-A signalling.

A Schematic structure of the Nogo protein isoforms Nogo-A. The inhibitory domain Nogo-A-Δ20 and Nogo-66 are indicated in red, transmembrane domains (TM) in dark grey. The Reticulon homology domain (RTN) is common to all three Nogo isoforms (black arrow). The Nogo-A-specific domain is encoded by the exon 3. **B** The transmembrane protein Nogo-A interacts with the Nogo-A-Δ20 domain with the S1PR2 and the Nogo-66 domain to Nogo receptor 1 (NgR1), which forms a complex with the transmembrane proteins LINGO1, and p75 or TROY. This binding leads, through still unknown intermediates, to an activation of the RhoA dependent pathways. The S1PR2 activates also RhoA via the G-protein G-13, the rhoGEF LARG. In addition to NgR1, Nogo-66 can interact with paired immunoglobulin-like receptor B (PirB), myelin-associated glycoprotein (MAG) and oligodendrocyte myelin glycoprotein (OMgp) interact also with NgR1 and PirB. (Adapted from: Schwab, 2010; Schwab and Strittmatter, 2014).

For signal transduction the NgR1interacts with co-receptors like the $P75^{NTR}$ or the related tumor necrosis factor alpha (TNF-α) receptor superfamily member 19 (TROY; Park et al., 2005; Shao et al., 2005). A second interaction partner of NgR1 is the leucine-rich repeat and Ig domain-containing Nogo receptor-interacting protein 1 (LINGO-1; Mi et al., 2004). Nogo-A is part of a family of neurite growth inhibitors including the myelin-associated glycoprotein (MAG), oligodendrocyte myelin glycoprotein (OMgp; Figure 3B) and the chondroitin sulfate proteoglycans also shown to bind the NgR1 (Domeniconi et al., 2002; Wang et al., 2002a; Imagama et al., 2011; Silver and Miller, 2004). The second inhibitory domain Nogo-A-Δ20 has just recently been shown to bind to the sphingosine1-phosphate receptor 2 (S1PR2; Kempf *et al.*, 2014). S1PR2 is a G protein-coupled receptor (GPCR) and belongs to a subfamily of five S1PRs (Figure 3B). The activation of S1PR2 by Nogo-A leads to neurite retraction, via the G proteins Gi/o, Gq, or G12/13 and the RhoA pathway resulting in a destabilization of the actin cytoskeleton within growth cones (Kempf et al., 2014; Singh and Hall, 2008; Spiegel and Milstien, 2003). Also NgR1 stimulation results in the regulation of the actin cytoskeleton in the growth cones as well as to changes in functional and structural plasticity. It is noteworthy that Nogo-A and the NgR1 has been found to be localized both at pre- and post-synaptic sites (Lee et al., 2008; Liu et al., 2003; Wang et al., 2002b).

2.3.4 Nogo-A restricts structural and functional plasticity in the adult naïve CNS

The first evidence that Nogo-A regulates activity-dependent plasticity processes were obtained when ocular dominance (OD) plasticity in the visual cortex was studied. It was hypothesized that Nogo-A signalling via the NgR1 receptor may limit plasticity in the intact CNS by stabilizing activity-dependent anatomical rearrangements. During the postnatal critical period (CP) neuronal circuits are refined in an experience-dependent manner. Alterations of sensory input (e.g. monocular deprivation, MD) occurring during this time result in changes in plasticity in the visual cortex and to a relative shift in OD toward the non-deprived eye (Hubel and Wiesel, 1962). After the end of the CP, mature neuronal circuits have been shown to be structurally more stable. Changes in response to MD can no longer occur (Hubel and Wiesel, 1962). This was also verified for mice showing a CP time window ranging from postnatal day 19 to 32 (Gordon and Stryker, 1996). Genetic deletion of Nogo-A or its receptors induces a significant expansion of the CP into adulthood (McGee et al., 2005; Syken et al., 2006). Taken together, these studies suggest that Nogo-A and their receptors restrict plasticity at the end of the CP and thereby ensure long-term network stability *in vivo*.

In the adult CNS synaptic plasticity (LTP / LTD) have been shown to be modified by guidance-related molecules like the Ephrin/Eph and Semaphorin/Plexin families (Shen and Cowan, 2010). As mentioned above also Nogo-A as well as NgR1 are expressed at both synaptic sites and may be potential candidates to influence synaptic plasticity (Aloy et al., 2006; Lee et al., 2008; Liu et al., 2003; Wang et al., 2002b). Indeed, studies analysing the role of Nogo-A and its receptors on synaptic plasticity (NgR1 and S1P2R) showed a restriction of long-term potentiation upon their activation (Delekate et al., 2011; Kempf et al., 2014; Lee et al., 2008; Mironova and Giger, 2013; Raiker et al., 2010). Interestingly, constitutive *nogo-a* or *ngR1*-KO mice didn't support previous results which might be due to genetic and/or developmental compensatory mechanisms. In *nogo-a* deficient mice Nogo-B as well as myelin-associated inhibitors like MAG and OMgp are upregulated and can still interact with their receptors providing a possible compensatory mechanism. (Delekate et al., 2011; Karlén et al., 2009; Lee et al., 2008; Raiker et al., 2010; Simonen et al., 2003). The Nogo receptor family consists of three isoforms, the loss of any one member is sufficient to reveal their inhibitory influence *in vitro*, whereas loss of all three NgRs is required *in vivo* (Wills et al., 2012). In line with this, a behavioural characterizations of *nogo-a* KO mice show normal anxiety-related behaviour, pain sensitivity, startle reactivity, spatial learning, and associative learning (Willi et al., 2009). However, a recent study used a microRNA-mediated acute down regulation of Nogo-A in transgenic rats to show that Nogo-A plays an important role in synaptic plasticity. The transgenic rats exhibited defects in cognition, sensory motor gating and social behaviour that are suggestive of schizophrenia-like behavioural phenotypes (Tews et al., 2013). In summary, these results open the possibility that Nogo-A signalling restricts different forms of synaptic strengthening in the adult CNS. Recent observations showed that Nogo-A and its receptors regulate also structural plasticity in the hippocampus and the cortex. Acute neutralisation of Nogo-A in mature organotypic hippocampal slice cultures leads to an alteration of axonal and dendritic complexity and a shift in dendritic spine distribution towards a less mature and more plastic type (Craveiro et al., 2008; Zagrebelsky et al., 2010). This implicates Nogo-A as a candidate to be involved in stabilizing the architecture of hippocampal neurons. This was also confirmed *in vivo* for the Nogo-A knockout and Nogo-A overexpressing transgenic mice for Purkinje cells in the cerebellum (Petrinovic et al., 2013). Indeed, also *in vivo* the knock-down of neuronal Nogo-A leads to an increase of filopodia-like protrusions of pyramidal neurons layer V of the neocortex (Pradhan et al., 2010). That Nogo-A signalling via the Nogo receptor 1 restricts anatomical plasticity was also reported in a study using the NgR1/2/3 triple knockout to study synaptogenesis (Wills et al., 2012) as well as the NgR1 knockout (Akbik et al., 2013) to analyse experience-dependent plasticity in the somatosensory cortex. Indeed, NgR1 was revealed to regulate

the experience-dependent turnover of dendritic spine and axonal varicosities in the somatosensory cortex (Akbik et al., 2013). Interestingly, transgenic mice overexpressing NgR1 show impaired long-term spatial memory (Karlén et al., 2009). Nogo-A actively suppresses anatomical plasticity in the adult CNS via a down regulation of growth-associated genes and transcription factors (Bareyre et al., 2002; Craveiro et al., 2008; Joset et al., 2010; Zagrebelsky et al., 1998). On the other hand, Nogo-A has been shown to regulate the actin cytoskeleton to induce growth cone collapse (Hsieh et al., 2006; Montani et al., 2009). Whether the regulation of actin dynamics within dendritic spines is required for the Nogo-A induced structural stabilization in the mature CNS remains an open question and was addressed in the study presented her.

2.4 The actin cytoskeleton within dendritic spines

Neurons keep their shape and architecture through the cytoskeleton. At the same time modifications in cytoskeleton dynamics are required for functional and structural changes (e.g. upon activity). Microtubules, neurofilaments and microfilaments are the three structural components of the neuronal cytoskeleton. Dendritic and axonal branches consists of a dense network of microtubules, which not only provides structural stability but also anchors organelles and serves as a track for the transport of cargoes (for review see: Conde and Cáceres, 2009). Also the actin microfilaments are found both in dendrites and axons and are particularly abundant at pre- and postsynaptic sites as well as in growth cones. Electron micrographs of spines showed a mesh like branched network in the spine heads and long linear bundles of actin filaments in the spine neck extending from the base towards the PSD (Fifková and Delay, 1982; Korobova and Svitkina, 2010). The actin treadmilling depends on the polymerisation of monomeric globular-actin (G-actin) at the barbed ends and its depolymerisation at the pointed ends of polymeric filamentous-actin (F-actin; Pollard and Borisy, 2003). Indeed, polymerisation or depolymerisation of the actin cytoskeleton are responsible for spontaneous and activity-driven remodelling of the spine structure(Bonhoeffer and Yuste, 2002; Dailey and Smith, 1996; Fischer et al., 1998; Hering and Sheng, 2001; Honkura et al., 2008; Izeddin et al., 2011). Interestingly, also long-lasting alterations of the synaptic efficacy have been shown to depend on the actin cytoskeleton (Kim and Lisman, 1999; Krucker et al., 2000). For example, a LTP like stimulus promotes actin polymerization and shifts the equilibrium of F- and G- actin towards F-actin associated with an enlargement of the spine volume (Okamoto et al., 2004; Matsusaki 2004, Fukazawa et al., 2003). Conversely, a stimulus known to weaken synaptic efficacy and to induce LTD (low-frequency stimulation) shifts

the ratio towards G-actin and causes actin loss and dendritic spine shrinkage (Okamoto et al., 2004; Zhou et al., 2004). Fluorescence recovery after photobleaching (FRAP) at single spines revealed that 85% of the actin cytoskeleton within spines is highly dynamic (Star et al., 2002) and that actin exists in distinct and locally restricted fractions (Honkura et al., 2008; Star et al., 2002). The 'cytoskeleton shell' of a spine (spine tip and periphery) is highly dynamic with a G- and F-actin turnover with a half-live (turnover time) of tens of seconds and characterized by morphological changes. In contrast, the spinoskeleton 'core' (centre and base of the spine) is more stable with a turnover time over tens of minutes (Honkura et al., 2008; Tatavarty et al., 2009). Taken together, these studies indicate that the actin cytoskeleton within dendritic spines supports the mobility as well as the stability of the spine size and shape. This raises the following question: what are the molecules regulating the structure and organisation of the actin cytoskeleton in such a precise way? Actin-binding proteins (ABPs) localizing to discrete regions within the spine contribute to the distinct regional specification of the actin fractions (Rácz and Weinberg, 2013). The spectrum of ABPs is multifaceted as can be deduced from the following list:

Capping proteins:

The barbed and pointed end of F-actin can be capped by Eps8 or adducin and tropomodulin, thereby, preventing the incorporation of new G-actin or depolymerisation respectively stabilizing the F-actin filament (Kuhlman et al., 1996; Stamatakou et al., 2013)). The capping activity for example of Eps8 is required for keeping a mature mushroom like spine morphology (Menna et al., 2013).

Depolymerisation:

ADF/cofilin decreases F-actin length by increasing the rate of depolymerisation of G-actin from the pointed end. This leads to the acceleration of F-actin treadmilling (Bamburg et al., 1980; Carlier et al., 1997). *In vitro* it was demonstrated that a low ratio of cofilin to actin subunits (less than 1%) results in F-actin severing of single long actin filament into several shorter ones (Andrianantoandro and Pollard, 2006; Bamburg and Bernstein, 2010). ADF/cofilin is required for changes of the spine head and stabilization during synaptic activity (Hotulainen et al., 2009; Van Troys et al., 2008). The postnatal knockout of cofilin demonstrates that cofilin is necessary to maintain an equilibrium between G- and F-actin in dendritic spines as well as stable spine density (Rust et al., 2010).

ADP/ATP exchanger:

The nucleotide exchange factor profilin enhances the exchange of ADP to ATP-actin and promotes F-actin polymerization (Goldschmidt-Clermont et al., 1992; Kovar et al., 2006). Profilin play also an important role in maintaining spine structure stability during synaptic plasticity (Ackermann and Matus, 2003; Michaelsen et al., 2010). Profilin containing

spines were shown to be lager in comparison to spines without profilin (Pilo Boyl et al., 2007).

Crosslinking proteins:

Cross-linking proteins like the Arp2/3 complex organize the actin cytoskeleton into three-dimensional bundles or networks. The Arp2/3 complex enhances actin nucleation and induces the branching and cross-linking of actin filaments (Mullins et al., 1998; Welch et al., 1998) which is required for spine maintenance and head growth. The nucleation of new actin branches is induced by the cortactin a nucleation factor class II that binds F-actin and the Arp2/3 complex (Uruno et al., 2001; Weaver et al., 2001). Postnatal loss of the Arp2/3 subunit ArpC3 or cortactin results in an altered actin turnover and a decrease in the number of spines (Hering and Sheng, 2003; Kim et al., 2013).

Motor proteins:

The actin-based molecular motor protein myosin can be included in the actin-binding proteins. Their function is to move organelles along F-actin or move F-actin filaments themselves (Kneussel and Wagner, 2013; Sellers, 2000). Various types of myosin forms have been identified as well as their localization in spine heads (Bridgman, 2004; Morales and Fifková, 1989). Myosin II for example is required for a proper spine head and neck morphology (Ryu et al., 2006).

(For reviews see: Cingolani and Goda, 2008; Hotulainen and Hoogenraad, 2010; Kennedy et al., 2005; Lamprecht, 2014; Pollard and Borisy, 2003; Schubert and Dotti, 2007; Sekino et al., 2007; Tada and Sheng, 2006).

The long-term stability of dendritic spines in the mature CNS is dependent on the control of the actin cytoskeleton dynamics, which in turn are regulated by many intra- and extra-cellular molecules like Nogo-A and BDNF. Signal transduction cascades via (1) Rho GTPases (RhoA, Rac1, and Cdc42) control (2) Rho effectors (ROCK, PAK, WAVE1 and N-WASP) which in turn control (3) ABPs (ADF/cofilin, Profilin, Arp2/3, Eps8 and MyosinII) to regulate cytoskeletal rearrangements (Figure 4). Indeed, the activation of Rho GTPases is required for the activity-dependent changes in spine size and structure (Murakoshi et al., 2011). A direct or indirect (via AMPA receptor blocking) activation of Rho-A causes a reduction in dendritic spine density, while Rho-A inhibition increases spine density (Kang et al., 2009; Tashiro et al., 2000; Yuste et al., 2000). Rho-A signalling through Rho-associated protein kinase (ROCK) stimulates LIM kinase (LIMK) to phosphorylate ADF/cofilin (Figure 4) leading to an inhibition of its actin severing activity and finally to a stability of dendritic spines (Arber et al., 1998; Murakoshi et al., 2011).

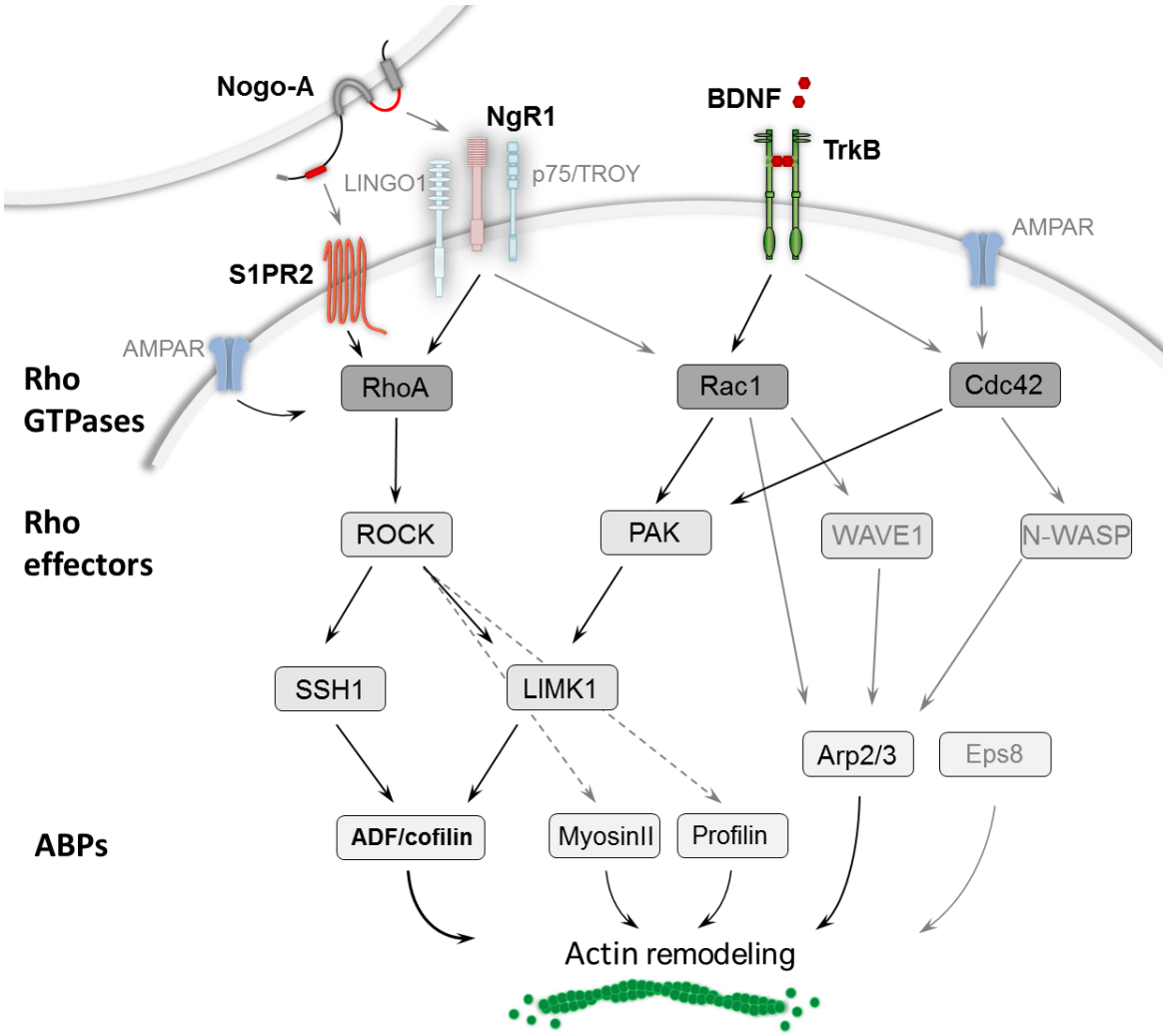

Figure 4: Nogo-A and BDNF signalling pathways involved in regulating actin at the synapse. Nogo-A signalling leads via the activation of the S1P2R, NgR1 (LINGO and P75NTR or TROY) or BDNF signalling via the TrkB receptor to a regulation of Rho GTPases like RhoA, Rac1 and Cdc42. Which in turn regulate Rho effectors like ROCK, PAK, WAVE1 and N-WASP regulate the actin binding proteins (ABPs) ADF/cofilin, Profilin, Arp2/3, Eps8 and MyosinII to control actin remodeling within dendritic spines. Further discussion and details are provided in the text (adapted from Dillon and Goda, 2005).

This modulation of actin dynamics via ADF/cofilin, regulated by LIMK and slingshot-phosphatase (SSH) during synaptic plasticity (Figure 4), also regulate postsynaptic receptor trafficking by AMPAR insertion in the PSD (Gu et al., 2010). AMPA receptor localization at the surface plays a crucial role in synaptic plasticity. LTP leads to an increase in the number of postsynaptic AMPA receptors (O'Brien et al., 1998; Shi et al., 1999). High-frequency stimulation / theta-burst stimulation (TBS) in hippocampal slices increases F-actin content within dendritic spine, which is prevented by blocking TrkB signalling and increased by the application of exogenous BDNF (Rex et al., 2007). Interestingly, an increased actin polymerisation was induced via Rac1- p21- activated kinase (PAK) - cofilin pathway which is required for the development of late LTP (L-LTP; Fukazawa et al., 2003; Rex et al., 2007) and is associated with increased spine size and

stability. Moreover, the GTPase Ras is activated via BDNF-TrkB signalling and thereby increases spine stability and spine enlargement (Yasuda et al., 2006). The exogenous application of BDNF in immature hippocampal neurons after 12 DIV leads to a gradual cortactin accumulation within the spine head and thereby may stabilize the actin cytoskeleton (Iki et al., 2005). Taken together, BDNF-TrkB signalling regulates activity-induced molecular pathways to stabilize the actin cytoskeleton and thereby maintaining dendritic spines stability. While it was clearly shown that Nogo-A and NgR1 signalling modulate dendritic spine shape and size (Lee et al., 2008; Zagrebelsky et al., 2010), the question of whether they regulate the actin cytoskeleton dynamics within spines is still open. The analysis of the Nogo-A signalling pathway in growth cones revealed an activation of the Rho-A/ROCK pathway resulting in a destabilization of the actin cytoskeleton via the phosphorylation of the LIMK and thereby the activation of cofilin (Nash et al., 2009; Niederöst et al., 2002; for reviews see: Kempf and Schwab, 2013; Mironova and Giger, 2013; Schwab, 2010). The Nogo-A-Δ20 domain signals via the S1PR2 (Kempf et al., 2014) which regulate the actin cytoskeleton of growth cones by G protein G13 signalling through Rho GEF LARG, and RhoA activation (Singh and Hall, 2008; Spiegel and Milstien, 2003; Toman et al., 2004). Overall, both inhibitory domains of Nogo-A regulate the actin cytoskeleton within growth cones via the activation of RhoA/ROCK and the inhibition of Rac1 pathway (Niederöst et al., 2002). This suggests that the actin cytoskeleton of dendritic spines could be a major target for Nogo-A signalling to maintain a mature spine architecture (for review see: Mironova & Giger, 2013). BDNF is able to regulate functional and structural plasticity and thereby might act as a plasticity promoting factor, in contrast Nogo-A function as a plasticity inhibitor by restricting plasticity. Together they could act in a yin–yang like mechanism by keeping the balance between plasticity and stability in the CNS.

2.5 Aim of this study

The functions of neural networks during development as well as in the adult brain are determined by the architecture of neurons and of the synaptic structures connecting them. The fine tuning of neural circuits relies upon both functional and structural plastic processes and is supposed to be crucial for the integration and storage of information in the brain, including learning and memory processes. Changes in dendritic spine architecture are correlated to the strength of their synapse and depend on the remodelling of the actin spinoskeleton. On the other hand after the end of development the overall neuronal morphology is remarkably stable and thereby is supposed to enable the storage of long-term memories. Still largely unknown are the molecules regulating the spatial and temporal specificity of plastic changes by mediating and modulating the balance between stability and plasticity of mature neuronal networks. In this context, I focused in my study on two promising candidates regulating this balance: the myelin associated inhibitor Nogo-A as a suppressor and the neurotrophin BDNF as a promoter of synaptic plasticity.

Recent studies indicate that Nogo-A signalling restricts functional and structural plasticity in the adult CNS. The present study was aimed at shedding some light in the acute regulation of structural plasticity by Nogo-A signalling and possibly underlying modulation of the actin cytoskeleton in this context. Furthermore, the still largely unexplored physiological relevance of the Nogo-A activity in regulating structural plasticity at spines was assessed during learning and its behavioural outcome *in vivo*.

BDNF signalling is involved in regulating numerous aspects of functional and structural plasticity in the mature CNS. Accordingly*, in vitro* experiments applying exogenous BDNF suggest a major role of BDNF in modulating neuronal architecture and structural plasticity at dendritic spines. On the other hand, *in vivo* the effects of endogenous BDNF in modulating the structure of neurons have been shown to be limited and to depend on the developmental stage, the brain area as well as the cell-type. The aim of this study was to clarify whether these contradictory results are the consequence of a different role of exogenous *versus* endogenous BDNF or whether they derive from comparing *in vitro versus in vivo* experiments.

3 Material and Methods

3.1 Mice strains

To examine the physiological role of Nogo-A in the mouse hippocampus as well as the influence of Nogo-A on spatial reference memory, either C57Bl/6 wild type or *nogo-a* deficient mice (*nogo-a* KO; Simonen et al., 2003; Dimou et al., 2006) were used. Briefly, to obtain mice where expression of Nogo-A is selectively abolished, parts of the *nogo* exons 2 and 3 and the intron in between were exchanged for a PGK-neo (phosphoglycerate kinase-neomycin resistance) gene.

3.2 Organotypic hippocampal slice cultures techniques

3.2.1 Preparation of organotypic hippocampal slice cultures

Hippocampal organotypic cultures were prepared from postnatal day 5 (P5) C57Bl/6 wild-type (WT) mice as previously described (Michaelsen-Preusse et al., 2014; Stoppini et al., 1991). The mice were decapitated with surgical scissors and the skin and bone was completely removed with forceps to expose the brain. The brain was horizontally cut (caudal to rostral) with a sharpened spatula starting between the Superior Colliculus and the Cerebellum (Figure 5A). The brain section was transferred upside down into the chilled drop of preparation solution (Figure 5B). The Cerebellum and Colliculus were gently detached and the meninges covering the hippocampi were carefully removed (Figure 5C). The Hemispheres were separated with a sharpened spatula along the midline (Figure 5D), and the exposed hippocampi were rolled out (Figure 5E) and separated from the cortex (Figure 5F). The hippocampi were dissected in ice-cold sterile Gey's balanced salt solution (GBSS). The hippocampi were transferred onto a teflon disc of the tissue chopper, and sliced transversally at a thickness of 400 µm using a McIllwain tissue chopper. After an incubation of 30 min at 4°C the slices were placed on Millicells CM membrane inserts (Millipore) and cultivated in medium in a 37°C, 5% CO_2, 99% humidity environment. To reduce the number of non-neuronal cells, a mixture of antimitotic drugs (cytosine arabinoside, uridine, and fluorodeoxyuridine; 10^{-6} – 10^{-7} M each; Sigma-Aldrich) was applied for 24 h three days after preparation and 50% medium was changed one a week. The medium was supplemented after 7-10 DIV with 1.25 µg/ml Fungizone as well as 100 U Penicillin and 100 µg/ml Streptomycin.

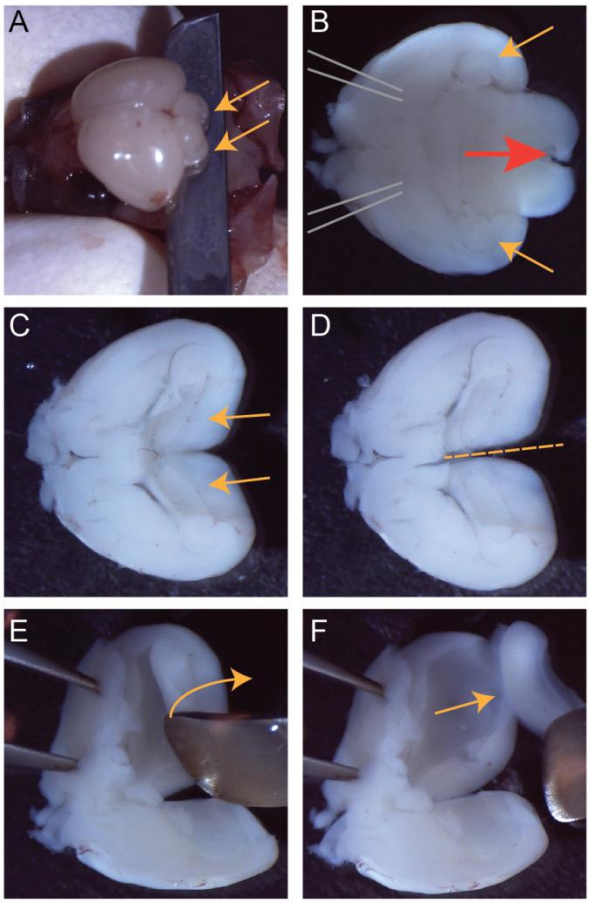

Figure 5: Dissection of the hippocampus for slice culture preparation.

A Shows how a spatula sharpened along the longer edge is used as a knife to perform a horizontal cut to separate the upper part of the brain, containing the hippocampi from the lower one.
B Shows the separated part of the brain from below containing the cortical hemispheres with inside the two hippocampi (*yellow arrows*). The *grey lines* show how the forceps are placed to hold the brain and the *red arrow* the direction along which the colliculi have to be removed. **C** After removing the colliculi the hippocampi are completely exposed (*yellow arrows*). **D** Shows how the two hemispheres are separated along the *midline*. **E** Shows how one hemisphere is held with a forceps through the cortex while a rounded spatula is used to flip the hippocampus.
F The *yellow arrow* shows how the hippocampus is separated from the cortex. Adapted from Michaelsen-Preusse et al., 2014.

3.2.2 Single cell DNA electroporation

In particular CA3 Neurons in the *stratum pyramidale* (sp) were electroporated of organotypic slice cultures 20-22 DIV (Figure 6A) and B. They showed a clear layered organisation *stratum radiatum* (SR) and *stratum oriens* (so) and especially the dense cell body layer *stratum pyramidale* (sp; Figure 6B). For the electroporation the Axoporator 800A (Axon Instruments / Molecular Devices Corp.) and an upright fluorescence microscope (Zeiss examiner) with a 4x Objective (air, NA 0.1, Zeiss) and a 40x Objective (water, NA 0.8, Zeiss) equipped with a differential interference contrast (DIC) video camera were used. For the single cell DNA electroporation a total DNA concentration of 150 ng/µl were used for eGFP-ß-actin (eGFP-actin) and for the co-electroporation equal amounts of eGFP-actin and mCherry-F (a modified version of mCherry carrying the 20-amino-acid farnesylation signal from c-Ha-Ras derived from eGFP-F, Clontech). The DNA was diluted in sterile electroporation buffer 24 h before the electroporation, centrifuged at 13,000 × g for 10 min and stored at 4°C. Right before the electroporation the centrifugation was repeated (13,000 × g for 10 min) and only the supernatant was filled into the patch pipet (approximately 4 µl) using the microloader tips (Eppendorf). The slices were kept in pre-warmed (37°C) sterile 1x Hank's Buffered Salt Solution HBSS (supplemented with 1.25 µg/ml Fungizone as well as 100 U Penicillin and 100 µg/ml

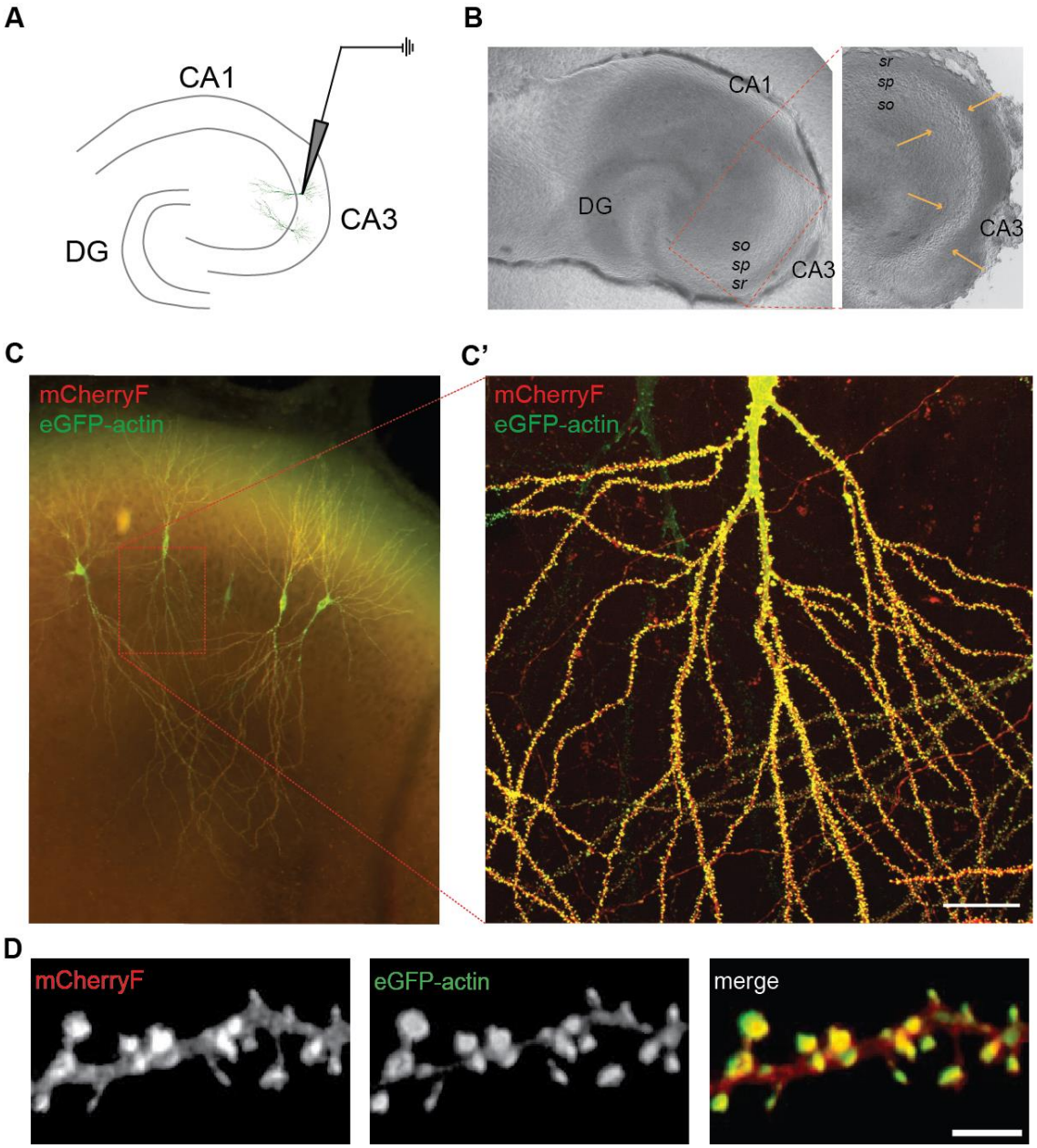

Figure 6: Single cell electroporation.
A schema of the hippocampus slice culture showed dentate gyrus (DG) and in the CA3 area the position of the electroporation. **B** transmitted light image of a 21 DIV hippocampal slice culture showed the dense and well-defined cell body layers especially in the dentate gyrus (DG) and in the CA3 area. The insert (left) showed the preserved layer organisation (stratum radiatum, SR and stratum oriens, so) and especially the dense cell body layer (stratum pyramidale, sp) in the CA3 region. **C** Shows five electroporated CA3 pyramidal neurons expressing both mCherry-F and eGFP-actin. **C'** Confocal image consisting of stacks of multiple optical sections showing the morphology of a mid-apical dendritic tree of a CA3 neuron expressing mCherry and eGFP-actin. Note all the dendrites are highly covered with dendritic spines and the cells does not show any sign of degeneration. Scale bar is 20µm. **D** maximum projection of confocal images showed with high magnification a part of a mid-apical dendrite, there spine shape (mCherry-F) and the actin content (eGFP-actin) colocalize within dendritic spines (merge). Scale bar 2 µm.

Streptomycin) and electroporated with one train of 5V, 200Hz, 100 ms, square pulses of 1 ms. The tip resistance of the electrode (GC150F-10, O.D. 1.5 mm x I.D. 0.86 mm, Harvard Apparatus (Kent): tip diameter 1-2 µm) was 5-10 MΩ at a pressure of 10-20 mlbar controlled by a pressure gauge (GDH200, Greisinger). The slices were used for FRAP measurements 24-72 h after the single cell electroporation. The electroporated CA3 neurons were used for experiments if they didn't show any sign of degeneration such as swelling of the cell body, fragmentation or retraction of the dendrites (Figure 6C and C'). The fluorescence intensity in pyramidal neurons was high enough to completely label both the basal and the apical dendritic tree and allowed detailed visualization of dendritic spines (Figure 6D; Michaelsen-Preusse et al., 2014).

Table 1: Plasmids used in this study (organotypic hippocampal slice cultures)

Plasmid	Description	Reference
pmCherry-F	farnesylated red fluorescent protein mcherry (CMV promoter)	Shaner et al., 2004; O'Brien, 2007
peGFP-actin	enhanced green fluorescent protein fused to ß-actin (CMV promoter)	Clontech

3.2.3 Treatment of hippocampal slice cultures

The loss-of-function for the Nogo-A signalling was obtained using specific antibodies or blockers as follows: (1) A Nogo-A specific blocking antibody (11C7, mouse IgG1), raised against a peptide corresponding to the rat Nogo-A sequence amino acids 623–640 (NiG-Δ20 region; Oertle et al., 2003). The 11C7 antibody is monospecific for Nogo-A in Western blots and shows no cross-reactivity with other Nogo variants (Dodd et al., 2005; Oertle et al., 2003). The Nogo-A function-blocking ability of the 11C7 antibody was confirmed *in vitro* as well as *in vivo* (Liebscher et al., 2005; Wiessner et al., 2003). Furthermore, (2) a function-blocking antibody against the Nogo receptor NgR (goat anti-Nogo receptor affinity-purified goat IgG; R&D Systems), (3) a specific blocker for the sphingosine-1-phosphate receptor 2 (S1PR2; JTE-013; Tocris, 5 µM in DMSO) and (4) a selective inhibitor of the Rho-associated protein kinase p160ROCK (y-27632 dihydrochloride, Tocris, 100 µM in H_2O) were used. A mouse IgG1 anti BrdU antibody was used as control. All antibody solutions were freshly diluted to a final concentration of 5 µg / ml in carbogenated ACSF containing 0.01% BSA. For inhibitors solved in DMSO or H_2O, an equal amount of solvent was used as control. The Nogo-A gain-of-function approach was performed diluting the inhibitory peptide Nogo-A-Δ20 (Oertle et al., 2003) to a concentration of 5 µg/ml in carbogenated ACSF containing 0.01% BSA.

Table 2: Antibodies and Reagents used in this study (organotypic hippocampal slice cultures)

Description	Work dilution	Source
αNogo-A, 11C7 (mouse IgG1)	5 µg / ml	Schwab, Zurich
αBrdU (mouse IgG1)	5 µg / ml	Schwab, Zurich
αNogo receptor NgR (goat IgG1)	5 µg / ml	R&D Systems
αsphingosine-1-phosphate receptor 2 (S1PR2), JTE-013	5 µm	Tocris
αRho-associated protein kinase p160ROCK, y-27632 dihydrochloride	100 µm	Tocris
inhibitory peptide Nogo-A-Δ20	5 µg/ml	Schwab, Zurich

3.2.4 Neuron selection in organotypic slice culture

The experiments in were performed at single spines of secondary or tertiary mid-apical dendritic branches of CA3 hippocampal neurons of organotypic slice culture. The overexpression of eGFP-ß-actin or mCherry-F resulted in the intense labeling of the entire dendritic arbor, as well as of all dendritic spines. Only cells without any sign of degeneration were selected for imaging and spines with an obvious head clearly separated from the dendrite were used.

3.3 Imaging

3.3.1 Fluorescence Recovery after Photobleaching (FRAP)

All FRAP experiments were performed 24-72 hours after electroporation (21-23 DIV) at single spines of secondary or tertiary dendritic mid-apical branches of CA3 hippocampal neurons. Only spines with an obvious head clearly separated from the dendrite were selected for the FRAP experiments. The slices were kept at 32 °C in an open imaging chamber with a continuous perfusion (1 ml / min) of ACSF (carbogenate with 95% O_2 and 5% CO_2) for 30 min before starting the experiment. Siliconized tubings were used and prewashed with ACSF containing 0.01% BSA to prevent sticking of the antibodies to the tubing and the chamber (Chen et al., 1999). The Olympus system BX61WI FluoView 1000 (FV1000) was used to excite eGFP-ß-actin with an excitation wavelength of 488 nm. The power of the excitation laser was adjusted to a low level (1-2%; 5-8 µW) to reduce photobleaching as much as possible still achieving a good signal-to-noise ratio. Scan speed was set to 8 µs per pixel and a line averaging of two (Kalman filtering) were used for an image size of 640 × 128 pixels (final pixel size of 76nm) with a 60x water immersion objective (NA1.0). To increase the z-section's depth the pinhole was opened to 400 µm and the gain and the offset were set to zero. The photobleaching of a single spine was performed using the SIM scanner unit Olympus FV5-LDPSU at an excitation wavelength

of 405 nm and a power of 28-32% (2.3-3 mW) for 28-30 ms. To determine the baseline and the fluorescence recovery 5 images were taken at two second intervals before and 55 after bleaching. In some experiments, the morphology of spines labelled with mCherry-F was imaged using the 594 nm laser line with a scanning speed of 12.5 µs, a line averaging of 2 (Kalman filtering) and a final pixel size of 60 nm. The minimal z-stack depth was set ensuring that all the spines of interests were included in the image and scanned the selected dendritic stretch at 0.35 µm increments along the z-axis (maximum of 15 to 20 z-planes). First the FRAP and then the spine morphology imaging was performed for the selected dendrite at an interval of 180 min.

3.3.2 Analysis of dendritic spine density and morphology

Confocal images were deconvolved using AutoQuantX2 (Media cybernetics, Inc.) and analysed with ImageJ (US National Institutes of Health). Dendritic spine density was counted in three dimensions by determining the number of spines per unit of dendritic length using the multipoint selection tool and the segmented line. The spine morphology was also analysed in three dimensions using the segmented line tool to measure maximum head width and the spine length (from the base at the dendrite its tip).

The statistical analysis was performed using GraphPad Prism. The data were analysed using a one-way ANOVA followed by a *post-hoc* Tukey's Multiple Comparison Test. Values of $p < 0.05$ were considered significant and plotted as follows $*p < 0.05$; $**p < 0.01$; $***p < 0.001$. All data are shown as mean ± standard error of the mean (SEM).

3.3.3 Analysis of the FRAP experiment

Images were analysed using the Olympus software FV1000, by drawing defined regions of interest (ROI) around the bleached spine (the free Area tool was used). For the background and bleaching correction four ROIs were placed next to the bleached spine and on the underlying dendrite respectively (Figure 7A) using the Ellipse tool. The average relative intensity of the ROIs was measured with the Series Analysis tool (Olympus FluoView FV1000) and exported into Microsoft Excel. The mean background (BG) ROIs (Figure 7A, ROIs B–E in green) and the bleaching correction (BL) ROIs (Figure 7A, ROIs F–I in blue) were calculated for each time point and plotted against time (Figure 7). The mean BL pre-bleaching was calculated using the five pre-bleaching images (time points −5 to −1) and a double normalization was used to correct for the loss of signal due to both the bleaching pulse and the bleaching during imaging (Phair et al., 2004).

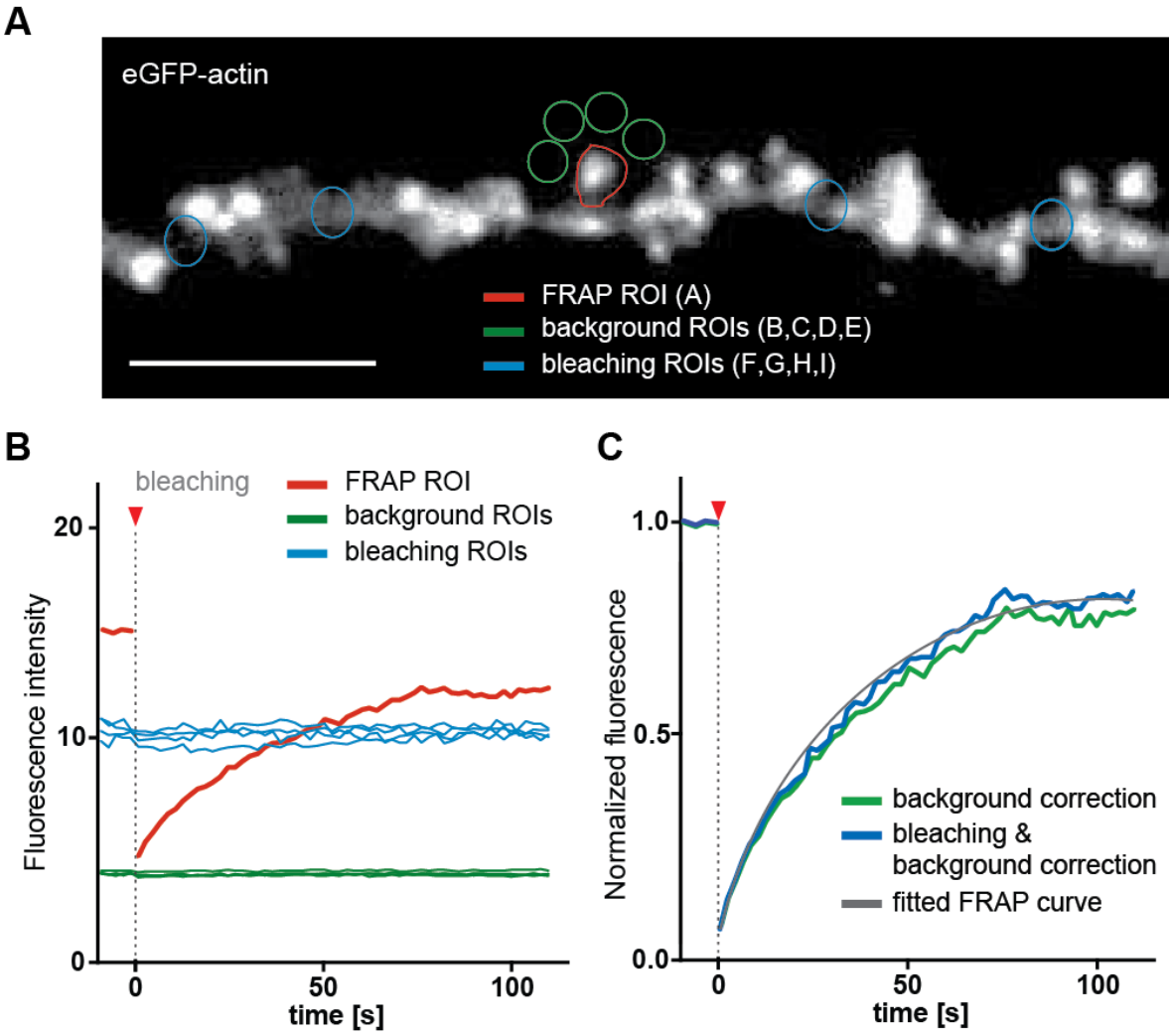

Figure 7: Analysis of the intensity values of the FRAP experiment
A representative image of a dendrite stretch (CA3 Pyramidal neuron) labelled with eGFP-actin and including the spine used for the FRAP experiment. The region of bleaching (*red* ROI, A) as well as the regions for the background (*green* ROIs, B, C, D, E) and bleaching correction (*blue* ROIs, F, G, H, I) are shown. Scale bar 5 µm. **B** the original fluorescence intensity values are plotted against the time for the ROIs in A. **C** the normalized fluorescence intensity including the background correction (*green*) is plotted *vs.* the time. The effect of applying a "bleaching correction" is shown in *blue*. The nonlinear fitting of the FRAP curve is shown in *grey*.

For each time point the normalized fluorescent intensity Fi was calculated (Fs fluorescent intensity of the bleached spine per time point (Figure 7, ROI A, red)).

$$Fi = (Fs - BG)\frac{BL\ prebleaching - BG}{BL\ after\ bleaching - BG}$$

The fluorescent intensity of each time point (Fi) was normalized by dividing it through the mean fluorescent intensity (Fi) before bleaching derived from the baseline time points −5 to −1. The turnover time (recovery half-time $t_{1/2}$) was calculated as the time in seconds at

which the fluorescence intensity reached half of its maximal pre-bleaching value. Based on the recovery curve the actin cytoskeleton dynamics within dendritic spines were divided into different actin fractions (Star et al., 2002; Zito et al., 2004). The 'immobile fraction' represents the stable actin fraction (fs, Figure 8A, red) within each spine. The 'mobile actin fraction' consists of a dynamic (ff, Figure 8A, green) and a monomeric ($1 - fs - ff$, Figure 8, blue) actin pool. The net recovery after photobleaching $F(t)$ is given by the equation below (were t is the time and λ is the time constant, inverse of the turnover rate; Star et al., 2002; Zito et al., 2004):

$$F(t) = 1 - fs - ffe - \frac{t}{\lambda}$$

The statistical analysis and nonlinear curve fitting (based on F(t)) of the fluorescence intensity were done using GraphPad Prism 5 by a 2-way repeated analysis of variance (ANOVA) inter-subject test followed by a two-tailed Student's t-test. For the actin fractions and the turnover time an unpaired two-tailed Student's t-test were used. Values of $p < 0.05$ were considered significant and plotted as followed *p < 0.05; **p < 0.01; ***p < 0.001. All data are indicated as mean ± standard error of the mean (SEM).

Different control conditions and pharmacological agents were used to modulate actin dynamics within dendritic spines to validated the FRAP technique and the analysis. First cytopasmatic eGFP (26.9 kDa) showed a fast recovery after photo bleaching with a turnover time $t_{1/2}$ of 0.34 ± 0.04 s and almost 100% recovery within 3 seconds after bleaching (Figure 8B). The turnover time for eGFP-actin (ß-actin fusion protein, 72 kDa) is 23.09 ± 2.25 s and displayed a stable actin fraction of 16.30 ± 2.01% (Figure 8C). The comparison of these results show a 68 fold increase of the turnover time and indicate that the eGFP-actin are not freely diffusible within the spine. The polymerization dynamics of actin filaments are governed by many factors including actin binding proteins. Therefore it was tested whether 15 min application of 2 µM cytochalasin D or 1 µM jasplakinolide influence the actin filament dynamic and if this could be revealed by the FRAP experiments. Cytochalasin D is a barbed end capping molecule that prevents actin polymerization (Cooper, 1987) and it was shown to reduce the actin turnover within dendritic spines (Star et al., 2002). Indeed, the turnover time was significantly increased 99.36 ± 2.72 s and cytochalasin D shifted the actin fraction towards the stable actin fraction (Figure 8C), by capping the barbed ends and the exchange of monomeric actin occurred only at the pointed end of the actin filaments (Cooper, 1987; Pollard et al., 2000). Complementary the application of the actin filament–stabilizing compound jasplakinolide (Bubb et al., 1994) converted nearly all actin 93.24 ± 1.04% to a stable form and

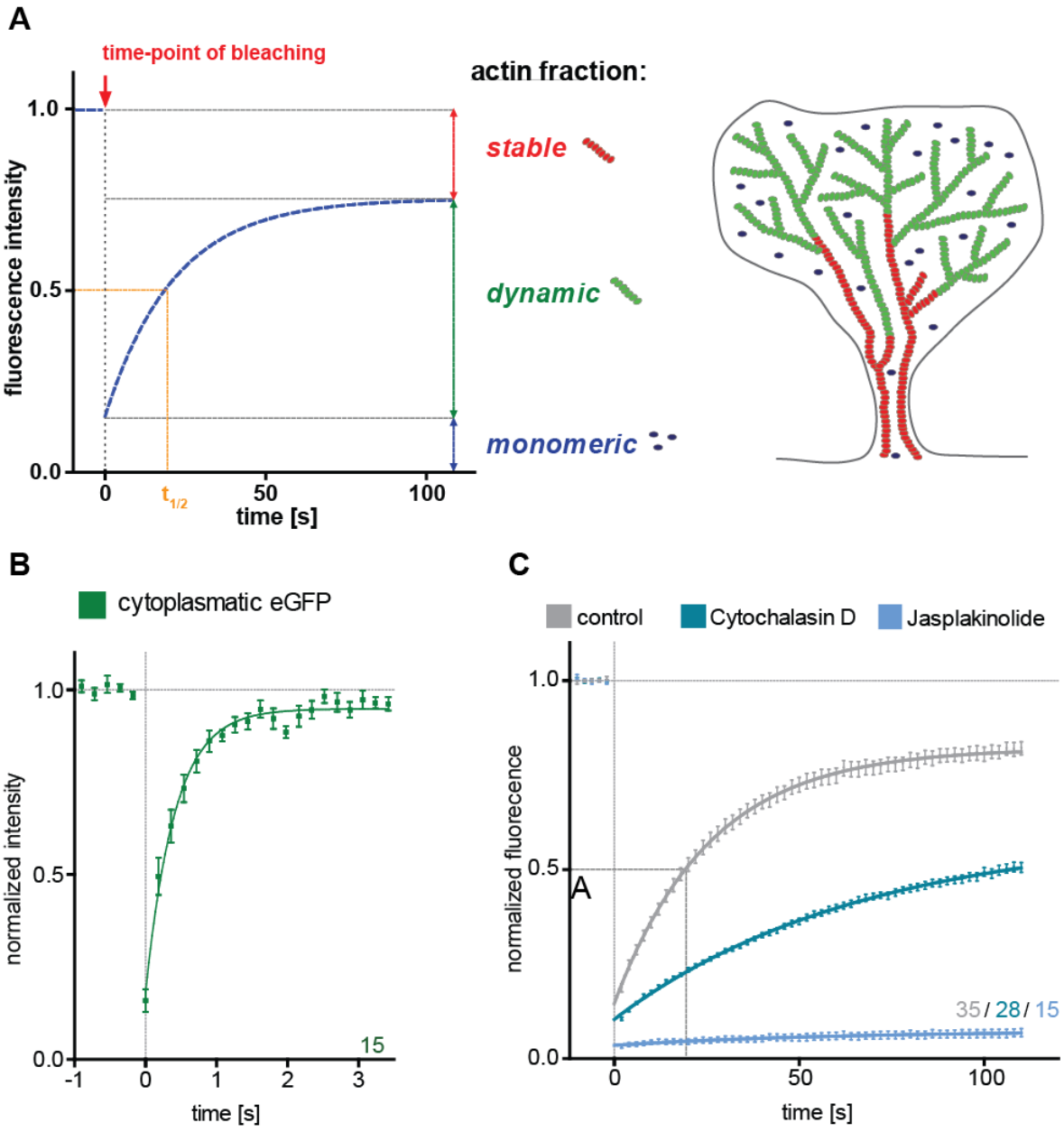

Figure 8: FRAP model to distinguish three actin fractions.
A the distribution of actin fractions is colour coded and illustrated for a FRAP curve and a dendritic spine (adapted from Star et al., 2002; Honkura et al., 2008). The stable actin fraction in *red* , the dynamic fraction in *green*, and the monomeric fraction in *blue*. The turnover time (recovery half-time $t_{1/2}$) is shown in o*range* in the FRAP curve. **B** fluorescence recovery curve after photobleaching for cytoplasmatic eGFP at single spines. **C** Fluorescence recovery curve after photobleaching for eGFP-actin at single spines under control conditions, 15min application of cytochalasin D (2 µM) and jasplakinolide (1 µM).

completely prevented recovery of actin after photobleaching (Figure 8C). These results together with previously published data support a model in which filament turnover determines the time course of fluorescence recovery after photobleaching and not a model in which recovery of fluorescence is determined by diffusion of filaments or unbound eGFP-actin (Star et al., 2002; Zito et al., 2004).

3.4 Preparation of acute hippocampal slices and DiOlistics

Hippocampal slices were prepared from the male wild-type C57Bl/6 and *nogo-a* KO mice at day 3 or 9 after the Morris water maze (MWM) training and control mice without MWM training. In brief, the mice were decapitated and the brain was quickly transferred for three minutes into ice-cold carbogenated (95% O_2, 5% CO_2) artificial cerebrospinal fluid (ACSF). The cerebellum and a part of the forebrain were removed; the hemispheres were separated, the striatum was removed and each hippocampus was gently rolled out with a spatula and separated from the cortex. One hippocampus was immediately frozen in liquid nitrogen and kept at -80°C for biochemical analysis. The other hippocampus was cut in 400µm thick transversal hippocampal acute slices (transversally to the longitudal axis) with the vibratome (VT 1200S; Leica). After an incubation phase of 1h in ACSF at room temperature the slices were fixed in 4% PFA overnight at 4°C and then washed with Phosphate Buffered Saline (PBS). The Diolistic was performed as previously described (Rauskolb et al., 2010). Briefly tungsten particles (50 mg; 1.7 µm in diameter; Bio-Rad) were mixed on a glass slide, with a 100 µl dye solution containing 3 mg of lipophilic dye DiI (Life Technologies) in 100µl of methylene chloride (Sigma-Aldrich; Grutzendler et al., 2003) and let dry. The dried dye-coated particles were removed from the glass slide, resuspended in 3 ml distilled water, and further diluted during sonication to a final concentration of 1:70. Finally, the solution containing the tungsten microcarriers was filled into Tefzel tubing (Biorad) previously briefly washed with a PVP containing solution (polyvinyl-pyrrolidone, 0.05 mg/ml in ethanol; Bio-Rad). To ensure homogenous distribution of the tungsten particles the tubing was continuously rotated while drying. The tubing was cut into 1 cm long bullets which were stored at room temperature. Dye-coated particles were delivered to the hippocampal slices using a hand held gene gun (Bio-Rad; Helios Gene Gun System) at a pressure of 90 psi (one shot per hippocampal slice). A membrane filter with a poor size of 3 µm (Millipore) was inserted between the barrel aligner and the slice to prevent large clusters of particles from damaging and staining the tissue. The slices were kept in PBS at room temperature for 2-3 days for the dye to diffuse. The slices were post fixed in 4% PFA and washed with PBS before being mounted using an anti-fading aqueous mounting medium (Fluoro-Gel Emsdiasum).

3.4.1 DiI imaging

Mid-apical dendritic stretches from CA3 neurons were imaged with a BX61WI FluoView 1000 (FV1000) Olympus confocal microscope. Image stacks were acquired using a 40x oil objective (NA1.3), z-step of 0.5 µm and a pixel size of 130 nm. For details of the analysis and statistics see 3.4.2: Analysis of dendritic spine density.

3.5 Morris water maze task

The Morris water maze (MWM) task was used to test spatial learning in rodents. It is based on the navigation in an open swimming arena equipped with distal cues to locate a submerged escape platform (Morris, 1984, 1981). Spatial learning is evaluated across repeated trials and days whereas reference memory is examined in a probe trail measuring the preference for the target quadrant when the platform is absent (Vorhees and Williams, 2006). The MWM experiments were used to assess spatial reference memory in adult male C57Bl/6 wild-type (WT) mice and Nogo-A $^{-/-}$ mice 3 month old (Simonen et al., 2003). An escape platform 10 cm in diameter was placed in a circular plastic pool (160 cm in diameter and 60 cm high) filled up to 30 cm with opaque water (Titandioxid, Euro OTC Pharma; water temperature 20°C). Three distal visual cues (triangle, circle and stripes) were positioned around the pool. The mice were maintained in a 12:12h light/dark cycle and all tests were performed under indirect light.

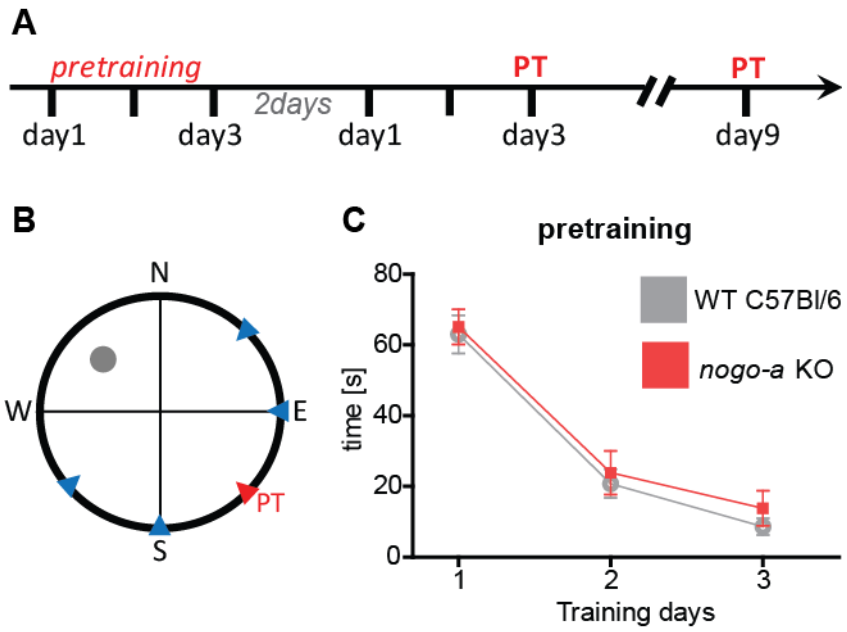

Figure 9: Organisation, pretraining and time course of the Morris water maze training. **A** Overview over the time course of the pertaining and the MWM training including the PTs at day 3 and 9. **B** Top view of the basin, divided in four quadrants via the cardinal point N north, E east, S south, W west. Blue triangle mark the starting position of the Morris water maze task, red triangle the release position of the probe trail (PT) and the grey circle the position of the hidden platform. **C** Pretraining mean latency of WT C57Bl/6 *versus* nogo-A KO mice over three days of the pretraining.

For the pre-training (3 days) the platform was clearly visible above the water surface and marked with a coloured mark. This served to familiarize the animals with the water maze and the experimenter. For the pre-training two trials for 90 s were performed and the release position on the opposite site of the visible platform was changed in a pseudo randomized order. The mice were carefully guided by the experimenter to the platform if

they failed to locate it within 90s. The mice had to remain 15 s on the platform before being returned to their home cage. WT C57Bl/6 and *nogo-A* KO mice learned equally to swim to the visible platform (Figure 9C). Only animals of (both mice species WT and *nogo-a* KO) that showed active swimming behaviour and no thighmotaxis at the last day of pretraining were used (after 2 days of recovery) for the MWM task. To assess spatial reference memory, the mice were trained to locate the hidden platform (1cm below the water surface) for 8 consecutive days (days 1–8, Figure 9A). The platform location was fixed, in the middle of quadrant NW and the release position (SW, S, E, NE) was changed in a pseudorandom order (Figure 9B). Each trial (4 per day with an interval of 3-5 min) was recorded and analysed by the tracking software VideoMot2. At day 3 and 9 of the acquisition phase reference memory was assessed by removing the platform and allowing the animal to freely swim for 45 s (starting position PT Figure 9B). All procedures described in the present study had been conducted in accordance with the applicable European and National regulations (Tierschutzgesetz) and approved by the responsible authority (Nds. Landesamtes für Verbraucherschutz und Lebensmittelsicherheit, LAVES Niedersachsen; Permit Number: 33.12 42502-04-13/1230; 31.7.2013).

3.5.1 Morris water maze data analysis

The recorded swim paths were analysed using Microsoft Excel and Matlab (The Mathworks, USA). As an index for spatial memory formation both in WT C57Bl/6 and Nogo-A deficient mice the escape latency was analysed. Reference memory in the probe trial was measured as the percentage of time spent in each quadrant and the number of crossings over the former platform location. The mice showed a series of different search patterns ranging from random to spatially precise or highly efficient. For qualitative aspects of spatial memory formation we analysed the individual search strategies used by the mice to locate the hidden platform (Brody and Holtzman, 2006; Garthe et al., 2009; Wolfer et al., 2001). Classification of searching behaviours was performed using a parameter-based algorithm, which allows the comparisons between the contributions of each strategy reliably (Figure 10; Garthe et al., 2009). The classification procedure was implemented as a script in Matlab and distinguished the following searching strategies: random search, scanning, chaining (all hippocampus independent) and the hippocampus dependent strategies: direct search, focal search and direct swimming were pooled and named direct search (Figure 10; Garthe et al., 2009). Statistical analysis was performed using IBM SPSS Statistics 20 software and the experimenter was blind to the genotype

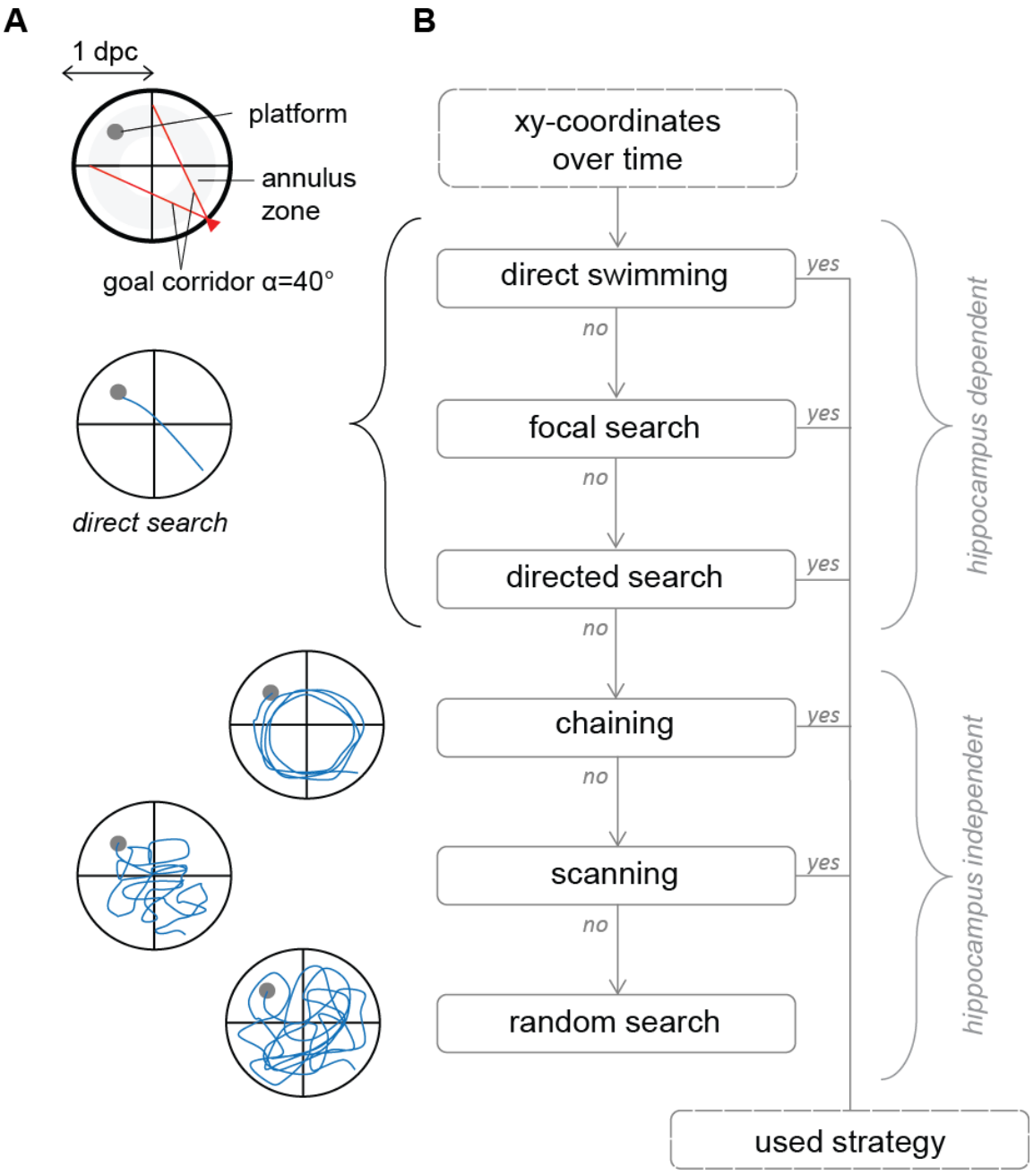

Figure 10: Algorithm-based classification of search strategies used during the Morris water maze task.

A criteria used in the classification of the search pattern, the basin was divided into distinct zones (annulus zone and goal corridor), distance to pool centre (dpc) to calculate the respective searching strategy. **B** the search patterns were identified using an algorithm-based classification (with Math lab). The xy-coordinates over the time were used to calculate the respective searching strategy in the outlined order. Direct swimming, focal search and directed search were categorized as direct search or as a hippocampus dependent searching pattern. Chaining scanning and random search were categorized as hippocampus independent searching pattern. Modified after Garthe et al., 2009.

both during the experiment and the analysis. The latency values were tested with a 2-way repeated analysis of variance (ANOVA). Scores obtained in the strategy analysis were analysed using 2-way repeated ANOVA followed by a non-parametric Mann–Whitney U-test. Quadrant preferences during the probe trials were analysed using a one-way ANOVA followed by a post-hoc Tukey's Multiple Comparison Test (GraphPad Prism). Values of $p < 0.05$ were considered significant and plotted as followed $*p < 0.05$; $**p < 0.01$; $***p < 0.001$. All data are indicated as mean ± standard error of the mean (SEM).

The parameters for the searching strategies are the following:

Random search:

- *Search behaviour covering the entire pool surface.*
  > 60% surface coverage

Scanning:

- *Search behaviour became increasingly restricted to the central pool.*

<60% and >10% surface coverage

<0.7 dpc (distance to pool centre)

For both random search and scanning any spatial or directional preference is absent.

Chaining:

- *Search behaviour became increasingly restricted to the goal annulus zone.*

>80% time in annulus zone

0.4 - 0.8 dpc

Directed search:

- *Search behaviour became directional restricted in a triangular way pointing towards the platform.*

80% in a 40° goal corridor (from the starting point)

Focal search:

- *Search behaviour became directed to the platform, searching near to the platform.*

<0.3 dpc to mean distance to the platform

<0.35 dpc to mean distance to swim path centroid

Direct swimming:

- *Search behaviour became directed to the platform.*

90% in a 10° goal corridor (from the starting point)

Modified after Garthe et al., 2009.

3.6 Western Blot

Tissues were homogenized with mechanical disruption and extracted on ice in RIPA buffer, pH 8.0, containing 0,1% SDS, 0,5% sodium deoxycholate (DOG), 1% NP-40 Nonidet P40 and protease inhibitors cocktail (Roche). Samples were incubated on ice for 40–60 min, and debris was pelleted by centrifugation (15,000 × g for 15 min at 4 °C). Total protein concentration of cleared lysates was measured by Bredford protein assay. Equal protein concentrations (20 µg per lane) from three animals per group (not-trained, 3 day training and 9 day training) were separated on 7.5% gels and transferred to polyvinylidene difluoride (PVDF) membranes. Membranes were blocked in tris-buffered saline / Tween with 5% milk powder and incubated with rabbit anti-Nogo antiserum Bianca (1:60,000) and mouse anti-tubulin antibody (1:2000; Sigma-Aldrich) overnight at 4 °C. The membranes were then washed in tris-buffered saline/Tween and subjected to secondary HRP conjugated antibodies goat anti-rabbit or goat anti-mouse (1:2000; Sigma-Aldrich) diluted in TBS-T for 90 min at room temperature. Immunoreactivity was visualized by chemoluminescence (Luminata, Millipore). For quantification the same samples were run independently three times. Densitometry of bands was conducted in EasyWin32 using the tubulin as loading control.

3.7 Primary hippocampal culture techniques

3.7.1 Preparation of primary hippocampal cultures

Primary hippocampal cultures were prepared from C57Bl/6 mice at embryonic day 18. Glass coverslips (13 mm diameter) were prepared in advance and were first incubated in a 10 M NaOH solution (5-6 h), sterilized at 225 °C for 6 h and coated with 0.5 mg/ml poly-L-lysine hydrobromide (Sigma) in boric acid buffer (overnight at 4°C or 3 h at 37 °C). Embryos were decapitated and the brains were kept in ice-cold Gey's balanced salt solution supplemented with glucose and adjusted to pH 7.2. After dissection the hippocampi were incubated for 10 min in trypsin/EDTA at 37°C and then mechanically dissociated with a Pasteur pipette. Cells were plated at high density (10^5/well) on the poly-L-lysine-coated coverslips (13 mm) and kept in Neurobasal medium (Lifetechnologies) supplemented with 2% B27 (Lifetechnologies) and 1% Glutamax at 37°C, 5% CO_2, and 99% humidity. For the neurite out growth assay after 3 days *in vitro* (DIV), the cells were plated at a density of 10^4 cells per well. Furthermore, for experiments were the synaptic activity was manipulated (e.g. with high Magnesium, 3.5 mM Mg^{2+}) and their controls, the cells were plated at a density of 70,000 cells per well and kept in Neurobasal medium (Gibco) supplemented with 2% BSA (Gibco), 200 µM L-Glutamin and 1% 100 × N_2 (Life Technologies) at 37°C, 5% CO_2, and 99% humidity.

3.7.2 Transfection of primary hippocampal neurons

Primary hippocampal neurons were transfected after 14 and 21 DIV with a farnesylated form of the enhanced green fluorescent protein (fEGFP) using Lipofectamine 2000 according to the manufacturer's protocol. To label F-actin the primary hippocampal cultures were co-transfected with fEGFP and an expression plasmid for the Lifeact peptide fused to a red fluorescent protein (RFP-LA; Riedl et al., 2008, 2010). Briefly, 0.8 µg DNA for transfection of a single plasmid or, for a co-transfection 0.4 µg pfEGFP and 0.6 µg pRFP-LA and 2 µl Lipofectamine 2000 per well were mixed in 100 µl Neurobasal medium without supplements (NB^-) and added after 20 min incubation at room temperature to the cultures drop-wise. The conditioned medium of the primary cultures was previously exchanged too NB^-. After 50 min of incubation the transfection medium was exchanged for the original Neurobasal medium. The cultures were kept for 24 h at 37°C, 5% CO_2, and 99% humidity before the treatment.

Table 3: Plasmids used in this study (primary hippocampal culture)

Plasmid	Description	Reference
pEGFP-F	farnesylated enhanced green fluorescent protein (CMV promoter)	Clontech
pRFP-Lifeact-N1	red fluorescent protein fused to lifeact (CMV promoter)	Riedel et al.,2008

3.7.3 Treatment of primary hippocampal neurons

Twenty-four hours after transfection, 1/3 of the culture medium was exchanged for a medium containing 0.1% Bovine Serum Albumine (BSA, 0.1% BSA/1x PBS) as a control treatment or 0.1% BSA combined with BDNF (Recombinant Human BDNF, 40 ng/ml, R&D Systems), BDNF blocking antibodies (BDNF-Abs, 1:500, M. Sendtner, Wuerzburg Germany) or TrkB receptor bodies (TrkB-Fc, Recombinant Human TrkB-Fc, 500 ng/ml, R&D Systems). BSA was added to the medium to prevent BDNF or the antibodies from sticking to the plastic (Chen et al., 1999). In a second set of control experiments the cultures were kept in Neurobasal medium (NB) without addition of BSA. As no significant difference between the two control conditions could be observed only the BSA control was used in the result part. After 24 h of treatment the cultures were fixed in 4% paraformaldehyde (PFA) in 0.1 M phosphate buffer (PB), washed and mounted with an anti-fading aqueous mounting medium (Fluoro-Gel Emsdiasum). In a second set of experiments neuronal activity was reduced in primary hippocampal cultures by increasing the Mg^{2+} concentration in the medium. Indeed, Mg^{2+} decreases the activation of voltage-gated channels thereby reducing neuronal excitability (Dribben et al., 2010; Mayer and Westbrook, 1987). To avoid effects on the early developmental stages Mg^{2+} concentration in the medium was increased starting at 7 DIV from 1.5 to 3.5 mM by adding $MgCl_2$ (50%

medium change, NB with 5.5 mM $MgCl_2$), fresh medium was added once a week (13 and 20 DIV; 50% medium change, NB with 3.5 mM $MgCl_2$). The treatment with BDNF or TrkB receptor bodies was performed for 24 h either in low (1.5 mM) or high (3.5 mM) Mg^{2+} containing medium.

Table 4: Antibodies and Reagents used in this study (primary hippocampal culture)

Description	**Work dilution**	**Source**
Recombinant Human **BDNF**	40 ng / ml	R&D Systems
Recombinant Human **TrkB-Fc** Chimera	500 ng / ml	R&D Systems
αBDNF antibodies (**BDNF-Abs**)	1:500	Sendtner, Würzburg

3.7.4 Immunohistochemistry

Primary hippocampal cultures (6 or 23 DIV) were fixed with 4% PFA, washed with PBS and incubated in a solution 0.2% Triton X-100, 10% goat serum and 0.1% BSA in phosphate buffer (PBS) to permeabilize the membrane and block unspecific binding sites. A rabbit polyclonal antibody anti-c-fos (Santa Cruz Biotechnology, Inc., sc-52; dilution 1:500), a mouse monoclonal antibody anti-CaMKII (Lifetechnologies, dilution 1:500), a rabbit polyclonal anti-MAP2 (Abcam, dilution 1:500) or a primary rabbit monoclonal anti-phospho-TrkA (Tyr674/675) / TrkB (Tyr706/707) antibody (Cell Signaling Technology; dilution 1:200) were diluted in blocking solution (10% goat serum, 0.1% BSA in PBS and 0.2% Triton X-100) and incubated at 4 °C overnight. Secondary anti-rabbit or anti-mouse antibodies conjugated with Cy2, Cy3, or Cy5 (Jackson Immuno Research) were diluted 1:500 in PBS and incubated for 2 h at room temperature. Alexa Fluor 350 phalloidin (Lifetechnologies) was diluted 1:50 in PBS and incubated for 3 h at room temperature to selectively stain F-actin. Finally, cultures were counterstained with DAPI (4',6-diamidino-2-phenylindole; Biotium) diluted 1:1000 in PBS for 5 min, washed and mounted using an anti-fading aqueous mounting medium (Fluoro-Gel Emsdiasum).

Table 5: Antibodies used in this study (primary hippocampal culture)

Antigen	**Organism**	**Work dilution**	**Source**
αCaMKII (Ca2+/calmodulin dep. kinase II)	mouse	1:500	Lifetechnologies
α-c-fos (Inc., sc-52)	rabbit	1:500	Santa Cruz Biotec.
MAP2 (microtubule associated protein)	rabbit	1:500	Abcam
Alexa Fluor 350 phalloidin		1:50	Lifetechnologies
anti-phospho-TrkA (Tyr674/675) / TrkB (Tyr706/707)	rabbit	1:200	Cell Signaling Tec.
Mouse/rabbit Cy2/Cy3/Cy5	goat	1:500	Jackson Immuno Res.

3.7.5 Neuron selection in primary hippocampal cultures

The transfection of the fEGFP expression plasmid under the control of the CMV promoter resulted in the intense labeling of the entire dendritic arbor as well as of all dendritic spines of individual pyramidal neurons. Only non-overlapping labelled pyramidal neurons were selected for our analysis allowing for an unambiguous reconstruction of the entire dendritic tree as well as the analysis for the spine density. Degenerating neurons were identified according to the presence of retraction bulbs and fragmentation of the dendritic processes and excluded from the analysis. Due to a recent report showing that Mg^{2+} (5 to 10 mM) increase neuronal apoptosis in primary hippocampal neurons (Dribben et al., 2010), special care was taken in selecting neurons kept in high magnesium medium (3.5 mM). Indeed, all neurons selected for the analysis showed a healthy cell body and dendritic tree with no signs of apoptosis.

3.7.6 Imaging of primary hippocampal cultures

The neurons selected for analysis were imaged using an Axioplan 2 microscope equipped with an ApoTome module (Zeiss). Each neuron was first imaged using a 20x objective (1.25 numerical aperture (NA). For the analysis of the spine density and spine morphology defined dendritic stretches were imaged using a 63x objective (1.32 NA) acquiring three-dimensional stacks z-sectioned at 0.5 µm.

3.7.7 Calcium imaging with primary hippocampal cultures

Primary hippocampal cultures 16 and 23 DIV were loaded with calcium indicator by incubating them for 15 min with the indicator solution (50 µg Oregon Green 488 BAPTA-1 AM (Lifetechnologies), dissolved in 50 µl DMSO and 2.5% Pluronic acid) at 37°C, 5% CO2, and 99% humidity. The cells were then transferred to HBSS (Hanks balanced salt solution) and kept 45 min at 37°C, 5% CO2, and 99% humidity. The coverslips were then transferred to the recording chamber, continuously perfused with HBSS and kept at 32°C. The live imaging was performed using an Olympus BX61WI microscope system (Cell^M software) and a CCD camera (VisiCam QE, Visitron Systems). Images were recorded at 6.67 Hz for 75 sec with an Olympus 20x water immersion objective (0.95 NA, XLUMPLAN FL, Olympus), whereby a pixel resolution of 0.77 µm / pixel was achieved. A frame rate of 150 ms and an exposure time of 61 ms were used. Primary hippocampal cultures were treated with BSA (0.1% BSA/1x PBS) or BDNF (Recombinant Human BDNF, 40 ng/ml, R&D Systems) by a 5 min bath-application. The analysis of calcium transients was performed using ImageJ (NIH) and calculating the fluorescence changes as average of all pixels within regions of interests (ROIs). The ROIs were set around the cell bodies of the neurons. For the background subtraction the ROI was drawn on a neighboring area

containing neuropil. The resulting changes in the intracellular calcium concentration are represented as $\Delta F/F_0$ in percent, where F_0 is the fluorescence at resting conditions ($\Delta F/F_0 = (F - F_0) / F_0$) taken before the application of BDNF (Lang et al., 2006). In addition, changes in the fluorescence intensity for the whole ΔF-stack were visualize using the plugin 'reslice' of the ImageJ Software to generate a pseudo-line scan . In the pseudo-line scan the y-axis corresponds to the respective line drawn on the stack whereas the x-axis corresponds to time.

3.7.8 Data analysis of primary hippocampal cultures

For the selected neurons dendritic complexity and length was analysed using a Sholl analysis (Sholl, 1953). The neurons were traced using the Neurolucida software (MicroBrightField), and the Sholl analysis was obtained with Neuroexplorer software (MicroBrightField), calculating the cumulative number of dendritic intersections at 10 µm interval distance points starting from the cell body. The total number of crossings for each cell was used as an index for total dendritic complexity. For 6 DIV neurons the total neurite length, number of primary neurites and number of branching points of were analysed by tracing MAP2 labelled neurites using the NeuronJ (Meijering et al., 2004) plugin for ImageJ (NIH) Software. Spine density was measured for portions of selected second or third order dendrite branches. The number of spines and the dendritic length were measured using the ImageJ software. The number of spines was normalized per micrometer of dendritic length and a minimal length of 250 µm of dendrite per cell was analysed. The maximal spine head diameter and maximal spine length (from the dendritic shaft to the spine head tip) were measured on three-dimensional stacks using the ImageJ (NIH) software. To examine the actin content in dendritic spine heads the mean fluorescent intensity of RFP-lifeact was measured with the area selection tool of ImageJ and normalized to the mean fluorescent intensity of the dendritic shaft (for normalization of the RFP overexpression, Figure 23B, indicated with the arrow heads). RFP-Lifeact and the immunocytochemistry for c-fos and phosphorylated TrkB were imaged keeping a constant exposure time. The mean fluorescent intensity values for the immunocytochemistry of c-fos and phosphorylated TrkB were measured with ImageJ (NIH) and normalized to the control condition. The analysis was done without knowledge of the treatment performed. The statistical analysis was performed using GraphPad Prism. The data obtained were compared between two different experimental conditions using an unpaired two-tailed Student's t-test. Data including more than 2 different groups were analysed using a One-Way ANOVA followed by a post-hoc Tukey's Multiple Comparison Test. Values of $p = 0.05$ were considered significant and plotted as follows $*p < 0.05$; $**p < 0.01$; $***p < 0.001$. All data are indicated as mean ± standard error of the mean (SEM).

3.8 Solutions and media

All reagents used in this thesis have been distributed by AppliChem, Invitrogen, PAA, Roth or Sigma. Exceptions were described separately.

Organotypic cultures:

Gey's Balanced Salt Solution pH 7.4 (GBSS)

Component	Molarity [mM]
$CaCl_2$ * 2 H_2O	1.5
KCl	5.0
KH_2PO_4	0.22
MgCl2 * 6 H_2O	1.0
$MgSO_4$ * 7 H_2O	0.28
NaCl	1.37
Na_2HCO_3	2.7
Na_2HPO_4	0.86
D-Glucose	5.5

Filtered sterile and kept at 4°C.

Kynurenic acid
Dissolved 946 mg Kynurenic acid in 5 ml 1 M NaOH; added 45 ml dH_2O; filtered sterile;
prepared 1 ml fractions and stored at -20°C.

Glucose (50%)
Glucose was dissolved in dH_2O 1:1 while heating, filtered sterile in warm state and stored at -20°C.

Preparation solution pH 7.2

GBSS	98 ml
Glucose (50%)	1 ml
Kynurenic acid	1 ml

Adjusted pH to 7.2 (1 M HCl) and filtered sterile.

Medium

BME	100 ml
HBSS	50 ml
Equine donor serum	50 ml
L-Glutamin (200 mM)	1 ml
Glucose (50%)	2 ml

Antimitotics

1M Uridine,	2.42 mg / 10 ml H_2O
1M Cytosin-β-D-Arabinofuranosid Hydrochlorid,	2.79 mg / 10 ml H_2O
1M 5-Fluoro-2´-Deoxyuridin,	2.46 mg / 10 ml H_2O

Stock solutions 1:1; sterile filtered and stored at -20°C.

Antibiotics and Fungicides

From DIV 7 on the medium was supplemented with 1.25 µg/ml Fungizone, 100 U Penicillin and 100 µg/ml Streptomycin.

Fungizone

Stock solution: 250 µg Fungizone/ml, diluted 1:200 = 1.25 µg Fungizone/ml culture medium or HBSS, 250 µl Fungizone Stock solution in 50 ml culture medium or HBSS.

Penicillin–Streptomycin

Stock solution: 5,000 U Penicillin–5,000 µg streptomycin /ml, diluted 1:50 = 100 U Pen–100 µg Strep / ml culture medium or HBSS, 1 ml Pen–Strep in 50 mL culture medium or HBSS.

Primary cultures:

Preparation solution pH 7.2

GBSS	98 ml
Glucose	1 ml

Adjusted pH to 7.2 (1 M HCl) and filtered sterile.

Medium normal Magnesium 1.5mM

Neurobasal	50 ml
B27	2 ml
GlutaMAX (200 mM)	125 µl

Medium high Magnesium 3.5mM

Neurobasal	50 ml
B27	1 ml
L-Glutamin (200mM)	125 µl
N2 (100x)	500 µl

Borate-Buffer pH 8.5 (Glass coverslips)

Dissolved 1.24 g boric acid and 1.9 g borax in 400 ml sterile H_2O and adjusted pH to 8.5.

Poly-L-Lysin stock solution

Dissolved 10 mg/ml in H_2O, stored at -20°C.

Cell and Molecular Biology:

ACSF (Artificial Cerebrospinal Fluid) used for live imaging experiments.

Component	Molarity [mM]
NaCl	124
KCl	4.9
$MgSO_4*7H_2O$	2.0
$CaCl_2*2H_2O$	2.0
KH_2PO_4	1.2
$NaHCO_3$	25.6
D-Glucose	10.0

ACSF used for the preparation of acute brain slices.

Component	Molarity [mM]
NaCl	125.0
KCl	2.5
$NaH_2PO_4 * H_2O$	1.25
$MgCl_2 * 6H_2O$	2.0
$NaHCO_3$	26.0
D- Glucose	25.0
$CaCl_2 * 2H_2O$	2.0

DNA electroporation buffer

Component	Molarity [mM]
NaCl	135
KCl	5.4
$MgCl_2$	1.0
$CaCl_2$	1.8
Hepes	5.0

Adjust pH of 7.2 and stored at 4°C.

Hank's Buffered Salt Solution - HBSS (500ml)

HBSS 10x	50 ml
$NaHCO_3$	175 mg
$CaCl_2 * 2 H_2O$	147 mg

Filled up with dH_2O, sterile filtered and stored at 4°C.

Phosphate buffered saline (PBS)

Component	Molarity [mM]
KCl	2.7
KH_2PO_4	1.5
NaCl	137
Na_2HPO_4	10.4

4% PFA in 0.2 M Phosphat Buffer pH 7.4

dH_2O	500 ml
PFA	40 g
0,2 M Phosphat	500 ml

4 Results

Learning and memory processes are correlated to both functional and structural changes at dendritic spines and axonal boutons (Bailey and Kandel, 1993; Caroni et al., 2012; Kasai et al., 2010; Lamprecht and LeDoux, 2004). Alterations in the size and shape of dendritic spines are correlated with their strength of synapses and heavily depend on remodelling of its underlying actin cytoskeleton (Dillon and Goda, 2005; Hotulainen and Hoogenraad, 2010; Okamoto et al., 2009). Interestingly, spine dynamics are tightly regulated by extracellular signals and most signalling pathways linking synaptic activity to spine morphology regulate actin dynamics (Hotulainen and Hoogenraad, 2010). In this context, I examined the role of two different molecules: the myelin associated protein Nogo-A and the neurotrophin BDNF (Brain-derived neurotrophic factor) in modulating or regulating the actin cytoskeleton and structural synaptic plasticity in the mature hippocampal network.

In the first part of my work, I addressed the question of whether Nogo-A signalling acutely controls the actin cytoskeleton dynamics at individual dendritic spines of hippocampal pyramidal neurons *in vitro*. Next, I examined whether Nogo-A is involved in regulating structural plasticity upon learning and memory processes *in vivo*. In the second part of my work, I asked whether BDNF signalling affects activity-dependent structural plasticity of mature hippocampal neurons *in vitro*.

4.1 Nogo-A modulates the actin cytoskeleton within dendritic spines and is involved in regulating structural plasticity upon learning

4.1.1 Nogo-A signalling transiently modulates actin cytoskeleton dynamics within dendritic spines to regulate their architecture

Recent studies demonstrated an important role of Nogo-A signalling in suppressing structural and functional plasticity in the mature and uninjured neuronal circuit of the CNS (for reviews see: Kempf and Schwab, 2013; Mironova and Giger, 2013; Schwab, 2010). These effects of Nogo-A are mediated via two extracellular domains and their receptors: Nogo-66 domain acting via the Nogo-66 receptor 1 (NgR1; Fournier et al., 2001) and Nogo-A-Δ20 via the sphingosine 1-phosphate receptor 2 (S1PR2; Kempf et al., 2014). In this study I applied a series of gain- or loss-of-function approaches for Nogo-A to investigate its role in modulating the actin cytoskeleton dynamics within dendritic spines of CA3 pyramidal neurons in 3-week-old organotypic hippocampal WT cultures. Filamentous actin is concentrated in dendritic spine heads (Figure 11A, left) and plays an important role in regulating structural and functional plasticity (Dillon and Goda, 2005; Hotulainen

and Hoogenraad, 2010; Matus, 2000; Okamoto et al., 2009). To determine if Nogo-A may influence the actin cytoskeleton dynamics fluorescence recovery after photobleaching (FRAP) was performed at individual dendritic spines of eGFP-actin expressing CA3 pyramidal neurons (Figure 11A, left). To distinguish possible early and late effects of actin dynamics, FRAP was performed 20 and 180 minutes after the application of different treatments. An anti-BrdU mouse IgG1 antibody was used as control.

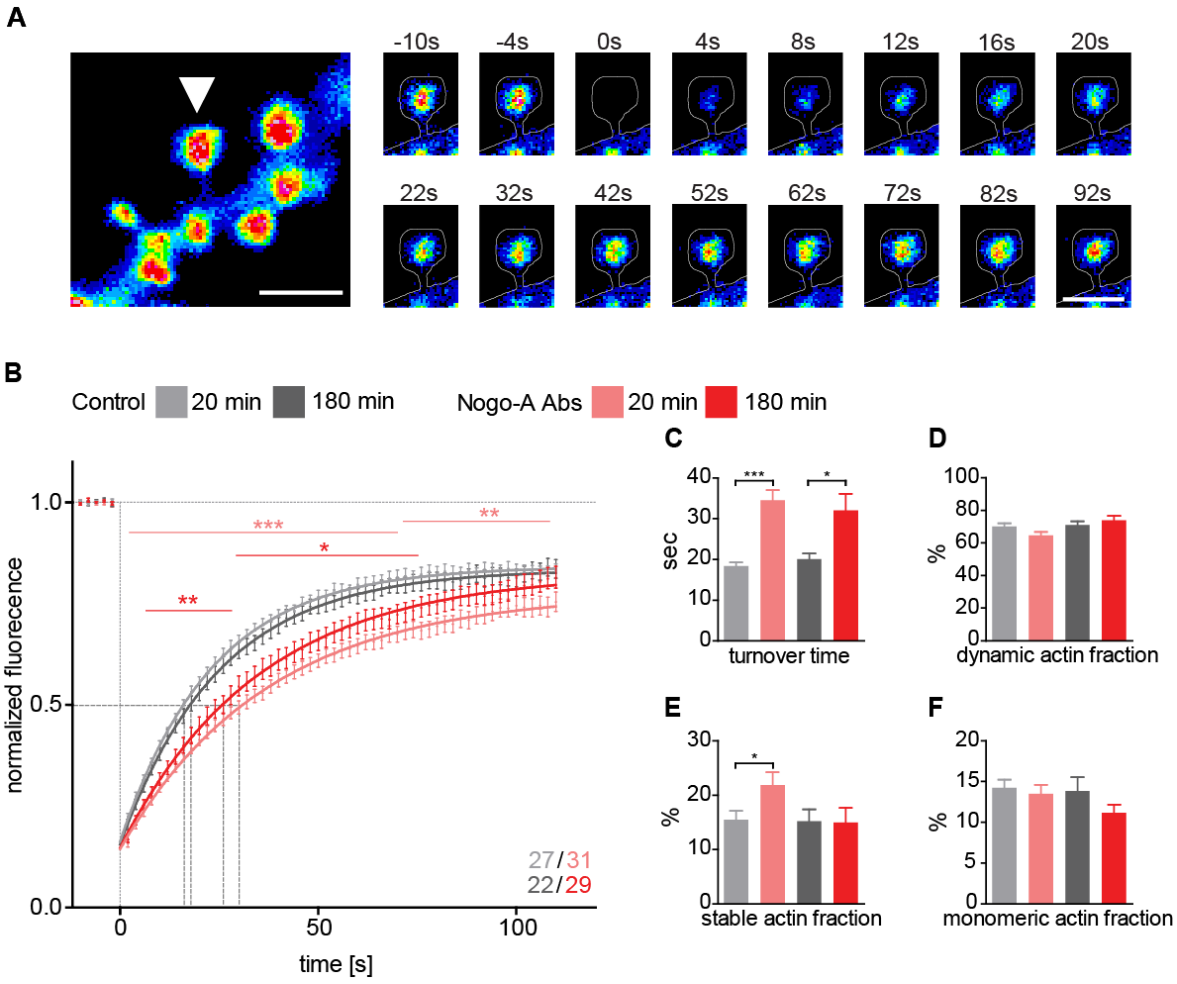

Figure 11: Nogo-A neutralisation affects transitory the actin cytoskeleton within dendritic spines of hippocampal pyramidal neurons.
A Maximum projection consisting of stacks of multiple optical sections, pseudo colour encodes for fluorescence intensity of the eGFP-actin content within dendritic spine of CA3 hippocampal pyramidal neuron. Scale bar, 2 µm (left) and the time series before and after bleaching of a single dendritic spine (time point of bleaching at 0s). Scale bar, 1 µm (right). **B** Fluorescence recovery curve after photobleaching for eGFP-actin at single spines under control conditions or Nogo-A Abs treatment after 20 and 180 min. Numbers of dendritic spines are indicated for each treatment. Analysis of the **C** turnover time, **D** dynamic actin fraction, **E** stable actin fraction and **F** monomeric actin fraction for control conditions compared to Nogo-A neutralisation after 20 and 180 min respectively. Data are presented as mean ± SEM. *p < 0.05, **p < 0.01; ***p < 0.001.

The actin cytoskeleton of single dendritic spines was imaged at 2 s intervals over 2 min before bleaching. The eGFP-actin fluorescence was constant and completely disappeared upon bleaching (Figure11A, right). Under control conditions the fluorescence intensity rapidly recovered after photobleaching and reached a plateau at 85% of the original pre-bleaching fluorescence after 110s. No significant differences in the fluorescence recovery profile could be observed between the two time points used (20 and 180 min; Figure 11B). Similar to previous data, this indicates that under control conditions 85% of the actin within dendritic spines exists in a mobile state and only a small fraction of 15% is stable 110 s after bleaching (Figure 11E; Star et al., 2002). Mobile actin consists in 70% dynamic actin fraction (Figure 11D) and 15% monomeric G-actin fraction (Figure 11F). No differences in mobile actin could be observed between the two time points (20 and 180 min; Table S1) under control conditions. Furthermore, the turnover time (recovery half-time t1/2; Figure 11C) was about 20 seconds both after 20 or 180 minutes of treatment (Table S1) and was in line with previous data (Stamatakou et al., 2013). Nogo-A was neutralised by bath application of the Nogo-A function blocking antibodies (Abs) 11c7 raised against the Nogo-A-Δ20 domain (Liebscher et al., 2005; Maier et al., 2009; Oertle et al., 2003). The actin cytoskeleton dynamics of single dendritic spines showed a dramatic change both after 20 and 180 min of Nogo-A neutralisation when compared to respective control conditions. Starting 6 s after bleaching the recovery curve recorded after 20 min of Nogo-A Abs treatment showed significantly lower intensity values than under control conditions. The significant differences in the recovery curve were maintained up to 110 s after bleaching (Figure 11B, control *vs.* Nogo-A 20 min $p < 0.01$). Also, when the FRAP experiment was performed 180 min after Nogo-A Abs treatment, the recovery curve showed significant lower intensity values between 10 and 76 s after bleaching in comparison to the control (Figure 11B, control *vs.* Nogo-A 180 min $p < 0.05$). To quantify the actin cytoskeleton dynamics within dendritic spines, the turnover time was calculated and showed a significant increase for both 20 min and 180 min Nogo-A neutralisation in comparison to controls (Figure 11C, Table S1, control *vs.* Nogo-A 20 min $p < 0.001$ and control *vs.* Nogo-A Abs 180 min $p < 0.05$). Moreover, the stable actin fraction was significantly increased after 20 min Nogo-A neutralisation in comparison to the control (Figure 11E, Table S1, control *vs.* Nogo-A Abs 20 min $p < 0.05$) while after 180 min of blocking Nogo-A the stable actin fraction was unaltered when compared to control condition (Figure 11E, Table S1). The analysis of the dynamic (Figure 11D) and monomeric actin fractions (Figure 11F) showed no significant changes between the controls and Nogo-A Abs treatment at both time points (Table S1).

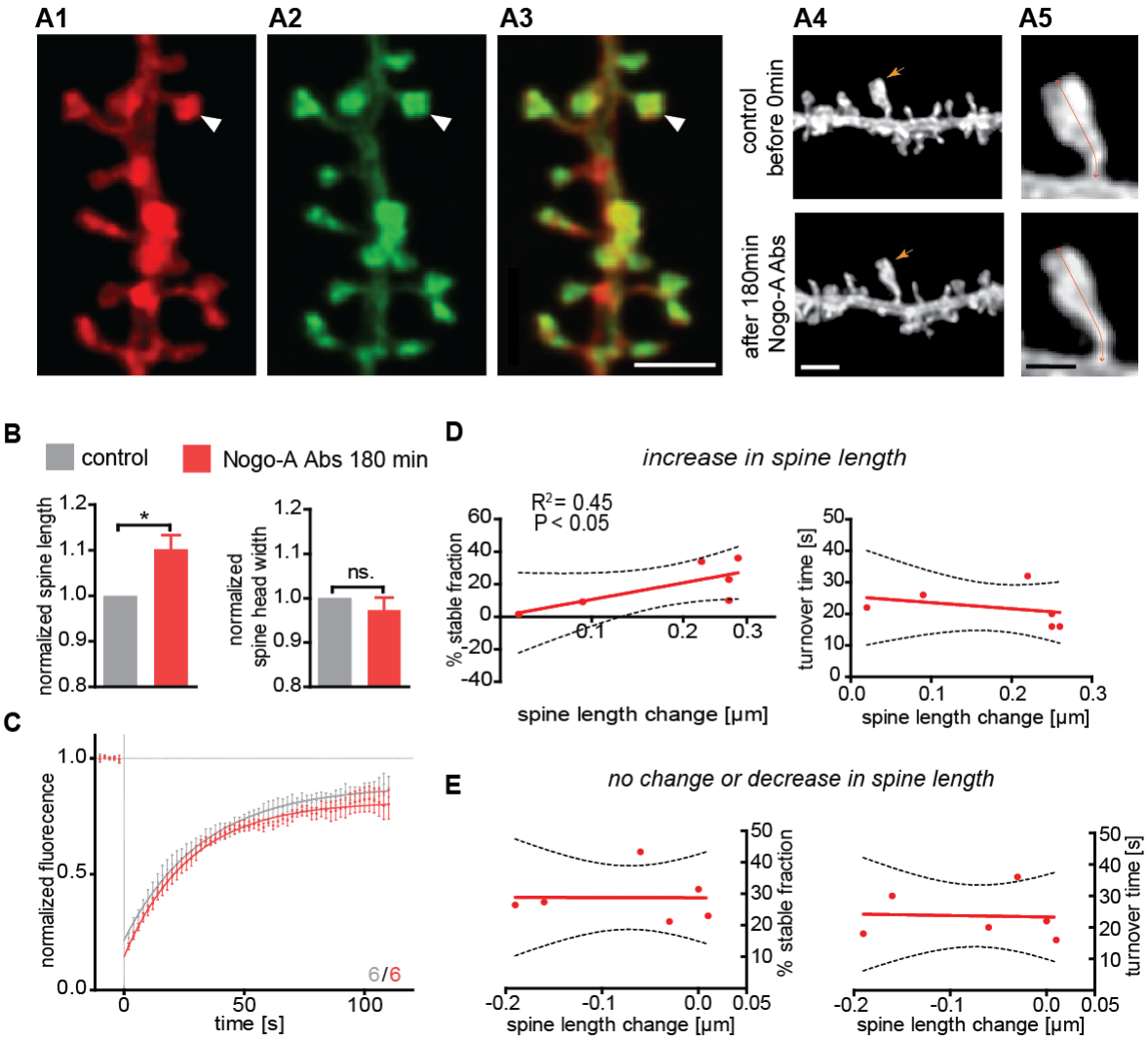

Figure 12: The stable actin fraction correlates with changes in spine length.
Confocal image consisting of stacks of multiple optical sections showing the morphology of a mid-apical dendritic stretch of a CA3 neuron, there spine shape **A1** (mCherry-F) and the actin content **A2** (eGFP-actin) colocalize (arrow head) within dendritic spines **A3** (merge). Scale bar 2 µm. Maximum projection of confocal images of spine morphology (mCherry-F) of two time points 0 min before and after 180 min Nogo-A neutralisation **A4**. Scale bar 2 µm. **A5** enlargement of one dendritic spines (highlighted with an arrow A4) with an increase in spine length (red line shows the measurement) after 180 min Nogo-A neutralisation. Scale bar 1 µm. **B** normalized spine length (left) and spine head width (right) before and after 180 min Nogo-A blocking. **C** only spine shown an elongation in length were included for further analysis. Fluorescence recovery curve after photobleaching for eGFP-actin at single spines before and after Nogo-A Abs treatment of 180 min. Numbers of dendritic spines are indicated for each condition. **D** spine with an increase in length displayed a correlation between spine length changes and the stable actin fraction (left, R^2=0.45, $p < 0.05$) but not with the turnover time (right). **E** the spine length changes of spine with no changes or decrease in spine length were not correlated to the stable actin faction (left) and the turnover time (right). Data are presented as mean ± SEM. *p < 0.05.

NgR1 had been shown to regulate the experience-dependent turnover of dendritic spines and axonal varicosities in the somatosensory cortex (Akbik et al., 2013). In addition, acute function blocking of Nogo-A plays a crucial role in the regulation of dendritic spine number and spine size in 3-weeks old hippocampal slice cultures (Kellner et al., under review). The transient stabilization of the actin cytoskeleton possibly supports the morphological changes occurring at the dendritic spine after acute Nogo-A neutralisation. To test this theory single cell electroporation was used to co-transfect CA3 pyramidal neurons with mCherry-F, to visualize the neuron's architecture and eGFP-actin (Figure 12A1 and A2) and simultaneously monitor changes in morphology and actin dynamics within the same dendritic spine. As expected eGFP-actin was specifically accumulated within the spine heads visualized with mCherry-F (Figure 12A3). The FRAP experiment as well as the imaging of the spine morphology was done before and after 180 min Nogo-A neutralisation (Figure 12A4). Spine morphology was analysed by measuring spine length and head width and displayed a significant increase of the spine length after 180 min Nogo-A neutralisation *versus* the normalized control (Figure 12A5, 2B left, Table S1, control *vs.* Nogo-A Abs 180 min $p < 0.05$). The head width wasn't influenced by the Nogo-A neutralisation (Figure 12B, right, Table S1). To assess the correlation between elongation and actin stabilization, only spines with a significant increase in length were further included in the analysis. The fluorescence recovery curve for eGFP-actin within selected spines showed lower intensity values after Nogo-A Abs treatment than the one recorded before (Figure 12C). Next, I examined whether the changes in the stable actin fraction were correlated to the spine elongation after Nogo-A neutralisation. Interestingly, the amount of stable actin within the selected spines was significantly correlated to the changes in spine length (Figure 12D left, Table S1, $R^2=0.45$, $p < 0.05$). The turnover time didn't show any correlation to the changes in spine length (Figure 12D right, Table S1). A correlation between the stable actin fraction and changes in spine length was only visible for spines that underwent elongation but not for spines that did not change or decreased in length (Figure 12E left Table S1). Also for spines without a change or decrease in length, the turnover time wasn't correlated to the changes in spine length (Figure 12E right, Table S1). These observations support the hypothesis that the morphological changes at spines observed up on Nogo-A loss-of-function are driven by an increase in the stable actin fraction within individual dendritic spines of CA3 hippocampal neurons.

4.1.2 Analysis of the signalling mediating activity of Nogo-A in regulating actin dynamics within spines

The actions of Nogo-A are mediated by two different inhibitory extracellular domains: Nogo-66 and Nogo-A-Δ20. First I'll focus on the Nogo-66 domain which signals via the Nogo-66 receptor 1 (NgR1; Fournier et al., 2001). An acute application of the Nogo-22 peptide in mature dissociated neurons was shown to reduce the gain and increase the loss of dendritic spines (Akbik et al., 2013). To further characterize this mechanism a specific function blocking antibody against the Nogo receptor (NgR Abs; Petrinovic et al., 2010) was tested for its ability to modulate actin cytoskeleton dynamics within dendritic spines. No significant difference could be observed between the recovery profiles of the control conditions anti-BrdU mouse IgG1 of the two time points (20 and 180 min; Figure 13A). Moreover, under control conditions the turnover time (about 20 seconds, Figure 13B) and the different actin fractions dynamic 70%, stable 16% and monomeric 14% (Figure 13C, D, E) were not significantly different between the two time points (Table S1).

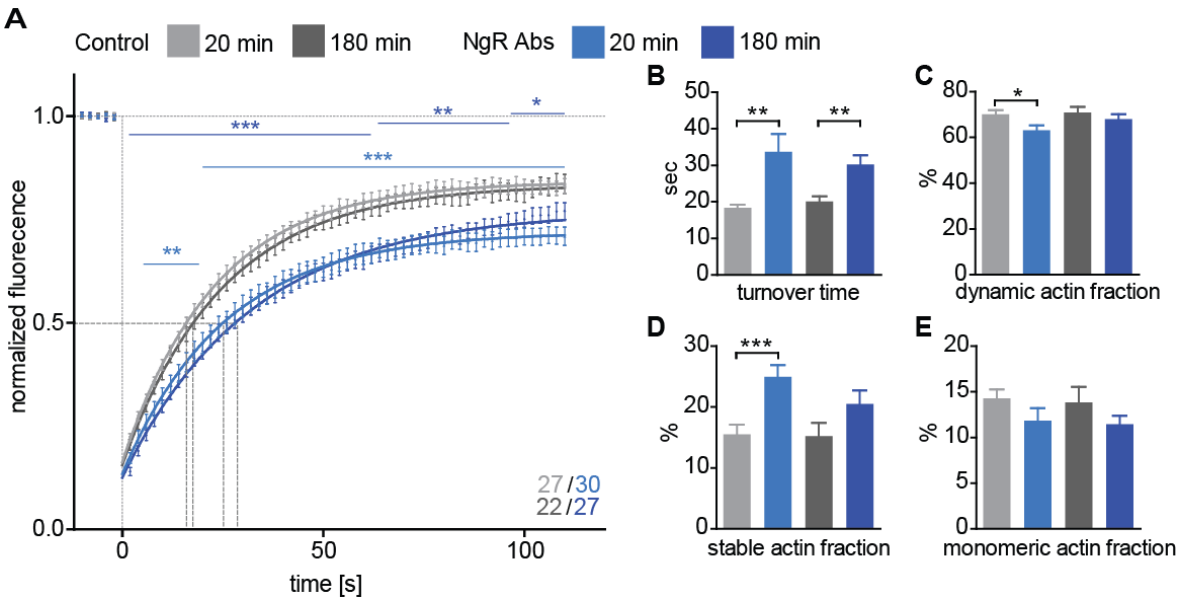

Figure 13: Nogo receptor blocking affects the actin cytoskeleton within dendritic spines of hippocampal pyramidal neurons.
A Fluorescence recovery curve after photobleaching for eGFP-actin at single spines under control conditions or NgR Abs treatment after 20 and 180 min. Numbers of dendritic spines are indicated for each treatment. Analysis of the **B** turnover time, **C** dynamic actin fraction, **D** stable actin fraction and **E** monomeric actin fraction for control conditions compared to NgR blocking after 20 and 180 min respectively. Data are presented as mean ± SEM. *p < 0.05, **p < 0.01; ***p < 0.001.

Similar to the Nogo-A loss-of-function experiments, blocking of NgR led to a significantly slower fluorescence recovery starting after 8 s and up to 110 s after photobleaching compared to the control conditions both after 20 and 180 min of treatment (Figure 13A, controls *vs.* NgR Abs 20 and 180 min $p < 0.01$). The turnover time was significantly

increased after 20 and 180 min blocking of the NgR in comparison to the control at the respective time points (Figure 13B. Table S1, controls *vs.* NgR Abs 20 and 180 min $p < 0.01$). The inhibition of the NgR after 20 min led to a significant decrease in the dynamic actin fraction *versus* the control conditions (Figure 13C, Table S1, control *vs.* NgR Abs 20 min, $p < 0.05$) no significant change could be observed after 180 min NgR Abs treatment. Similarly the stable actin fraction was transiently increased after 20 min NgR blocking *versus* control and slightly higher after 180 min (Figure 13D, Table S1, control *vs.* NgR Abs 20 min $p < 0.001$). The monomeric actin fraction was slightly reduced after NgR blocking at both time points (Figure 13E, Table S1). In summary, the acute inhibition of the NgR reproduced the stabilization of the actin cytoskeleton observed within dendritic spines upon a loss-of-function for Nogo-A (Figure 11B). To further characterize the mechanisms mediating the actions of Nogo-A, I next focused on the sphingosine 1-phosphate receptor 2 (S1PR2) which has been recently described to specifically bind the Nogo-A-Δ20 domain (Kempf et al., 2014). Interestingly, Nogo-A-Δ20 S1PR2 signals via the G protein G_{13}, leukemia-associated Rho guanine exchange factor (RhoGEF) LARG and activates RhoA to mediate inhibition of neurite outgrowth and cell spreading (Kempf et al., 2014). Thus, an acute inhibition of the S1PR2 may also influence actin dynamics within dendritic spines of CA3 hippocampal neurons. No significant difference could be observed between the kinetics of the recovery for eGFP-actin under control conditions (DMSO) at 20 and 180 min (Figure 14A). Moreover, the turnover time (Figure 14B) as well as the different actin fraction dynamic, stable and monomeric (Figure 14C, D, E) were not significantly different between the two time points (Table S1). A 20 min inhibition of the S1PR2 via the application of a specific antagonist (JTE-013) caused a significantly slower recovery after photobleaching of eGFP-actin starting 36 s after bleaching and up to 110 s when compared to the controls (Figure 14A control *vs.* JTE-013 20 min $p < 0.05$). Blocking the S1PR2 over 180 min led to a slightly slower increase of the fluorescent intensity values after photobleaching starting already after 10 s and up to 110 s in comparison to the control (Figure 14A, control *vs.* JTE-013 180 min $p < 0.05$). Moreover, 20 min S1PR2 inhibition had no significant effect on the turnover time in comparison to the control whereas after 180 min the turnover was significantly increased (Figure 14B, Table S1, control *vs.* JTE-013 180 min $p < 0.05$). The JTE-013 application resulted after 20 and 180 min in a significant reduction of the dynamic actin fraction in comparison to the controls (Figure 14C, Table S1, controls *vs.* JTE-013 20 and 180 min $p < 0.05$). The slower recovery observed upon S1PR2

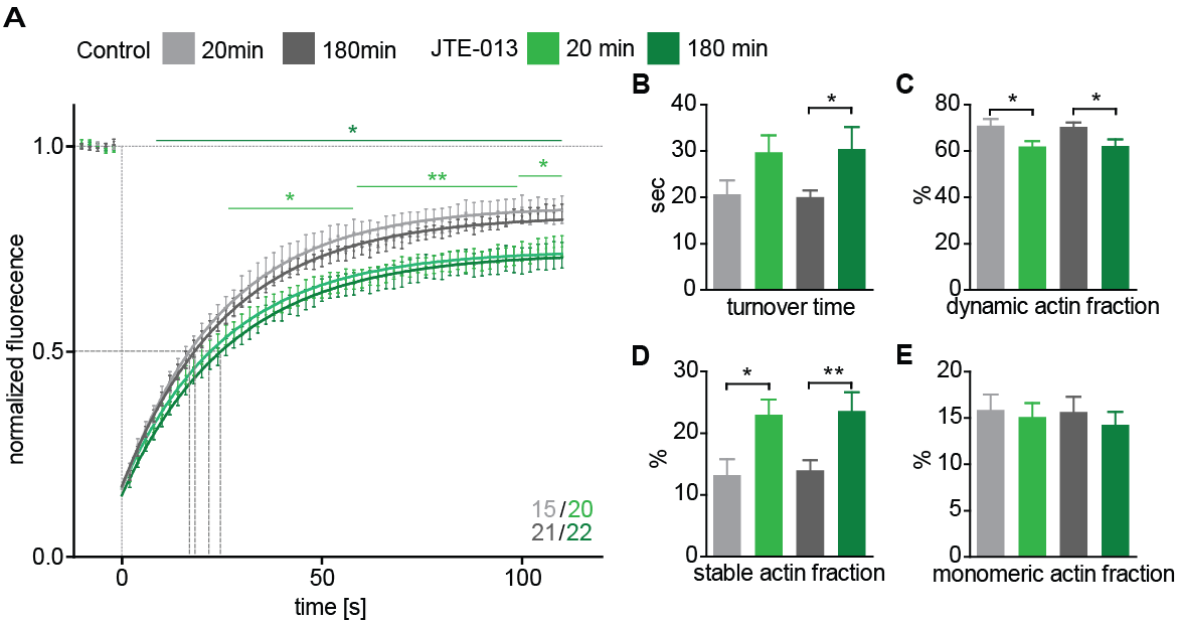

Figure 14: Blocking the sphingosine 1-phosphate receptor 2 affects the actin cytoskeleton within dendritic spines of hippocampal pyramidal neurons.
A Fluorescence recovery curve after photobleaching for eGFP-actin at single spines under control conditions or S1PR2 blocking after 20 and 180 min. Numbers of dendritic spines are indicated for each treatment. Analysis of the **B** turnover time, **C** dynamic actin fraction, **D** stable actin fraction and **E** monomeric actin fraction for control conditions compared to S1PR2 blocking after 20 and 180 min respectively. Data are presented as mean ± SEM. *p < 0.05, **p < 0.01.

inhibition could be accounted for a significant increase in the stable actin fraction for both time points in comparison to the relative control conditions (Figure 14D, Table S1, control *vs.* JTE-013 20 min $p < 0.05$, control *vs.* JTE-013 180 min $p < 0.01$). The monomeric actin fraction wasn't altered in comparison to the control for both time points (Figure 14E, Table S1). Taken together, also the acute blocking of the S1PR2 led to a significant alteration of the actin dynamics within dendritic spines of CA3 neurons and seemed to be stronger and longer lasting then blocking either Nogo-A or the Nogo receptor.

4.1.3 Application of the active Nogo-A-Δ20 peptide

To further investigated the role of Nogo-A in modulating actin cytoskeleton dynamics within dendritic spines I used a gain-of-function approach by applying the Nogo-A-Δ20 peptide (Delekate et al., 2011), the most active portion of the Nogo- specific inhibitory domain (Oertle et al., 2003). The soluble peptide Nogo-A-Δ20 was shown to be fast internalized into signalling endosomes upon binding (Joset et al., 2010). The continued peptide application is supposed to result in a clearance of the receptor complex from the surface resulting in a long-term dominant negative effect (Delekate et al., 2011; Kempf et al., 2014). In addition, the neurite outgrowth inhibitory and growth cone collapsing activity of Nogo-A-Δ20 depend on its ability to modulate actin dynamics via the small GTPase

RhoA and Rac1 (Joset et al., 2010; Kempf et al., 2014; Niederöst et al., 2002). Therefore, I addressed whether an acute application of Nogo-A-Δ20 peptide might influence actin cytoskeleton dynamics within dendritic spines in comparison to a 0.01% BSA containing ACSF solution (control) treatment. The control conditions exhibited a fast recovery of the fluorescent intensity after photobleaching with a turnover time of about 24 seconds (Figure 15A, B, Table S1) indicating equivalent actin dynamics as for previous control treatments (Table S1). The application of the Nogo-A-Δ20 peptide for 5 min (gain-of-function) resulted in a significantly faster recovery after photobleaching in comparison to the control, starting 14 seconds after the bleaching and up to 110 seconds the intensity values were significantly increased in comparison to the control (Figure 15A control *vs.* Nogo-A-Δ20 5 min $p < 0.05$). On the contrary, after 20 min incubation with Nogo-A-Δ20 peptide

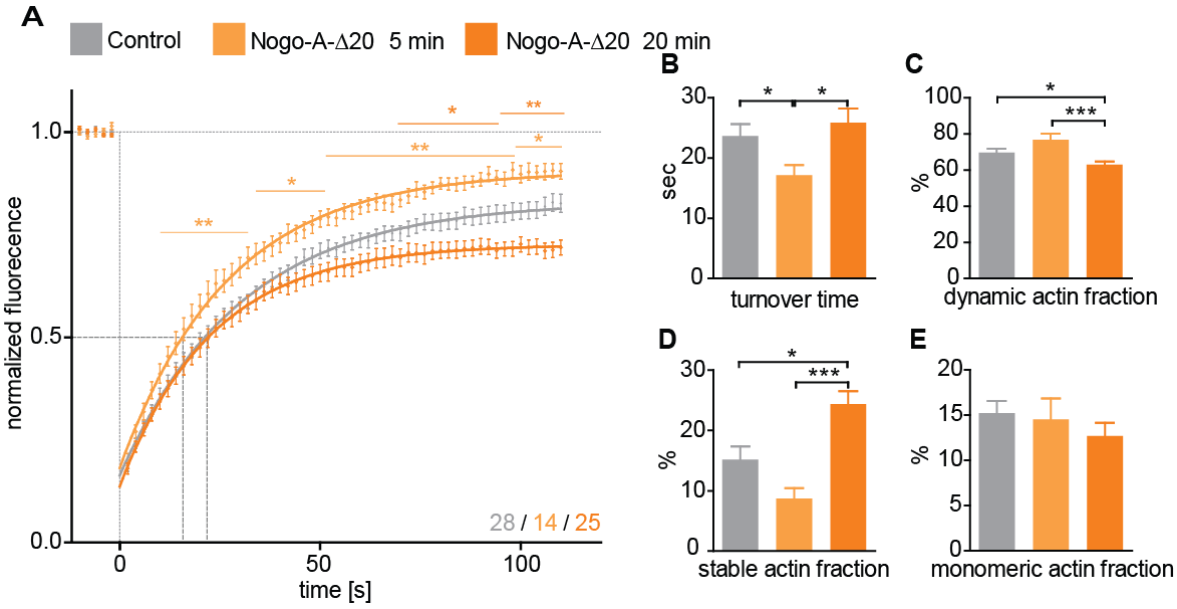

Figure 15: Application of the Nogo-A-Δ20 peptide affects the actin cytoskeleton within dendritic spines of hippocampal pyramidal neurons.

A Fluorescence recovery curve after photobleaching for eGFP-actin at single spines under control conditions or Nogo-A-Δ20 peptide application of 5 and 20 min. Numbers of dendritic spines are indicated for each treatment. Analysis of the **B** turnover time, **C** dynamic actin fraction, **D** stable actin fraction and **E** monomeric actin fraction for control conditions compared to Nogo-A-Δ20 peptide application of 5 and 20 min. Data are presented as mean ± SEM. *$p < 0.05$, **$p < 0.01$; ***$p < 0.001$.

(loss-of-function) the intensity values of the recovery curve were significantly decreased in comparison to the control starting 58 s after bleaching (Figure 15A, control *vs.* Nogo-A-Δ20 20 min $p < 0.05$). Accordingly, while the turnover time was significantly decreased after 5 min Nogo-A-Δ20 peptide incubation, a 20 min incubation resulted in its increase in comparison to the control (Figure 15B, Table S1, control *vs.* Nogo-A-Δ20 5 min $p < 0.05$).

For the dynamic actin fraction the 5 min application of Nogo-A-Δ20 caused an increase and after 20 min a significant decrease in comparison to control conditions (Figure 15C, Table S1, control *vs.* Nogo-A-Δ20 20 min $p < 0.05$). The incubation with the Nogo-A-Δ20 peptide affected the stable actin fraction by decreasing it after 5 min and significantly increasing it after 20 min relative to the control (Figure 15D, Table S1, control *vs.* Nogo-A-Δ20 20 min $p < 0.05$). The monomeric actin fraction was not significantly altered (Figure 15E, Table S1). In summary, after 5 min Nogo-A-Δ20 peptide application the actin cytoskeleton became more dynamic (gain-of-function), while after an incubation of 20 min the actin cytoskeleton was stabilized (loss-of-function). Overall, these observations indicate that Nogo-A acutely modulates the actin cytoskeleton within dendritic spines of CA3 hippocampal pyramidal neurons by destabilizing it in a rapid and transitory manner.

4.1.4 Blocking the Rho-kinase ROCK

The neurite outgrowth inhibitory and growth cone collapsing activity of Nogo-A depend on its ability to activate the small GTPase RhoA (Kempf et al., 2014; Niederöst et al., 2002). To further determine the Nogo-A actions on the actin cytoskeleton, the effector

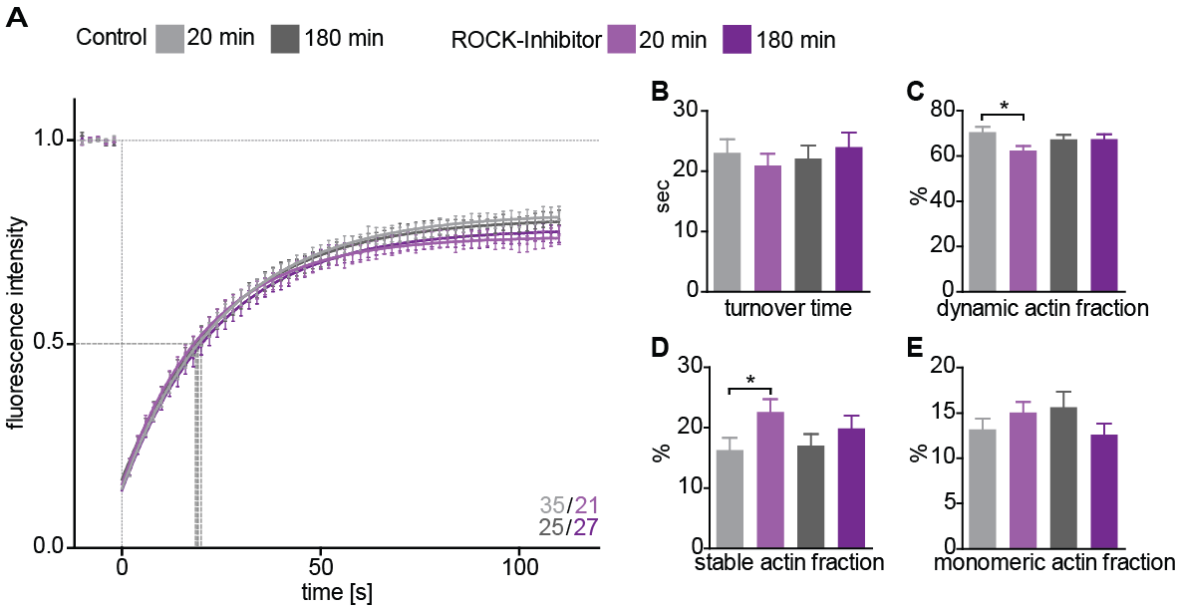

Figure 16: Blocking the Rho-kinase ROCK didn't affects the actin cytoskeleton within dendritic spines of hippocampal pyramidal neurons.

A Fluorescence recovery curve after photobleaching for eGFP-actin at single spines under control conditions or blocking of the Rho-kinase ROCK after 20 and 180 min. Numbers of dendritic spines are indicated for each treatment. Analysis of the **B** turnover time, **C** dynamic actin fraction, **D** stable actin fraction and **E** monomeric actin fraction for control conditions compared to the blocking of the Rho-kinase ROCK after 20 and 180 min respectively. Data are presented as mean ± SEM. *$p < 0.05$.

Rho- kinase ROCK was inactivated by the application of the specific blocker Y27632 (Kinases et al., 2000) and the actin dynamics of single dendritic spines were analysed. The FRAP experiment was performed 20 and 180 min after ROCK inhibition. No difference between control conditions (H_2O control) at 20 and 180 min could be found. The fluorescent intensity after photobleaching for the controls was progressively increasing with a turnover time of about 22-23 seconds and a dynamic actin fraction of 67-70% (Figure 16A, B, C; Table S1). Interestingly, the FRAP curve didn't display any significantly difference after 20 and 180 min of ROCK inactivation in comparison to the respective control conditions (Figure 16A). Also the turnover time and the monomeric actin fraction were unchanged after Y27632 treatment (Figure 16B and E; Table S1). Whereas 20 min after the beginning of the ROCK inhibition the dynamic actin fraction showed a significant reduction and the stable actin fraction a significant increase *versus* the control (Figure 16C, D, Table S1, control *vs.* Y27632 20 min $p < 0.05$). Both actin fractions were not significantly altered after 180 min of ROCK inhibition in comparison to the control conditions (Figure 16C, D, Table S1). Overall, the acute blocking of the Rho-kinase ROCK display a transient mild stabilization of the actin cytoskeleton as previously shown upon the neutralisation of the Nogo-A signalling.

4.1.5 Nogo-A enhances learning and memory acquisition *in vivo*

The activity- and experience-dependent changes in the number, size and shape of dendritic spines have been associated to learning processes in the mouse somatosensory and visual cortex (Holtmaat and Svoboda, 2009). Interestingly, the Nogo receptor signalling was shown to regulate experience dependent structural plasticity as well as learning in two paradigms linked to structural changes in the somatosensory cortex and hippocampus (Akbik et al., 2013; Karlén et al., 2009). Acutely interfering with Nogo-A signalling results in an increase in dendritic spine number and length in CA3 hippocampal neurons (Kellner et al., under review) correlated to a rapid regulation of the dynamics of the spine actin cytoskeleton. To investigate whether Nogo-A is involved in regulating learning and memory processes at the behavioural level, I tested spatial memory acquisition and reference memory formation analysing learning in the Morris water maze (MWM) paradigm (Vorhees and Williams, 2006) and testing male wild type (WT) and *nogo-a* knockout (KO) mice in two independent probe trails at day 3 and 9 (Figure 17). Indeed, spatial learning abilities as tested in the Morris water maze are thought to be dependent on the hippocampus (Morris et al., 1982). After a pretraining of two days the mice were trained for 8 consecutive days to locate a platform hidden in the middle of quadrant NW and the release position (SW, S, E, NE) was changed in a

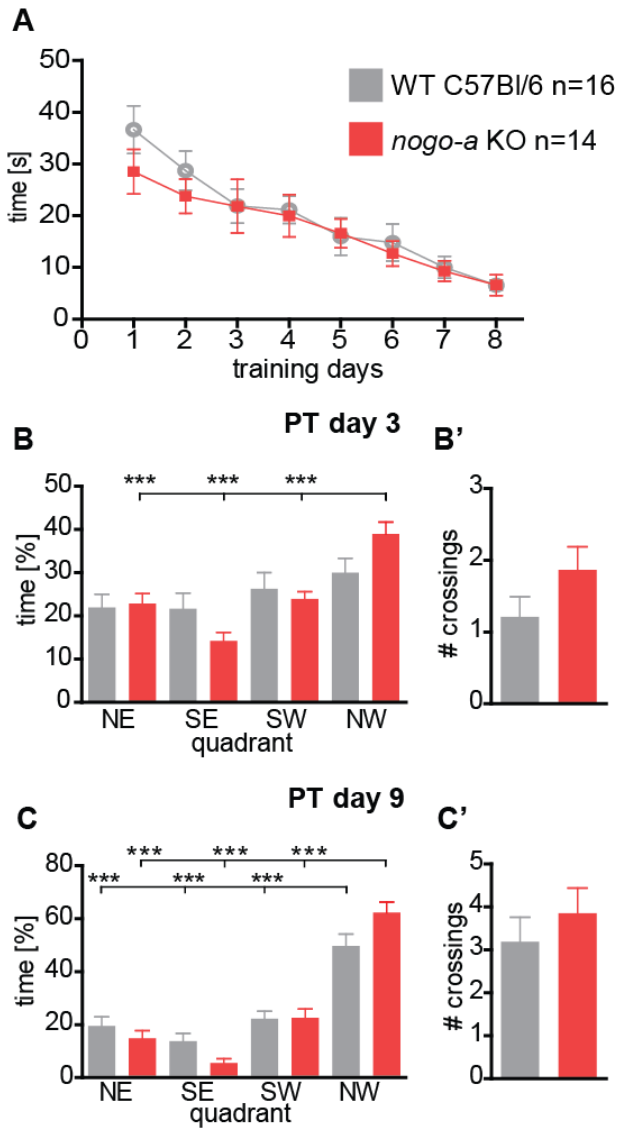

Figure 17: N*ogo-a* KO mice display a transitory effect in spatial learning in the Morris water maze.

A Escape latency to reach the hidden platform during acquisition of 8 days for WT and *nogo-a* KO mice. n= number of mice. Performance of search behaviour, shown as percent time spent in each quadrant and the number of annulus crossings, on probe trial at day 3 (**B** and **B'**) and the probe trial at day 9 (**C** and **C'**) of the Morris water maze task (target quadrant NW). Data are presented as mean ± SEM. ***p < 0.001

pseudorandom way. The escape latency improved equally in WT C57Bl/6 and *nogo-a* KO mice during the 8 days training period (Figure 17A, WT (day 1) 36.65 ± 4.61 s to (day 8) 6.58 ± 1.03 s, $F_{7,105}$=13,23; p < 0.001 and *nogo-a* KO (day 1) 28.53 ± 4.30 s to (day 8) 6.59 ± 2.02 s, $F_{7,91}$=5.91; p < 0.001). Reference memory formation was determined by analysing the preference for the target quadrant north-west (NW) when the platform was removed (probe trials).To assess whether the lack of Nogo-A might have already an effect on the early phase of spatial memory acquisition, the first probe trial was performed after 2 days of training (day 3). While WT mice didn't show any quadrant preference at this time point *nogo-a* KO mice showed a highly significant preference for the NW quadrant in comparison to the other quadrants (Figure 17B, Table S2, quadrant preference NW: WT 30.04 ± 3.31% and *nogo-a* KO 38.95 ± 2.75%, p < 0.001). Analysis of the number of platform crossings showed a slight increase at this time point for the mice lacking *nogo-a* in comparison to WT mice (Figure 17B', Table S2). A second probe trial was performed after 8 days of training (day 9). At this time point, the search behaviour across the four quadrants was comparable between the two genotypes, both showing a significant

preference for the NW quadrant (Figure 17C, Table S2, quadrant preference NW: WT 47.79 ± 4.39%, $p < 0.001$ and *nogo-a* KO 60.12 ± 3.93, $p < 0.001$). The analysis of the number of platform crossings at day 9 exhibited for both genotypes an equal increase in comparison to day 3, without a difference between the two groups (Figure 17C', Table S2). Taken together, these data demonstrate that formation of a reference memory during spatial learning is accelerated in mice lacking *nogo-a* in comparison to WT as it is already present after 3 days of training. However, at later time points (day 9) during training in the water maze no difference in spatial learning could be observed between the two genotypes. To evaluate the qualitative aspects of spatial learning the searching strategies applied to find the platform were analysed. This approach allows differentiating between hippocampus-dependent, allocentric *versus* hippocampus-independent, egocentric search strategies (Garthe and Kempermann, 2013). Over the acquisition period both WT and nogo-a KO mice used progressively less hippocampus-independent and more hippocampus-dependent strategies (Figure 18A', Table S3, WT: $F_{7,105}= 7.58$ $p < 0.001$; *nogo-a* KO: $F_{7,91}= 10.34$ $p < 0.001$). Interestingly, at days 3 of the training period *nogo-a* KO mice used less hippocampus-independent (Figure 18A, arrow, Table S3, WT 71.88 ± 7.17% *vs. nogo-a* KO 57.14 ± 5.52%; p=0.122 ns) and more hippocampus-dependent strategies than WT mice (Figure 18A', arrow, Table S3, WT 28.13 ± 7.17% *vs. nogo-a* KO 42.86 ± 5.52%; p=0.122 ns).To perform a more detailed analysis the searching strategies were classified in four categories: direct search, chaining, scanning and random search (Figure 18B; Garthe et al., 2009). The contribution of the direct search increased equally in both groups of mice during the acquisition period of 8 days (Figure 18B and B'), whereas the contribution of random search decreased (Figure 18B and B'). The percentage of chaining used during the 8 days training in the MWM for both was constant for both genotypes without any significant difference between WT and *nogo-a* KO mice (Figure 18B and B'). The contribution of the scanning strategy increased progressively to day 3 and was than stable up to day 8 without showing any significant difference between the two genotypes. To summarise the results: no significant differences could be observed between WT and *nogo-a* KO for the escape latency during the acquisition period of 8 days in the MWM. Interestingly, however, *nogo-a* KO mice formed a reference memory considerably earlier than WT mice as revealed by the probe trail performed at day 3. On the contrary, there wasn't any significant difference in reference memory between the two genotypes when the probe trial was performed at day 9. Moreover, the contribution of hippocampus-dependent searching strategy was higher in *nogo-a* KO mice than in WT specifically at day 3 bot not at day 8 of the training. The detailed analysis of the four searching strategies during the 8 days of MWM didn't show any significant differences between WT and *nogo-a* KO mice.

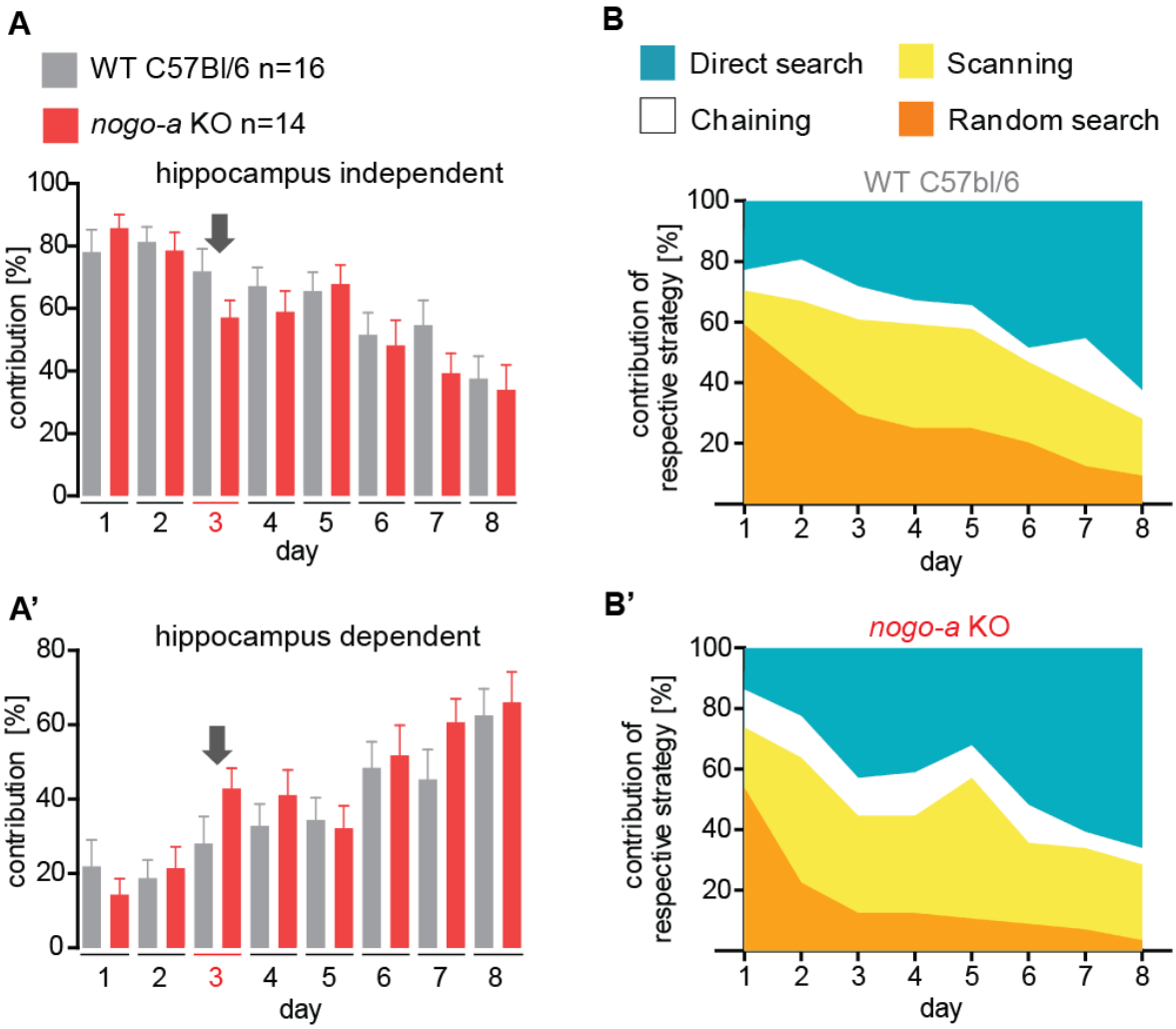

Figure 18: Qualitative analysis of spatial learning in *nogo-A* knockout mice.

Classification of **A** hippocampus independent and **A'** hippocampus-dependent searching strategies (contribution in percent) over 8 days of the Morris water maze task are displayed (arrows highlight day 3) for WT and *nogo-a* KO mice. n= number of mice. The searching strategies (direct search, chaining, scanning, random search) are colour coded and the contribution of the respective strategy in percent are presented for each day of the MWM task for **B** WT and **B'** *nogo-a* KO mice. Data are presented as mean ± SEM.

4.1.6 Nogo-A modulates structural plasticity at spines during leaning *in vivo*

Recent studies have provided evidence that learning is correlated to specific changes at dendritic spines which are suggested to provide a structural substrate for memory storage and learning processes (Caroni et al., 2012). Indeed, long-term *in vivo* imaging in the mouse somatosensory and visual cortex studies reveal that activity and experience-dependent alteration in the number and structure of dendritic spines are associated to learning processes and long-lasting memories (Holtmaat and Svoboda, 2009). To assess whether the effect of deleting *nogo-a* on reference memory formation in the MWM is correlated to structural changes at spines, dendritic spine density for the apical dendrite of hippocampal CA3 neurons was analysed during and after training in the MWM and compared to the one of not trained mice. A diolistic approach was used to label the neurons (Figure 19A) including their dendritic spines with DiI (Figure 19A'; Rauskolb et al., 2010). The spine number was compared between WT and *nogo-a* KO mice under

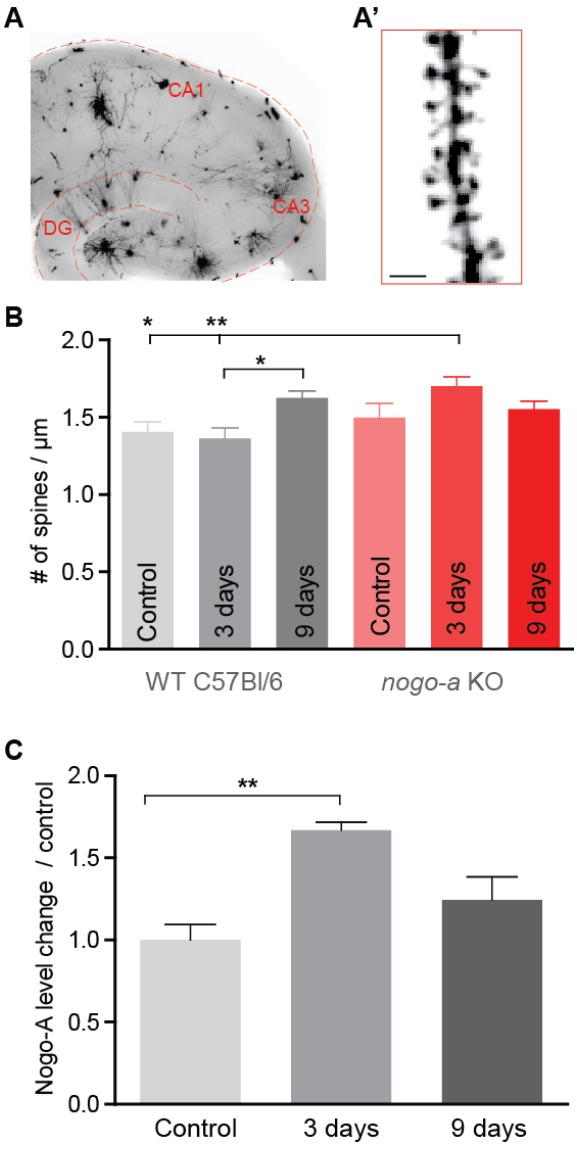

Figure 19: Nogo-A regulates structural plasticity upon learning.

A acute hippocampus slice stained with DiI, highlighted a mid-apical dendritic stretch covered with spines **A'**. Scale bar 2 µm. **B** Spine density of mid-apical CA3 neurons for WT and *nogo-a* KO mice, control (without MWM training) and after 3 or 9 days of the Morris water maze task. **C** Normalized Nogo-A proteins levels of WT mice control (without MWM training) and after 3 or 9 days of the Morris water maze task. Data are presented as mean ± SEM. *p < 0.05, **p < 0.01.

three different conditions: (1) control untrained, (2) after 3 day MWM and (3) after 9 days of MWM training (Figure 19B). While the spine number for WT neurons did not show any difference between not-trained and 3 days training, it was significantly higher at 9 days in comparison to 3 days training (Figure 19B, WT (day 3) 1.36 ± 0.07 *vs.* WT (day 9) 1.63 ± 0.05 spines / µm $p < 0.05$). Interestingly, in the *nogo-a* KO mice the number of dendritic spines transiently increased already after 3 days MWM training. The spine density increase in the *nogo-a* KO mice (day 3) is significant in comparison to WT control and WT 3 days training (Figure 19B, Table S3, WT (Control) 1.41 ± 0.06 and WT (day 3) 1.36 ± 0.07 spines / µm *vs*. *nogo-a* KO (day 3) 1.70 ± 0.06, $p < 0.05$). The increase in spine number wasn't maintained in *nogo-a* KO mice at day 9 of the MWM training (Figure 19B, Table S3). An increase of the number of dendritic spine has been correlated to learning and memory processes (Xu et al., 2009; Yang et al., 2009a). While here spine density in CA3 hippocampal neurons was significantly increased in *nogo-a* KO after 3 days of MWM training, in WT mice it was significantly increased only at day 9 of the MWM training. Indeed, this is correlated with the performance in the probe trial early at day 3 which revealed that the *nogo-a* KO mice form a reference memory significantly faster than WT mice, and the initial and transient advantage of *nogo-a* KO mice in forming a reference memory is disappeared after 9 days of training.

Previous studies in aged rats reported an increase in Nogo-A expression in the hippocampus is correlated to cognitive decline and deficits of spatial learning and memory (Vanguilder et al., 2012). However, Nogo-A levels were reported to be activity-dependent down-regulated in the dentate gyrus (Mingorance et al., 2004) but not in the CA1 or CA3 region of the hippocampus (Karlsson et al., 2013). In this context also Nogo-A protein levels in WT mice hippocampi after MWM training were quantified. A significant increase in Nogo-A levels was detected at day 3 of the MWM training but not at day 9 in comparison to control untrained mice (Figure 19C, Table S3, control 1 ± 0.08 *vs.* 3 days training 1.57 ± 0.08, $p < 0.01$). In summary, *nogo-a* KO mice showed a transitory improved learning which was correlated with a significant increase in the spine density at day 3. However, in WT mice Nogo-A levels were transitory increased after 3 days of training correlated to delayed increase in spine density at day 9. Therefore it is suggestive to conclude that endogenous Nogo-A restricts structural plasticity in the hippocampus upon learning.

4.2 The BDNF effects on dendritic spines of mature hippocampal neurons depend on neuronal activity

4.2.1 Endogenous BDNF regulates dendritic spine density and morphology in mature primary hippocampal neurons

After studying a molecule, limiting synaptic plasticity, I also studied BDNF as a paradigmatic molecule which might meditate and promote functional and structural changes. A clear inconsistency exists between previous work showing a significant effect of the application of exogenous BDNF in modulating the dendritic architecture of hippocampal neurons *in vitro* (Ji et al., 2005, 2010; Tyler and Pozzo-miller, 2001) and data from our group and others showing that a global deprivation of BDNF throughout the CNS *in vivo* results in only minimal morphological alterations of mature hippocampal neurons (Minichiello et al., 1999; Zakharenko et al., 2003; Rauskolb et al., 2010, for a review see Zagrebelsky and Korte, 2013). In this context, I analysed under standardised and controlled culture conditions the role of BDNF in modulating dendritic spine number and morphology as well as dendritic architecture of primary hippocampal neurons. To map the action of BDNF I used different gain- and loss-of-function experiments in developing, young and mature primary neurons and examined the role of BDNF in an activity-dependent manner. The dendrite and dendritic spine architecture of mature 3-week-old (22 DIV) primary hippocampal neurons (Papa et al., 1995), expressing a membrane targeted farnesylated EGFP (fEGFP; Figure 20B) were analysed upon the application of either a gain- or loss-of-function approach for BDNF (Figure 20A,B). The neurons included in the analysis were identified as excitatory by their pyramidal like morphology (Figure 21A) and by the expression of the Ca^{2+}/calmodulin-dependent protein kinase (CaMKII; Figure 20B'). While 22 DIV fEGFP-expressing neurons treated for 24 hours with exogenous BDNF showed no obvious alterations in dendritic spine density when compared to controls (Figure 20B), treating the neurons with BDNF function blocking antibodies (BDNF-Abs) led to a strong reduction in dendritic spine density (Figure 20B). This observation was confirmed by the quantification of dendritic spine density showing no significant difference between BDNF and control treated cells (Figure 20C Table S4). On the other hand, a significant reduction in dendritic spine density was observed for neurons treated with BDNF blocking antibodies (Figure 20C, Table S4; control *vs.* BDNF-Abs, $p < 0.001$; BDNF *vs.* BDNF-Abs $p < 0.001$). These observations suggest that while the endogenous BDNF may be crucial for the maintenance of dendritic spines in mature primary hippocampal neurons, exogenous BDNF does not play a role in this context. Next, I assessed whether BDNF regulates spine morphology in mature hippocampal neurons by analysing the effects of adding or blocking BDNF on dendritic spine length and head

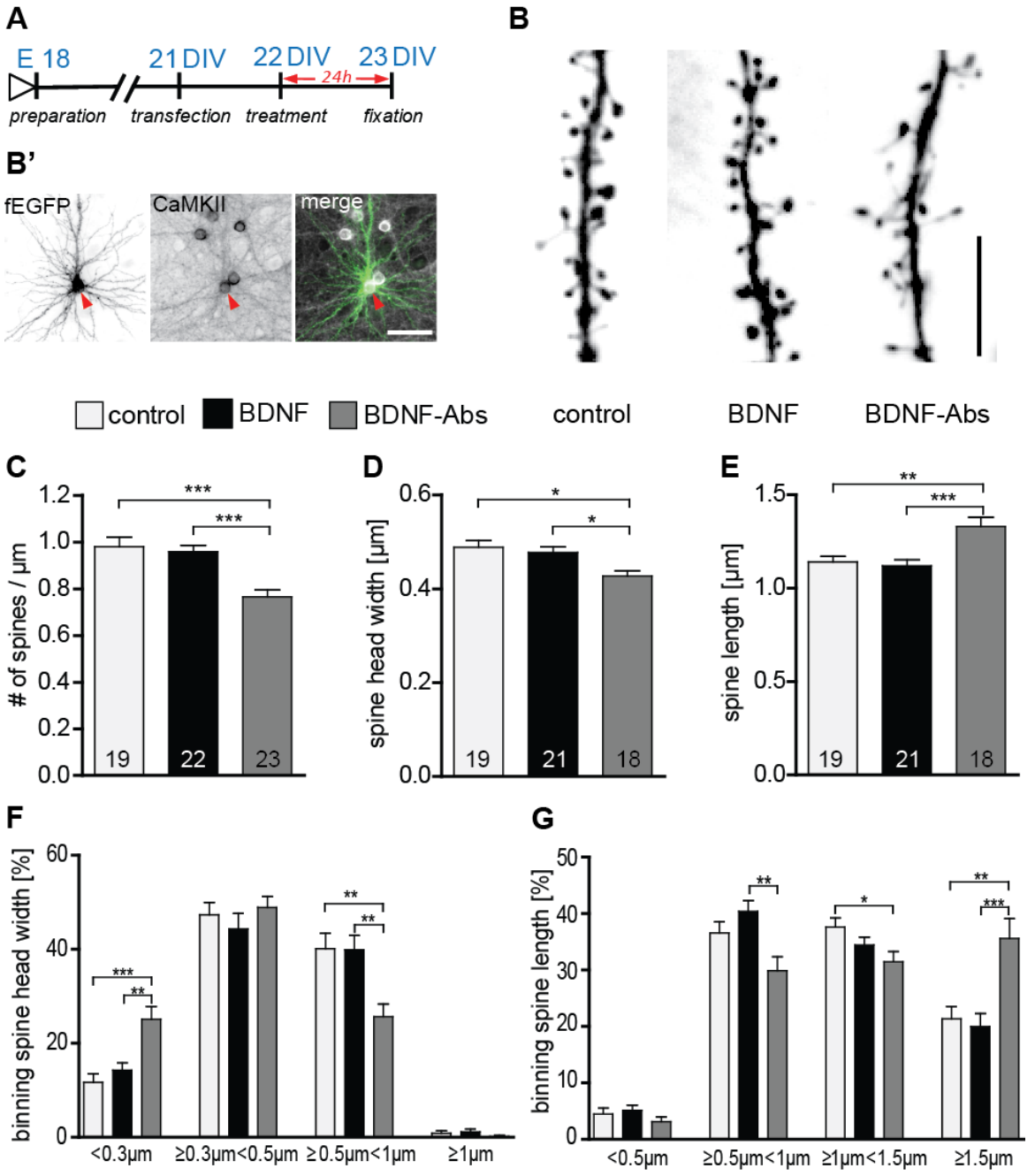

Figure 20: BDNF signalling regulates dendritic spine density and morphology in mature primary hippocampal neurons. A Experimental timeline. DIV23 hippocampal neurons were treated for 24 h before fixation. **B** High-magnification image of typical dendritic stretches from control (left), BDNF (middle) and BDNF antibodies (right) treated neurons. Scale bar, 5 µm. **B'** Representative image of a typical DIV23 fEGFP expressing hippocampal neuron show a close up of the cell body labelled with fEGFP (left) or with an immunohistochemistry against CaMKII (middle) merged to show colocalization (right): scale bars are 50 µm. **C** Graphs comparing dendritic spine density between BSA (control), BDNF and BDNF antibodies (BDNF-Abs) treated DIV22 hippocampal neurons. **D** Histogram comparing the spine head width between hippocampal neurons upon BSA (control), BDNF or BDNF antibodies (BDNF-Abs) treatment. **E** Histogram of the dendritic spine length in control, BDNF or BDNF antibodies (BDNF-Abs) treated neurons. **F** Graph showing the binning of spines according to their spine head width and comparing the proportion of spines within each category in response to a BSA (control), BDNF or BDNF antibodies (BDNF-Abs) treatment. **G** Graph showing the binning of spines according to their spine length and comparing

the proportion of spines within each category in response to a BSA (control), BDNF or BDNF antibodies (BDNF-Abs) treatment. The number in the columns represents the number of cells analysed. Data are presented as mean ± SEM. *p < 0.05, **p < 0.01; ***p < 0.001.

width. When compared to the controls spine head width as well as spine length (Figure 20B) did not show any major difference after a 24 hour treatment with BDNF. On the other hand, neurons treated with BDNF blocking antibodies showed clearly longer and thinner spines than control neurons (Figure 20B). Indeed, quantification of spine morphology upon BDNF antibody treatment showed a significant decrease in spine head width (Figure 20D, Table S4; control *vs*. BDNF-Abs and BDNF *vs.* BDNF-Abs, $p < 0.05$) associated to a significant increase in dendritic spine length (Figure 20E, Table S4; control *vs*. BDNF-Abs $p < 0.01$, BDNF *vs.* BDNF-Abs $p < 0.001$). Treatment with exogenous BDNF did not result in any significant change in dendritic spine head width (Figure 20D, Table S4). Under these conditions dendritic spine length was only slightly reduced when compared to controls but significantly lower than in neurons treated with BDNF blocking antibodies (Figure 20E, Table S4; BDNF *vs.* BDNF-Abs, $p < 0.001$). Next, dendritic spines were separated according to their spine shape into four categories based on their head width. A significant increase in spines with a small head (Figure 20F; <0.3 µm; control *vs.* BDNF-Abs $p < 0.001$, BDNF *vs.* BDNF-Abs $p < 0.01$) accompanied by a significant decrease in larger spine heads (Figure 20F; ≥0.5 µm <1 µm; control *vs.* BDNF-Abs $p < 0.01$, BDNF *vs.* BDNF-Abs $p < 0.001$) was observed when a treatment with BDNF blocking antibodies was compared to a control treatment or to a treatment with exogenous BDNF (Figure 20F). Application of BDNF (gain-of-function experiment) did not result in any significant alteration in spine head size when compared to the control conditions (Figure 20F). Binning the spines according to their length did not show any difference for BDNF treated neurons but resulted in a significant alteration in spine length distribution upon BDNF antibody treatment (loss-of-function; Figure 20G). While under these conditions spines shorter than 1.5 µm were significantly decreased (Figure 20G; ≥0.5 µm <1 µm $p < 0.01$ to the BDNF treatment; ≥1 µm <1.5 µm $p < 0.05$ to the control), those longer than 1.5 µm were significantly increased in comparison to the control conditions or the BDNF treatment (Figure 20G; $p < 0.01$ to the control, $p < 0.001$ to BDNF treatment). Finally, the effects of either a gain- or a loss-of-function for BDNF on dendritic architecture were analysed using a Sholl analysis to compare dendritic complexity (Sholl, 1953; Figure 21A). No significant differences in the detailed analysis of dendritic complexity and length using the Sholl analysis could be observed between the three different treatments (Figure 21B; control, BDNF, BDNF-Abs). Accordingly, also total dendritic complexity was not significantly different in BDNF or BDNF- antibody-treated cells *versus* control cells (Figure 21C, Table S4).

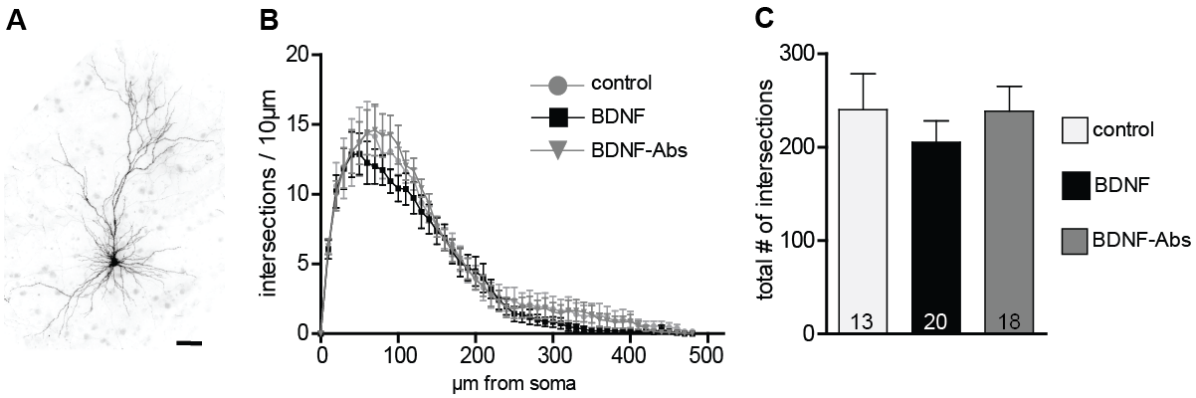

Figure 21: Dendritic complexity of mature primary hippocampal neurons in not regulated by BDNF signalling. A Representative image of a typical DIV23 fEGFP expressing hippocampal neuron used in the experiments. **B** Graph plotting dendritic complexity in relation to the distance to the cell body of hippocampal neurons under control conditions or treated with BDNF or BDNF antibodies (BDNF-Abs). **C** Histogram of the total number of intersections for BSA (control), BDNF and BDNF antibodies (BDNF-Abs) treated neurons. The number in the columns represents the number of cells analysed. Data are presented as mean ± SEM.

Taken together, these results demonstrate that the exogenous application of BDNF, in mature primary hippocampal neurons, does not influence dendritic spine density, morphology and dendrite complexity. On the other hand, the loss-of-function experiments show that the endogenous BDNF is essential for maintaining spine density and the mature morphology of dendritic spines in primary hippocampal neurons.

4.2.2 Endogenous BDNF regulates dendritic spine density and morphology in young primary hippocampal neurons

In the next series of experiments I tested whether the different effects of exogenous *versus* endogenous BDNF on neuronal structure might depend on the age of the treated primary hippocampal neurons. To this aim, I analysed whether a gain- or a loss-of-function approach for BDNF regulates the dendritic architecture or spine number and morphology in 2 weeks-old primary hippocampal neurons (15 DIV; Figure 22A). When 15 DIV fEGFP-expressing neurons treated for 24 hours with BDNF were compared to control neurons, no obvious difference in dendritic spine density or morphology could be observed. Accordingly, the quantification of spine density did not result in any significant difference between BDNF treated and control neurons (Figure 22B, Table S4). However, as for mature hippocampal neurons, also here the application of BDNF blocking antibodies led to a highly significant reduction in dendritic spine density (Figure 22B, Table S4; control *vs.* BDNF-Abs and BDNF *vs*. BDNF-Abs $p < 0.001$). Next, I assessed whether BDNF regulates spine morphology

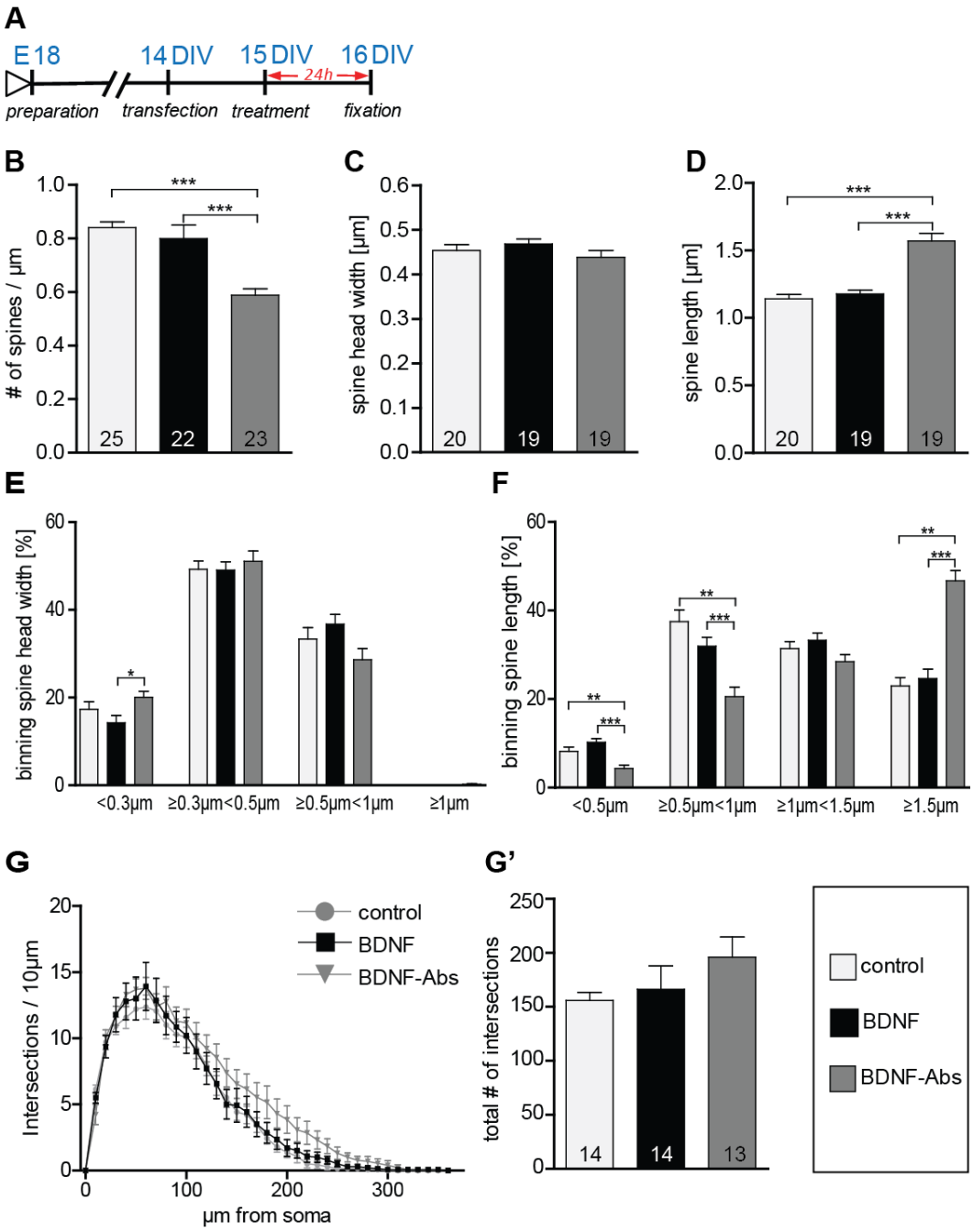

Figure 22: BDNF signalling regulates dendritic spine density and morphology in young primary hippocampal neurons. A Experimental timeline. DIV16 hippocampal neurons were treated for 24 h before fixation. **B** Graphs comparing dendritic spine density between control, BDNF and BDNF-antibodies (BDNF-Abs) treated DIV16 hippocampal neurons. **C** Histogram comparing the spine head width between hippocampal neurons upon BSA (control), BDNF or BDNF antibodies treatment. **D** Histogram of the dendritic spine length in BSA (control), BDNF or BDNF antibodies (BDNF-Abs) treated neurons. **E** Graph showing the binning of spines according to their spine head width and comparing the proportion of spines within each category in response to a BSA (control), BDNF or BDNF antibodies (BDNF-Abs) treatment. **F** Graph showing the binning of spines according to their spine length and comparing the proportion of spines within each category in response to a BSA (control), BDNF or BDNF antibodies (BDNF-Abs) treatment. **G** Graph plotting dendritic complexity in relation to the distance to the cell body of hippocampal neurons under control conditions or treated with BDNF or BDNF antibodies (BDNF-Abs). **G'** Histogram of the total number of intersections for BSA (control), BDNF and BDNF antibodies (BDNF-Abs) treated neurons. The number in the columns represents the number of cells analysed. Data are presented as mean ± SEM. *p < 0.05, **p < 0.01; ***p < 0.001.

comparing the maximal spine head width and spine length between different treatments. Application of exogenous BDNF for 24 hours did not result in any significant alteration of the spine head width (Figure 22C, Table S4) and length (Figure 22D, Table S4) in comparison to the control condition. Interestingly, while the loss-of-function experiments did not result in any significant change in spine head width (Figure 22C, Table S4) a significant increase in dendritic spine length could be observed after application of BDNF blocking antibodies in comparison to both, the control and the BDNF treatment (Figure 22D, Table S4; control *vs.* BDNF-Abs and BDNF *vs*. BDNF-Abs $p < 0.001$). Binning the spines according to their head width and comparing the different treatments within each spine head category resulted in a significant increase in the proportion of spines with a small head for the BDNF blocking antibody treatment only when compared to the BDNF treatment (Figure 22E; BDNF *vs.* BDNF-Abs $p < 0.05$). No significant changes could be observed for the spine head width distribution upon BDNF application (Figure 22E) when compared to the control condition. Binning the spines according to their length showed for neurons treated with BDNF blocking antibodies a significant decrease in the shorter spine category (Figure 22F; <0.5 µm, control *vs.* BDNF-Abs $p < 0.01$, BDNF *vs.* BDNF-Abs $p < 0.001$; and ≥0.5 µm <1 µm, control *vs.* BDNF-Abs $p < 0.01$, BDNF *vs.* BNF-Abs $p < 0.001$) accompanied by a significant increase in longer spines (Figure 22F; >1.5 µm, control *vs.* BDNF-Abs $p < 0.01$, BDNF *vs.* BDNF-Abs $p < 0.001$). Finally, I also analysed whether the effect of BDNF on dendrite architecture might be age dependent. However, also for 15 DIV hippocampal neurons when either a BDNF or a BDNF antibody treatment was compared to the controls, no significant alteration in dendritic complexity could be observed for the Sholl analysis (Figure 22G). Accordingly, I did not observe any significant differences in total complexity between the different treatments (Figure 22G′, Table S4).

All in all the results described above indicate that endogenous BDNF is necessary for dendritic spine growth and the regulation of spine length in developing primary hippocampal neurons. Interestingly, maintaining the spine head width in younger hippocampal neurons does not dependent on endogenous BDNF signalling.

4.2.3 Endogenous BDNF regulates actin concentration within dendritic spine

The actin cytoskeleton is involved in regulating cell mobility and morphology. Actin is highly enriched within the dendritic spine head, (for a review see: Cingolani and Goda, 2008), for that reason I tested whether BDNF may regulate actin in dendritic spines in order to shape and change spine morphology. To test this hypothesis RFP-Lifeact (Riedl et al., 2008, 2010) was used to detect possible changes in the F-actin content in dendritic spines upon changes in BDNF signalling. The RFP-Lifeact expression plasmid was co-transfected with fEGFP and resulted in 99.7% colocalization of RFP-Lifeact within spines (Figure 23A,B) as well as with F-actin labelled using Alexa Fluor 350 Phalloidin (Figure 23B). In line with our observations above the exogenous application of BDNF for 24 hours to 22 or 15 DIV primary hippocampal neurons did not result in any change in the normalized mean fluorescent intensity for RFP-Lifeact in comparison to the control group (Figure 23C,D, Table S4). However, in the loss-of-function experiments the treatment with BDNF blocking antibodies resulted in a highly significant decrease in the F-actin content within the head of dendritic spines both in 16 DIV (Figure 23D, Table S4; control *vs.* BDNF-Abs $p < 0.001$, BDNF *vs.* BDNF-Abs $p < 0.001$) and 23 DIV primary hippocampal neurons (Figure 23D, Table S4; control *vs.* BDNF-Abs $p < 0.01$, BDNF *vs.* BDNF-Abs $p < 0.001$). Taken together, these results show that endogenous BDNF modulates the actin cytoskeleton within dendritic spines as well as their morphology.

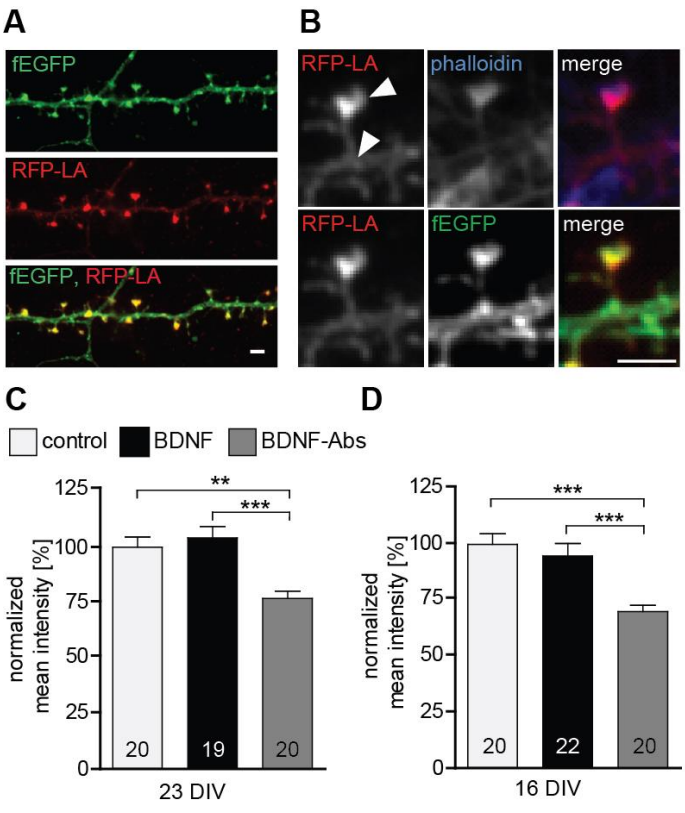

Figure 23: Actin content within dendritic spines. A Maximal intensity projection of a representative dendrite of hippocampal neurons expressing fEGFP (above) and RFP-Lifeact (middle) merged to show colocalization (below). Scale bar, 2 µm. **B** High magnification images showing a single dendritic spine expressing fEGFP (above) and RFP-Lifeact (middle) and merged to show their colocalization in the spine head (below) Scale bar, 2 µm. **C** Histogram plotting the normalized mean fluorescent intensity for RFP-Lifeact within the spine head of DIV23 BSA (control), BDNF and BDNF antibodies (BDNF-Abs) treated neurons. **D** Histogram showing the normalized mean intensity for RFP-Lifeact within the spine head of DIV16 hippocampal neurons. The number in the columns represents the number of cells analysed. Data are presented as mean ± SEM. **p < 0.01; ***p < 0.001.

4.2.4 Mature primary hippocampal neurons are responsive to an acute treatment with exogenous BDNF

The results, so far, clearly support a role for endogenous BDNF in the hippocampus by completely reproducing *in vitro* the mild alterations observed in the morphology of hippocampal neurons upon a global BDNF deprivation *in vivo* (Rauskolb et al., 2010). On the other hand, the data fail to replicate previous work showing an effect of BDNF application in regulating dendrite and spine architecture (Ji et al., 2005; Tyler and Pozzo-miller, 2001). To address this discrepancy I first confirmed that the BDNF used in this study is indeed active and that it is able to elicit clear neuronal responses in primary hippocampal neuronal cultures. To this aim I tested three critical events known to occur upon a BDNF application: (1) activation of the TrkB receptor was tested by analysing its phosphorylation levels (Ji et al., 2010); (2) calcium imaging was used to test the ability of BDNF to induce local calcium transients in hippocampal neurons (Berninger et al., 1993) and (3) immunohistochemistry was used to visualize the activation of the immediate early gene (IEG) c-fos (Marty et al., 1996). An immunohistochemistry against phosphorylated TrkB receptor performed 15 min after BDNF application (Figure 24A) showed an obvious increase in the levels of TrkB receptor phosphorylation when compared to control treated neurons (Figure 24B). This observation was confirmed by a significant increase in the normalized intensity for the phospho-TrkB immunohistochemistry (Figure 24C, Table S5; control *vs.* BDNF $p < 0.001$)

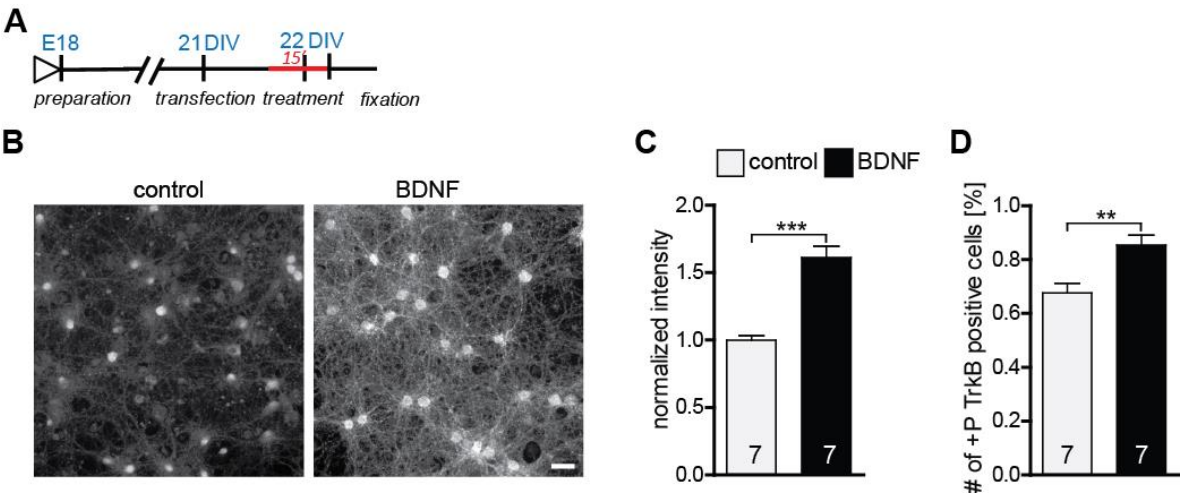

Figure 24: TrkB receptor phosphorylation.
A Experimental timeline. DIV22 primary hippocampal neurons were treated 15 min with BDNF before fixation. **B** Images of primary hippocampal cultures (22 DIV) treated with either BSA (control, left) or BDNF (right) and stained with an anti-phospho-TrkB receptor antibodies. Scale bar, 40 µm. **C** Histogram showing the normalized fluorescence intensity for the phospho-TrkB receptor under control conditions or treated with BDNF. **D** Graph showing the number of phospho-TrkB positive hippocampal neurons in control and BDNF treated hippocampal primary cultures. The number in the columns represents the number of analysed experiments. Data are presented as mean ± SEM. $^{**}p < 0.01$; $^{***}p < 0.001$.

as well as by a clear shift in the proportion of positive *versus* negative cells for phospho-TrkB. Indeed, upon BDNF treatment significantly more neurons resulted to be positive for phospho-TrkB immunohistochemistry and significantly less to be negative for it (Figure 24D, Table S5; control *vs.* BDNF $p < 0.01$). The activation of the PLCγ signalling pathway upon BDNF binding to the TrkB receptor leads to an increase in the intracellular calcium levels (Blum and Konnerth, 2005; Minichiello, 2009; Segal and Greenberg, 1996) and was specifically shown for hippocampal cultures (Berninger et al., 1993; Canossa et al., 1997; Finkbeiner et al., 1997). Here, the frequency of global calcium transients as readout for a neuronal response to an acute BDNF application was analysed

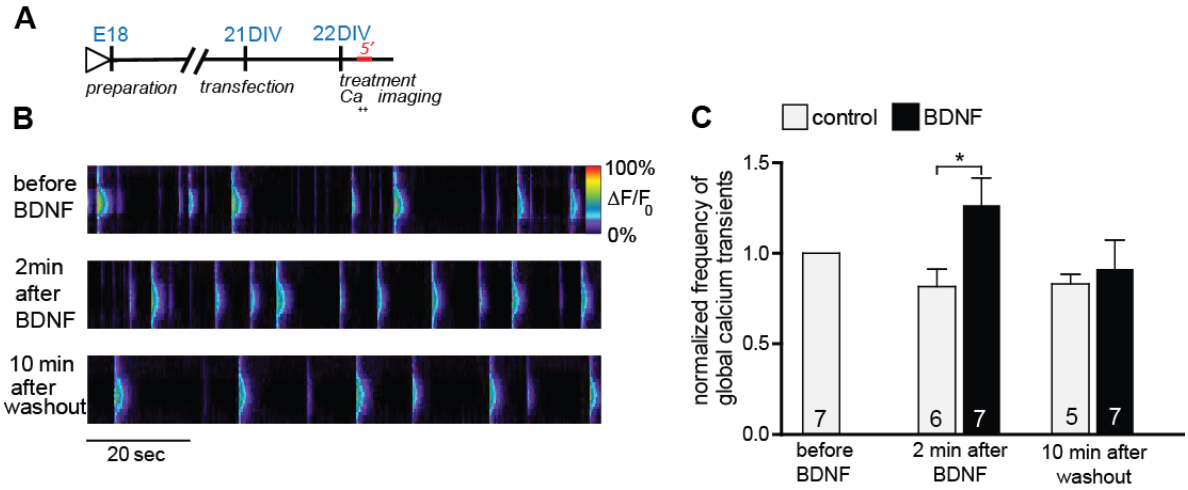

Figure 25: Local calcium transients in hippocampal neurons.
A Experimental timeline. DIV22 primary hippocampal neurons were treated 5 min with BDNF during calcium imaging. **B** Pseudo line-scan showing the global calcium transients occurring in hippocampal primary cultures before, during and after BDNF applications. **C** Graph showing the frequency of calcium transients in hippocampal primary neurons before, during and after BDNF application. The number in the columns represents the number of analysed experiments. Data are presented as mean ± SEM. *$p < 0.05$.

(Figure 25A; Lang et al., 2007; Lohmann, 2009). A clear increase in the frequency of calcium transients in DIV22 primary hippocampal neurons could be observed upon the acute application of BDNF (Figure 25B; Gödecke, 2012). Indeed, at a quantitative analysis the frequency of calcium transients resulted to be significantly increased after BDNF treatment in comparison to a control treatment (Figure 25C, Table S5; BDNF *vs.* control $p < 0.05$). The increase in the frequency in calcium transients upon BDNF application was transient as 10 min after BDNF washout the frequency was back to the pre-treatment levels (Figure 25C, Table S5; Gödecke, 2012). Finally, to verify that the application of BDNF leads to the expression of IEGs immunohistochemistry for c-fos was used. This IEG is known to be activated upon an acute treatment with BDNF (Figure 26A; Marty et al., 1996; Gascon et al., 2005). An immunohistochemistry for c-fos showed a clear

colocalization between c-fos and the nucleus of neurons (Figure 26B). Quantitative analysis performed 3 hours after the stimulation with BDNF (Figure 26A) showed significantly higher intensity values for the c-fos immunohistochemistry (Figure 26C, Table S5; $p < 0.01$) and a significant increase in the number of c-fos positive cells in comparison to control (Figure 26D, Table S5; $p < 0.001$). In summary, these observations indicate that the BDNF used in these experiments is active and leads to the activation of the TrkB-receptor, an increase in the frequency of calcium transients and an activation of transcription (up regulation of the immediate early gene *c-fos*) in mature primary hippocampal neurons.

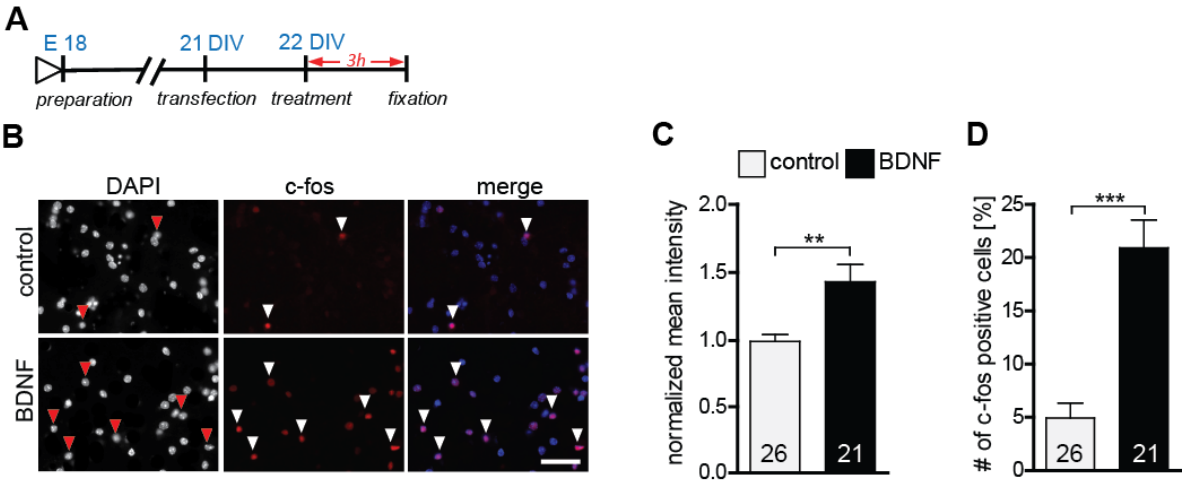

Figure 26: Activation of the immediate early gene *c-fos*.
A Experimental timeline. DIV22 primary hippocampal neurons were treated for 3 h with BDNF before fixation. **B** Images of primary hippocampal cultures (22 DIV) treated with either BSA (control, above) or BDNF (below) and stained with an anti-c-fos antibody. Scale bar, 20 µm. **C** Graph comparing the normalized mean intensity for the immunohistochemistry against c-fos in control or BDNF treated hippocampal primary neurons. **D** Histogram of the number of c-fos positive neurons in control and BDNF treated hippocampal cultures. The number in the columns represents the number of analysed experiments. Data are presented as mean ± SEM. **p < 0.01; ***p < 0.001.

4.2.5 Exogenous BDNF regulates neurite outgrowth and complexity in young primary hippocampal neurons

Previous studies have revealed BDNF to promote neurite outgrowth and dendritic complexity in developing cortical neurons (McAllister et al., 1995; Shimada et al., 1998). In view of the lack of effects on dendritic architecture observed in my work upon BDNF application to either DIV15 or DIV22 hippocampal primary neurons, we tested whether the effect of BDNF on dendrites might be age-dependent (Thieme, 2011). Indeed, BDNF has been shown to regulate neurite outgrowth in development hippocampal neurons (Ji et al., 2005, 2010). Therefore, young hippocampal neurons 3 DIV were treated with either a gain- or a loss-of-function approach for BDNF.

After 3 days of treatment (Figure 27A) an immunohistochemistry for Microtubule-associated protein 2 (MAP2) was used to visualize the developing neurites (Figure 27B; up control, middle BDNF, lower TrkB-Fc). Morphometric analysis for neurite growth was performed by quantifying three parameters: total neurite length, number of primary neurites and number of branching points (Figure 27C–E, Table S6). The total neurite length was higher after BDNF application than in control treated neurons (Figure 27C, Table S6; BDNF *vs.* control, $p < 0.001$). Interestingly, the loss-of-function experiments with either a BDNF-Abs or TrkB-Fc did not show any significant difference in neurite length when compared to the control conditions (Figure 27C, Table S6). The specificity of the TrkB-Fc in neutralising BDNF was determined by a co-application of BDNF and TrkB-Fc. Quantitative analysis revealed that application of TrkB-Fc completely prevented the positive effect of a BDNF treatment on total neurite length (Figure 27C, Table S6). The number of primary neurites after BDNF application showed a slight increase when compared to the control (Figure 27D, Table S6; BDNF *vs.* control, $p < 0.01$), whereas the treatment with BDNF-Abs or TrkB-Fc did not alter their number (Figure 27D, Table S6). The significant increase in primary neurites observed after BDNF treatment could be prevented by a co-treatment with TrkB-Fc (Figure 27D, Table S6).

Next, we determined whether a BDNF application might affect neurite complexity by analysing the number of branching points of MAP2 labelled processes. Indeed, a BDNF treatment resulted in a 2-fold increase in complexity in comparison to control (Figure 27E, Table S6; BDNF *vs.* control, $p < 0.001$). On the contrary, treatment with BDNF-Abs or TrkB-Fc did not influence the number of branching points when compared to the control (Figure 27E, Table S6). Additionally, the positive effect of BDNF on neurite complexity was prevented by a co-treatment with BDNF and TrkB-Fc (Figure 27E, Table S6). These results suggest that the application of BDNF promotes neurite outgrowth by increasing both neurite elongation and branching in developing DIV3 hippocampal primary neurons

(Thieme, 2011). The two loss-of-function approaches for BDNF did not affect the neurite architecture of primary hippocampal neurons (3–6 DIV) during their early development.

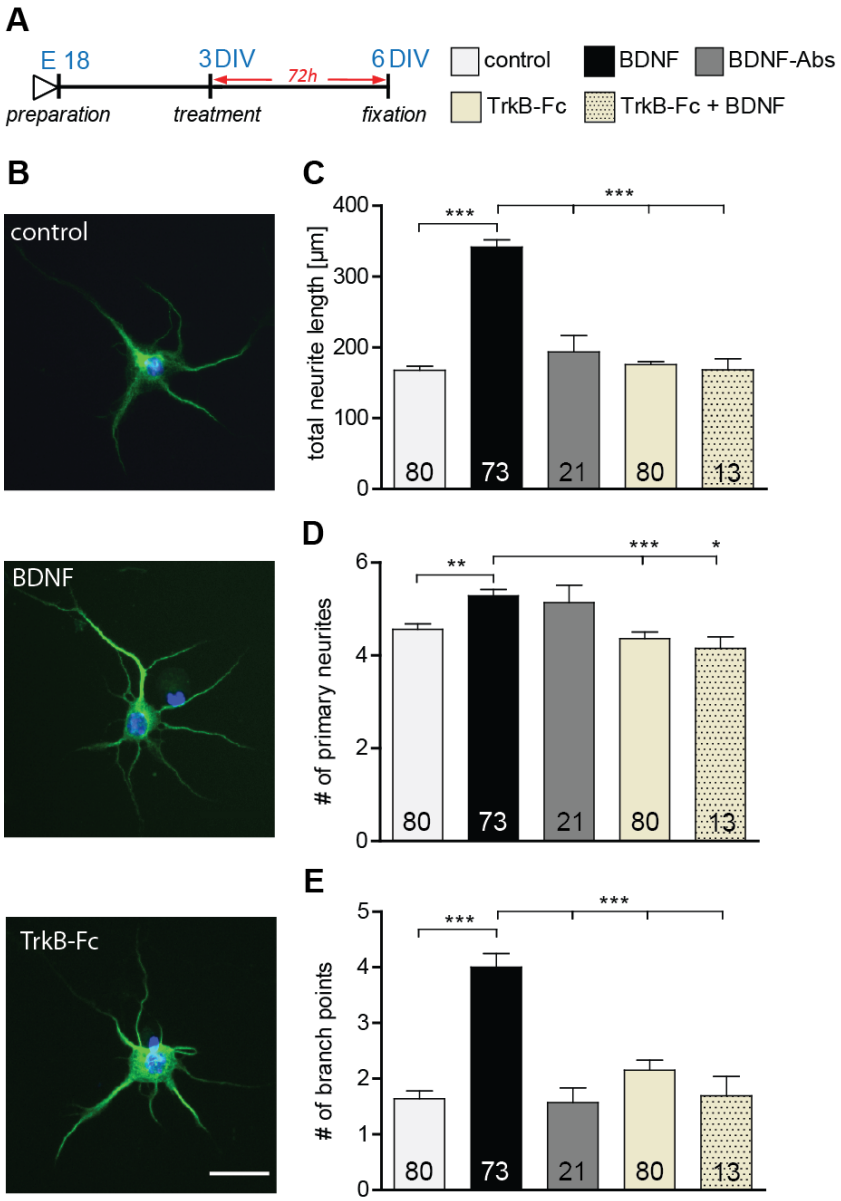

Figure 27: Exogenous BDNF regulates neurite complexity.
A Experimental timeline. BSA (control), BDNF, BDNF antibodies (BDNF-Abs) or TrkB receptor bodies (TrkB-Fc) were applied on DIV3 hippocampal neurons for 72 h. **B** Micrographs showing MAP2 positive BSA (control; above), BDNF (middle) or BDNF antibodies (BDNF-Abs; below) treated primary hippocampal neurons. Scale bar, 25 µm. **C** Histogram comparing neurite length of DIV6 hippocampal neurons after application of BSA (control), BDNF, BDNF antibodies (BDNF-Abs), TrkB receptor bodies (TrkB-Fc) or combined BDNF and TrkB receptor bodies (TrkB-Fc). **D** Histogram comparing the number of primary neurites of DIV6 hippocampal neurons after application of BSA (control), BDNF, BDNF antibodies (BDNF-Abs), TrkB receptor bodies (TrkB-Fc) or combined BDNF and TrkB receptor bodies (TrkB-Fc). **E** Histogram comparing the number of branching points for the dendrites of DIV6 hippocampal neurons after application of BSA (control), BDNF, BDNF antibodies (BDNF-Abs), TrkB receptor bodies (TrkB-Fc) or combined BDNF and TrkB receptor bodies (TrkB-Fc). The number in the columns represents the number of cells analysed. Data are presented as mean ± SEM. *$p < 0.05$, **$p < 0.01$; ***$p < 0.001$.

4.2.6 Role of neuronal activity in regulating the sensitivity of mature hippocampal neurons upon exogenous BDNF application

BDNF synthesis and release have been shown to occur in an activity-dependent way (Gärtner and Staiger, 2002; Thoenen, 1991). Therefore, one possible explanation for the discrepancies in the effect of BDNF application on neuronal morphology *in vitro* (Ji et al., 2005, 2010; Rauskolb et al., 2010) may lie in the different levels of neuronal activity in the primary cultures. Indeed, in cultures with a higher neuronal activity the levels of endogenous BDNF may be already high and thus mask the effects of BDNF application. To test this hypothesis primary hippocampal neurons were kept for 2 weeks in a medium containing a higher concentration of Magnesium (3.5 mM Mg^{2+}; Figure 28A) to reduce neuronal activity and the effects of a 24 hour treatment with BDNF (in NB medium with low, 1.5 mM Mg^{2+}) on the number and structure of dendritic spines were analysed. Calcium imaging was used to compare the levels of neuronal activity in hippocampal

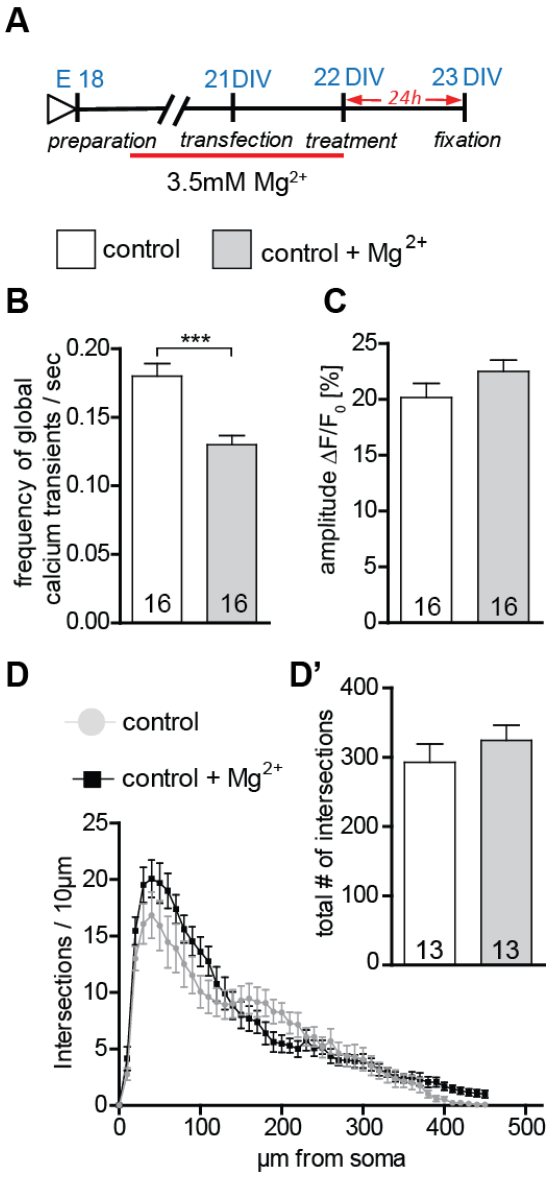

Figure 28: High Mg^{2+} concentration reduces neuronal activity. A Experimental timeline. Primary neurons were cultivated for 2 weeks in high (3.5 mM Mg^{2+}) medium and treated with BSA (control), BDNF or TrkB-Fc in low (1.5 mM Mg^{2+}). **B** Graph comparing the frequency of calcium transients in hippocampal primary neurons cultivated in high or low Mg^{2+} containing medium. **C** Graph comparing the amplitude of calcium transients in hippocampal primary neurons cultivated in high or low Mg^{2+} containing medium. **D** Graph plotting dendritic complexity in relation to the distance to the cell body of hippocampal neurons under control (1.5 mM) Mg^{2+} conditions or high (3.5 mM) Mg^{2+}. **D'** Histogram of the total number of intersections in hippocampal primary neurons cultivated in control or high Mg^{2+} containing medium. The number in the columns represents the number of cells analysed. Data are presented as mean ± SEM. ***p < 0.001.

neurons grown under high Mg^{2+} to those of neurons grown under control (low Mg^{2+}) conditions. While no significant difference could be detected regarding the amplitude of global calcium transients between the two groups (Figure 28C, Table S7), their frequency was significantly decreased in neurons kept in high Mg^{2+} when compared to control neurons (Figure 28B, Table S7; $p < 0.001$) suggesting a long-term reduction in neuronal activity. While no significant differences in dendritic complexity could be observed between the two different culturing conditions (Figure 28D,D', neurons kept in 1.5 *vs.* 3.5 mM Mg^{2+}; Table S7). A significantly lower dendritic spine density could be observed when comparing control neurons kept in high Mg^{2+} with control neurons kept in low Mg^{2+} medium (Figure 29B, Table S7; $p < 0.001$). On the other hand, no significant differences in spine density could be detected upon a BDNF or a TrkB-Fc treatment for neurons grown under high Mg^{2+} conditions when compared to the control high Mg^{2+} conditions (Figure 29B, Table S7). Next, a possible effect of BDNF on dendritic spine morphology was analysed. Interestingly, compared to control treated neurons BDNF treatment in cultures kept in high Mg^{2+} resulted in a slight increase in dendritic spine width (Figure 29C, Table S7) and a slight decrease in spine length (Figure 29D, Table S7), but the difference did not reach significance. No significant differences were observed both for the head width and for the length when TrkB-Fc treated cells in high Mg^{2+} were compared to high Mg^{2+} controls (Figure 29C, D, Table S7). To better clarify the mild spine head increase observed in neurons kept in high Mg^{2+} medium upon BDNF treatment spines were binned into four categories according to their head width. Comparing spine head width within each category showed a significant increase upon BDNF treatment in the proportion of spines with larger heads (Figure 29E; ≥0.5 µm <1 µm; $p < 0.05$) with a comparable significant decrease in the proportion of spine with small heads (Figure 29E; <0.3 µm; $p < 0.05$) when compared to control neurons cultivated in high Mg^{2+}. No significant difference was observed between the control and TrkB-Fc treatments in any of the spine head width categories under the same conditions (Figure 29E). Comparing the effect of a control, a BDNF or a TrkB-Fc treatment within different categories of dendritic spine binned according to their length did not show any significant difference (Figure 29F). The data described above suggest that indeed a chronic reduction in neuronal activity during the cultivation time might reduce the endogenous BDNF levels in hippocampal primary neurons and thereby increase their sensitivity to an exogenous BDNF application to modulate dendritic spine morphology.

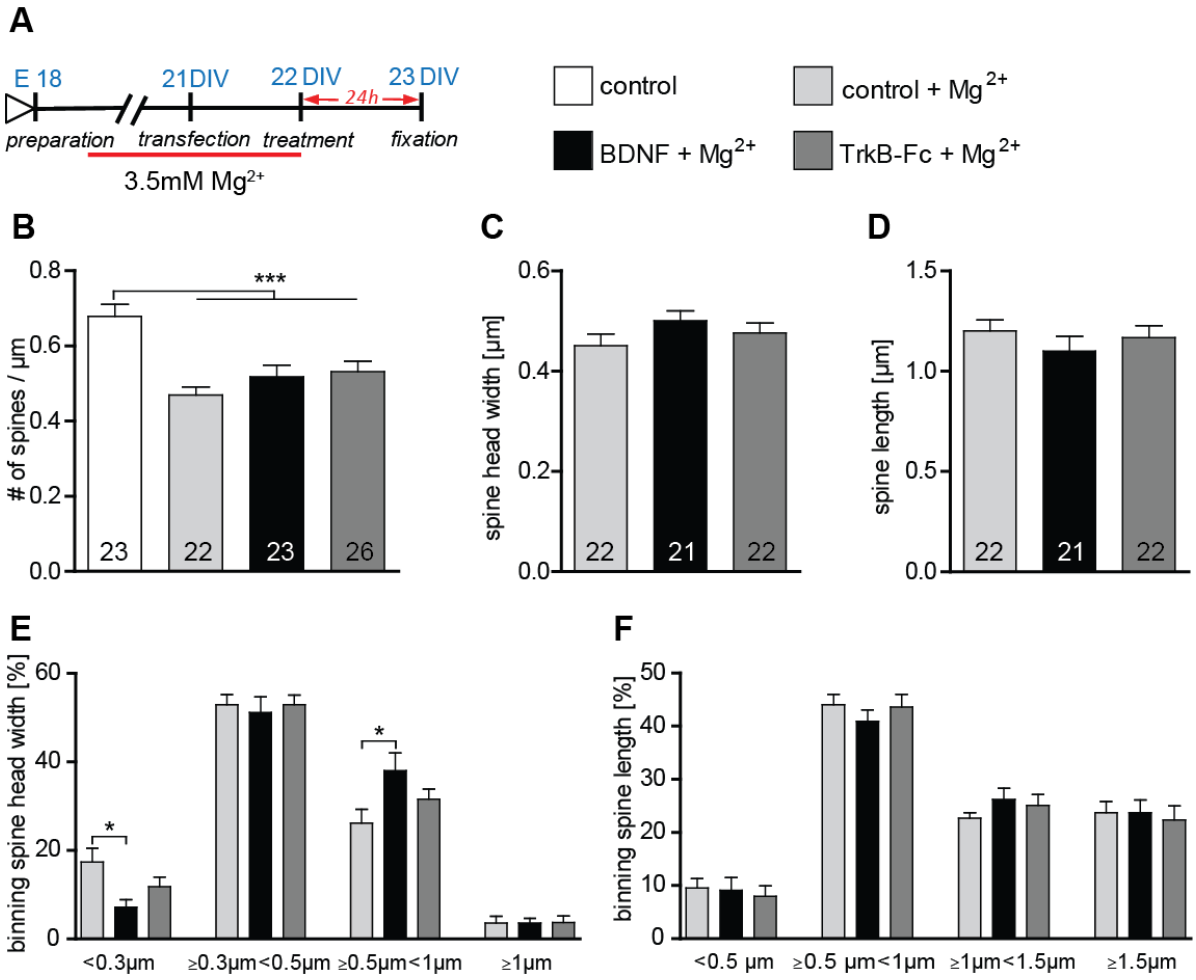

Figure 29: Exogenous BDNF in modulating dendritic spine morphology under reduced neuronal activity. A Experimental timeline. Primary neurons were cultivated for 2 weeks in high (3.5 mM Mg^{2+}) medium and treated with BSA (control), BDNF or TrkB-Fc in low (1.5 mM Mg^{2+}). **B** Graphs comparing dendritic spine density between neurons cultivated in low or high Mg^{2+} and treated with BSA (control), BDNF and TrkB receptor bodies (TrkB-Fc). **C** Histogram comparing the spine head width between primary hippocampal neurons cultivated in high Mg^{2+} and treated with BSA (control), BDNF and TrkB receptor bodies (TrkB-Fc). **D** Histogram of the dendritic spine length between primary hippocampal neurons cultivated in high Mg^{2+} and treated with BSA (control), BDNF and TrkB receptor bodies (TrkB-Fc). **E** Graph showing the binning of spines according to their spine head width and comparing the proportion of spines within each category in response to a BSA (control), BDNF or BDNF antibodies (BDNF-Abs) treatment. **F** Graph showing the binning of spines according to their spine length and comparing the proportion of spines within each category in response to a control, BDNF or TrkB receptor bodies (TrkB-Fc) treatment. The number in the columns represents the number of cells analysed. Data are presented as mean ± SEM. *$p < 0.05$, ***$p < 0.001$.

BDNF has been shown to modulate dendritic spine morphology upon activity-dependent synaptic plasticity Tanaka (Tanaka et al., 2008). To assess whether under these culture condition neuronal activity governs the BDNF effect on dendritic spine morphology, hippocampal primary neurons were kept for two weeks in a high Mg^{2+} (3.5 mM) medium and treated with BDNF in the same medium (Figure 30A) in order to reduce neuronal activity also during the BDNF treatment. Under these conditions a significantly lower

dendritic spine density could be observed when comparing control neurons kept in high Mg^{2+} to control neurons in low Mg^{2+} medium (Figure 30B, Table S7; $p < 0.05$). Moreover, dendritic spine density of neurons treated either with BDNF or with TrkB-Fc in high Mg^{2+} was significantly lower than in controls neurons (low Mg^{2+}, Figure 30B, Table S7; BDNF *vs.* low Mg^{2+} control $p < 0.05$; TrkB-Fc *vs.* low Mg^{2+} control $p < 0.001$) but it was not significantly different than in not treated cells kept in high Mg^{2+}.

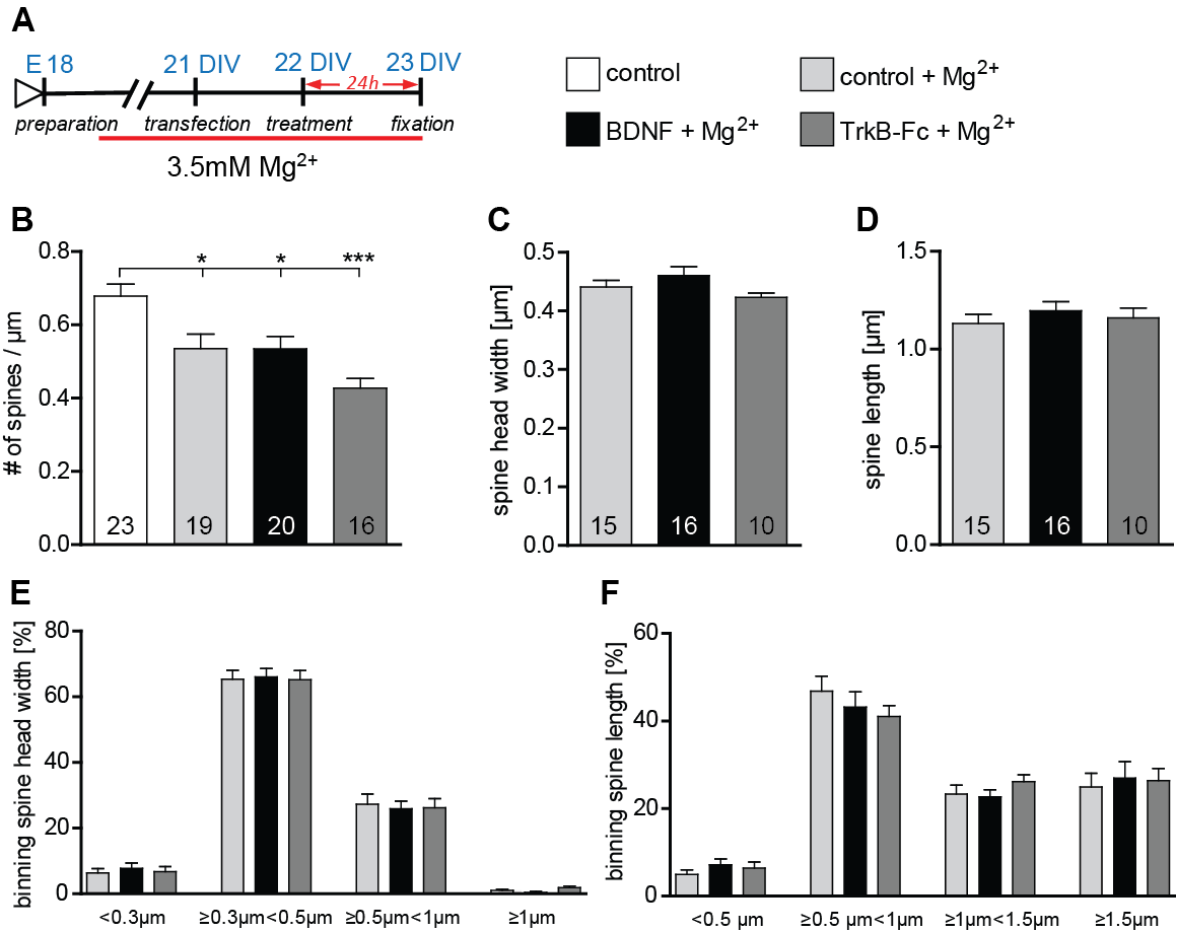

Figure 30: Reducing neuronal activity during the treatment blocks the effect of exogenous BDNF in modulating dendritic spine morphology. A Experimental timeline. Primary neurons were cultivated for 2 weeks in high Mg^{2+} medium and treated with BSA (control), BDNF or TrkB-Fc in high Mg^{2+}. **B** Graphs comparing dendritic spine density between neurons cultivated in low or high Mg^{2+} and treated with BSA (control), BDNF and TrkB receptor bodies (TrkB-Fc) in high Mg^{2+}. **C** Histogram comparing the spine head width between primary hippocampal neurons cultivated and treated in high Mg^{2+} with BSA (control), BDNF and TrkB receptor bodies (TrkB-Fc). **D** Histogram of the dendritic spine length between primary hippocampal neurons cultivated and treated in high Mg^{2+} with BSA (control), BDNF and TrkB receptor bodies (TrkB-Fc). **E** Graph showing the binning of spines according to their spine head width and comparing the proportion of spines within each category in response to a BSA (control), BDNF or BDNF antibodies (BDNF-Abs) treatment in high Mg^{2+}. **F** Graph showing the binning of spines according to their spine length and comparing the proportion of spines within each category in response to a BSA (control), BDNF or TrkB receptor bodies (TrkB-Fc) treatment in high Mg^{2+}. The number in the columns represents the number of cells analysed. Data are presented as mean ± SEM. *$p < 0.05$, ***$p < 0.001$.

Interestingly, both a BDNF treatment as well as a treatment with TrkB-Fc performed in high Mg^{2+} did not affect either activity also during the BDNF treatment. Under these conditions a significantly lower dendritic spine density could be observed when comparing control neurons kept in high Mg^{2+} to control neurons in low Mg^{2+} medium (Figure 30B, Table S7; $p < 0.05$). Moreover, dendritic spine density of neurons treated either with BDNF or with TrkB-Fc in high Mg^{2+} was significantly lower than in controls neurons (low Mg^{2+}, Figure 30B, Table S7; BDNF *vs.* low Mg^{2+} control $p < 0.05$; TrkB-Fc *vs.* low Mg^{2+} control $p < 0.001$) but it was not significantly different than in not treated cells kept in high Mg^{2+}. Interestingly, both a BDNF treatment as well as a treatment with TrkB-Fc performed in high Mg^{2+} did not affect either spine head width (Figure 30C, Table S7) or spine length (Figure 30D, Table S7) when compared to a control treatment in high Mg^{2+}. Also binning the spines according to their head width (Figure 30E) or to their length (Figure 30F) did not show any alteration in the spine size distributions both for a BDNF and a TrkB-Fc applications compared to a control treatment performed in high Mg^{2+}. In summary, the results above indicate that BDNF application indeed modulates dendritic spine architecture in an activity-dependent manner.

5 Discussion

The main cellular mechanism of learning and memory processes in the adult brain is considered to be the plasticity of neurons, which is the ability to modify the function and morphology of their synaptic connection in response to changes in neuronal activity. The fine-tuning of synaptic connectivity involves a variety of extracellular molecules that regulate functional and structural plasticity in a precise spatial and temporal manner. The cytoskeleton within synapses is the common denominator on which different signalling pathways controlling synapse-morphology and -strength converge. Filamentous actin is the main constituent of the cytoskeleton in spines and its dynamics have been shown to underlie the tight balance between stability and plasticity of neuronal networks in the CNS. In this work I investigated the role of two molecules known to either restrict or promote synaptic plasticity and their signalling pathway in modulating the actin cytoskeleton as well as structural plasticity of dendritic spines at mature hippocampal neurons. In the first part I addressed the role of Nogo-A and its signalling in regulating the actin cytoskeleton within dendritic spines and thereby maintaining the balance between the plasticity and stability of the neuronal circuitry required to store long-term information in the mature CNS. I show that Nogo-A signalling rapidly modulates the spine actin cytoskeleton to control structural plasticity at dendritic spines of CA3 hippocampal pyramidal neurons. Interfering with Nogo-A signalling transiently increases F-actin stability within minutes and results in an increase in dendritic spine number and length (Figure 31). Moreover, my results support the notion that Nogo-A signalling regulates learning and memory processes *in vivo* possibly by restricting structural plasticity. In summary, these data provide a cellular mechanism underlying the action of Nogo-A in regulating synaptic plasticity and show an important function for Nogo-A in maintaining the balance between plasticity and stability for the proper functions of the mature CNS network.

The second part of my work describes the necessity for endogens BDNF in the activity-dependent maintenance of a mature spine phenotype in excitatory mature hippocampal neurons (Figure 32). Specifically, I analysed at defined maturation stages (development, young and mature) the dendritic architecture of hippocampal neurons and show that the effects exerted by BDNF in this context are dependent on the neuron's maturation stage. Furthermore, I also shed some light on why published *in vivo* and *in vitro* results concerning morphological effects of BDNF are often contradictory.

5.1 Nogo-A rapidly modulates actin dynamics to control structural plasticity of dendritic spines and regulates memory acquisition

5.1.1 Use of FRAP to detect actin dynamics within mature dendritic spines

Filamentous actin is the main constituent of the cytoskeleton in dendritic spines, and the modulation of actin dynamics, is controlled by different signalling pathways to determine spine number and morphology (Cingolani and Goda, 2008; Hotulainen and Hoogenraad, 2010; Matus, 2000; Okamoto et al., 2009). Indeed, actin polymerization is supposed to generate a propulsive force toward the cell membrane (Mogilner and Oster, 1996) possibly generating force promoting the expansion of the spine head and thereby defining spine morphology (Honkura et al., 2008). Accordingly, the inhibition of actin polymerization by the application of latrunculin A induces spine shrinkage (Allison et al., 1998; Korkotian and Segal, 2001; Okamura et al., 2004) leading to the hypothesis that the spine number and morphology might be continuously maintained in a precise balance between the propulsive force of the F-actin fraction and the mechanical pressure imposed by the surrounding neuropil (Honkura et al., 2008). To test whether Nogo-A signalling is involved in regulating actin dynamics and thereby controlling spine morphology I established an new technique to the lab - fluorescence recovery after photobleaching (FRAP) at individual spines of eGFP-actin expressing CA3 hippocampal pyramidal neurons. I used the FRAP technique in order to analyse actin turnover and to provide quantitative estimates of F-actin filament stability within single spines. By this means I could confirm earlier results: recovery of the fluorescence after photobleaching occurred in two distinct components (Star et al., 2002; Zito et al., 2004), showing that 85% of the actin within spines exists in a mobile state and only 15% in a stable fraction (within a time frame of 110 s). The mobile actin portion (85%) can be further subdivided in a 70% dynamic F-actin fraction and 15% monomeric G-actin fraction. Moreover, similar to previous data (Stamatakou et al., 2013), all control spines showed an average turnover time of about 20 s implying a fast treadmilling (highly dynamic exchange of monomers between filaments and monomers). My FRAP data support the view of a highly dynamic actin cytoskeleton within mature dendritic spines of CA3 pyramidal neurons in organotypic slices. Previous studies showed that the spine-head volume is proportional to the total amount of F-actin and specifically to the stable actin fraction (Honkura et al., 2008; Okamoto et al., 2004). To avoid that different spine sizes and by this different amounts of stable actin within spines may influence the FRAP results, only mushroom like spines with a clear head and on average the same spine head size were used for experiments. Moreover, a series of preliminary experiments was performed to demonstrate that the fluorescent recovery after photobleaching indeed visualizes the F-actin treadmilling.

As previously described from Star et al. (2002) and confirmed here, the fluorescent intensity values of cytoplasmic eGFP recovered within seconds and the application of Cytochalasin D or jasplakinolide resulted in a dramatic reduction of the actin turnover, indicating a fast diffusion in the organotypic slice within minutes (see Figure 8C). Moreover, the turnover time for the fluorescence recovery of cytoplasmic GFP (0.34 s) is significantly faster than the one for eGFP-actin (20 s) indicating that the latter is not freely diffusible within the spine. These observations indicate that the FRAP experiment used in this study reliably detect the actin turnover within single mature dendritic spines (Star et al., 2002). A weakness of the FRAP experiments is that the portion of monomeric G-actin is relative because it is determined by the first imaging time point after the bleaching which is set by the experimenter. Furthermore, the FRAP experiments are limited to only a few single dendritic spines and changes over time can only be displayed after a full recovery of the stable actin fraction in 15-20 min (Honkura et al., 2008). Yet, FRAP experiments allow to examine the turnover time and the different actin fractions (dynamic, stable and monomeric) of single dendritic spines (Michaelsen-Preusse et al., 2014; Star et al., 2002), which cannot be determined with any other imaging technique.

5.1.2 Nogo-A restricts structural plasticity

Recent studies started to elucidate the role of Nogo-A in structural plasticity in the adult and intact (uninjured) CNS (for reviews see: Kempf and Schwab, 2013; Mironova and Giger, 2013). In organotypic hippocampal slice cultures Nogo-A was shown to regulate axonal and dendritic architecture of mature pyramidal neurons via a receptor-mediated mechanism (Craveiro et al., 2008; Zagrebelsky et al., 2010). A similar result was obtained analysing a triple knockout of the Nogo receptor (NgR1/2/3; Wills et al., 2012). Moreover, the neutralisation of Nogo-A in organotypic hippocampal slice cultures shifted the spine type distribution towards a more immature phenotype (Zagrebelsky et al., 2010). Also the Nogo-A receptors NgR1 and PirB have been shown to regulate the experience-dependent turnover of dendritic spines and axonal varicosities in the somatosensory and visual cortex, respectively (Akbik et al., 2013; Djurisic et al., 2013). In our recent study we asked whether Nogo-A acutely regulates structural plasticity and what are the molecular mechanisms mediating this action of Nogo-A (Kellner et al., under review). The loss-of-function experiments, performed by acutely blocking Nogo-A or the receptors NgR or S1PR2 revealed an increase in dendritic spine density and length within one hour of treatment (Figure 31). Accordingly, gain-of-function experiments by the application of the Nogo-A-Δ20 peptide showed a transitory decrease in spine length within minutes. The spine density increase after blocking NgR1 or S1PR2 remained lower than upon Nogo-A neutralisation possibly indicating a cooperative effect of the two receptors. Yet, no change

of the spine density after a chronic neutralisation of Nogo-A in CA3 pyramidal neurons were shown (Zagrebelsky et al., 2010), suggesting that the gained spines are not maintained over days. Similarly, while the analysis of spine morphology upon an acute Nogo-A neutralisation induced spine elongation without changes in spine head width its long-term neutralisation caused more stubby like spines (Zagrebelsky et al., 2010). This suggests that a chronic neutralisation of Nogo-A may conduct changes in the network homeostasis and finally may support changes in synaptic plasticity as a compensatory mechanism. This needs to be further examined with time-lapse imaging over days. Taken together, Nogo-A signalling acutely restrict structural plasticity at individual dendritic spines of CA3 pyramidal neurons on a fast timescale.

5.1.3 Nogo-A signalling controls actin dynamics

Nogo-A signalling triggers the activation of the small GTPase RhoA and suppression of Rac1 resulting in growth cone collapse and axonal repulsion (Kempf et al., 2014; Niederöst et al., 2002; Yiu and He, 2006). Inactivated RhoA is increased in *nogo-a* KO mice resulting in an increased LIMK1 phosphorylation via ROCK and in the deactivation of the actin severing protein cofilin (Montani et al., 2009). These signalling events in *nogo-a* KO mice, lead to increased growth cone motility through the increase in actin polymerization required for the formation and extension of filopodia in growth cones (Montani et al., 2009). Interestingly, in primary hippocampal neurons as well as *in vivo* NgR1 restricts dendritic and synaptic growth through RhoA activation, probably by limiting the number of synaptic contacts made during development (Wills et al., 2012). Furthermore the Nogo-A-Δ20 peptide binds to S1PR2 and signals via the G protein G13, the Rho GEF LARG to activate RhoA (Kempf et al., 2014). The inhibitory effects of Nogo-A on neurite outgrowth and oligodendrocyte-mediated growth cone collapse were also abolished by inactivating the Rho-kinase ROCK (Niederöst et al., 2002). These studies suggest that Nogo-A signalling may regulates the actin cytoskeleton via the RhoA–ROCK pathway. The inactivation of RhoA has been shown to result in more and longer spines suggesting that RhoA can repress the maintenance and elongation of spines (Tashiro et al., 2000). Here I showed that a similar regulation of actin dynamics via ROCK takes place within mature dendritic spines to control their architecture and thereby suppressing their structural plasticity. Neutralising Nogo-A signalling in mature hippocampal neurons results in the fast stabilization of the actin cytoskeleton shown by an increase in turnover time and in the stable actin fraction already after 20 minutes of Nogo-A or NgR1 and S1PR2-receptor blockade (Figure 31). This stabilizing effect on the actin cytoskeleton is transient for the Nogo-A signalling via the NgR1. It is noteworthy that, blocking the S1PR2 leads to a strong and long lasting stabilizing effect on the actin cytoskeleton beyond 180 minutes.

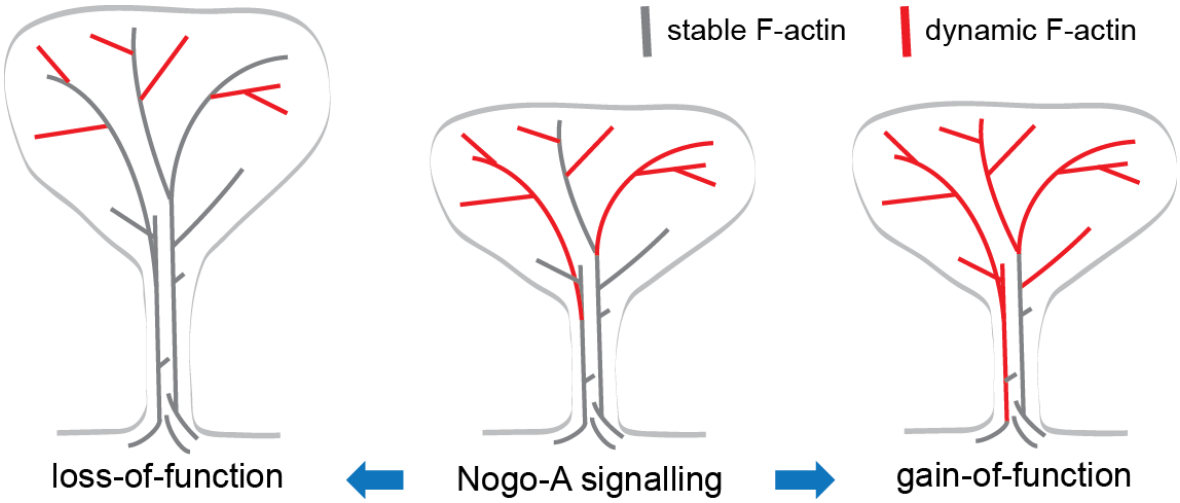

Figure 31: Control of the actin cytoskeleton via Nogo-A signalling.
Scheme showing a dendritic spine within the stable F-actin (grey) and dynamic F-actin (red) under the gain- and loss-of-function of Nogo-A signalling.

To block the S1PR2 I used the selective antagonist JTE-013 which was shown to counteract Nogo-A-Δ20-mediated inhibition of neurite outgrowth and cell spreading (Kempf et al., 2014). Yet, to block Nogo-A and its receptors different antibodies and blockers were used whose kinetics and blocking efficiency may be not identical and therefore may lead to different outcomes in blocking the Nogo-A signalling. The long lasting effect on the actin cytoskeleton achieved by blocking the S1PR2 might be mediated also via RhoA signalling like the blocking of the NgR1 (Kempf et al., 2014). Yet, S1PR2 has also been shown to regulate Ca^{2+} homeostasis (Rapizzi et al., 2007; Spiegel and Milstien, 2003) and, a misregulation of the intracellular Ca^{2+} homeostasis might indirectly influence diverse molecular mechanism to alter actin dynamics (Oertner and Matus, 2005). Calcium activates cascades of kinases and phosphatases in dendritic spines, resulting in changes in cellular functions and leading to functional and structural plasticity (for review see: (Sala and Segal, 2014). Indeed, calcium triggers the activation of the CaMKII that can reorganize actin filaments, bundles them and consolidates the remodelled spine morphology (Okamoto et al., 2009). A transient rise in the calcium concentration in dendritic spines has been shown to lead to an increase in spine length (Korkotian and Segal, 1999). The stabilization of the actin cytoskeleton and the increase of the spine length after Nogo-A blocking (Figure 31) might be indirectly mediated by calcium. It is noteworthy, that the application of Nogo-A-Δ20 leads in the growth cone to a release of Ca^{2+} from internal stores necessary to induce growth cone collapse (Bandtlow et al., 1993). The gain-of-function approaches by the application of Nogo-A-Δ20 or Nogo-66 peptides reduce the amplitude of post-tetanic stimulation (Delekate et al., 2011) or LTP (Raiker et al., 2010). Interestingly, here I showed a decrease of the actin turnover time directly after Nogo-A-Δ20 application and thereby a more mobile actin cytoskeleton

(Figure 31). A longer incubation of the peptide upon 20 min correlates with a stabilization of the actin cytoskeleton which were also achieved by neutralising Nogo-A (loss-of-function experiments). Joset and colleagues (2010) described an internalization of the Nogo-A-Δ20 starting 15 min after application of the peptide on neuronal cells. The binding of Nogo-A-Δ20 to its receptor leads to endocytosis and thereby to a loss-of-function of the S1PR2 complex (Kempf et al., 2014; Schwab, 2010). This biphasic action after Nogo-A-Δ20 application of a transient destabilization followed by a stabilization of the actin cytoskeleton within dendritic spines supports previous observations in LTP experiments (Delekate et al., 2011).

As indicated above Nogo-A signalling might regulate actin dynamics in dendritic spines via RhoA, ROCK signalling (Mironova and Giger, 2013). Rex and colleges showed that the inhibition of ROCK upon LTP induction leads to a dysregulation of cofilin and a lack of LTP maintenance (Rex et al., 2009). Also here I show that the inhibition of ROCK leads to a transient stabilization of the actin cytoskeleton. Nevertheless, this effect is mild in comparison to the effect achieved with the inhibition of the Nogo-A action, suggesting that the timing of the direct ROCK inhibition might be different or the inhibition is compensated. Indeed, ROCK activates via LIMK cofilin to regulate actin dynamics, the LIMK can also be regulated via PAK controlled by the Rho-GTPases Rac1 or Cdc42 to compensate the inhibition of ROCK. A further actin regulatory protein that may play an important role in this context is Myosin II, known to regulate the retrograde flow of G-actin and thereby possibly influencing the dynamics and organisation of the actin cytoskeleton (Medeiros et al., 2006). The inhibition of myosin II in mature hippocampal neurons results in a stabilization of the actin cytoskeleton within spines (Rex et al., 2010) and in an increase in spine number and spine length (Ryu et al., 2006; Schubert and Dotti, 2007). In *nogo-a* KO mice it has been observed that myosin II is down-regulated (Montani et al., 2009), correlating to an increase in neurite motility by regulating contractility of actin-bundles and the retrograde actin-flow within growth cones (Medeiros et al., 2006). In further experiments are needed to examine whether Nogo-A signalling might regulate Myosin II via the RhoA or PAK pathway. Although I cannot determine the detailed signalling pathway my data strengthen the view that Nogo-A controls structural plasticity at spines by regulating actin dynamics possibly via the RhoA-ROCK pathway and by this means it might regulate cofilin and Myosin II. A regulation of the Ca^{2+} homeostasis might contribute to the effect seen upon Nogo-A neutralisation to regulate dendritic spine dynamics.

5.1.4 Linking actin cytoskeleton dynamics to functional and structural plasticity

Electrophysiological recordings revealed that Nogo-A and its receptors play a crucial role in restricting activity-dependent synaptic plasticity (Delekate et al., 2011; Kempf et al., 2014; Lee et al., 2008; Raiker et al., 2010). Loss-of-function experiments of Nogo-A or of its receptors NgR1 or S1PR2 result in higher potentiation during LTP (Delekate et al., 2011; Kempf et al., 2014), whereas in a gain-of-function approach the application of Nogo-A-Δ20 or Nogo-66 peptides reduces the amplitude of post-tetanic stimulation (Delekate et al., 2011) or LTP (Raiker et al., 2010). We show in our current study an increase in spine density upon Nogo-A neutralisation associated with a higher number of new AMPA receptor clusters at spines suggesting an increase in active synapses (Kramer, 2013; Kellner et al., under review). Activity-dependent alterations in the strength of synapses are driven by a collaborative interaction between functional and structural changes (Matsuzaki et al., 2004a; Yuste and Bonhoeffer, 2001). Induction of LTP is accompanied by a rapid insertion of AMPA receptors and by their increased clustering at the surface of dendritic membranes (Kessels and Malinow, 2009; Lu et al., 2001; Pickard et al., 2001) underlying the associated increase in synaptic strength. Electron microscopy verified that AMPARs are located in the cytoskeleton shell of the spine (Harris and Stevens, 1989; Nusser et al., 1998; Takumi et al., 1999). The inhibition of actin polymerization applying latrunculin A has been shown to block the functional expression of AMPARs (Kim and Lisman, 1999; Krucker et al., 2000) and at the same time reduces F-actin dynamics at spines (Honkura et al., 2008). Furthermore AMPARs are anchored via adaptor molecules to actin filaments (Lisman and Zhabotinsky, 2001) and ADF/cofilin mediates the actin dynamics to regulate AMPAR trafficking specifically during synaptic plasticity (Gu et al., 2010). In this way changes in the dynamics of the actin cytoskeleton modulates both synaptic strength and as discussed above structural changes at synapse. I showed an acute role of Nogo-A signalling in modulating the actin cytoskeleton within dendritic spines at a time scale of minutes and hours comparable to the effects observed on LTP and correlated with an increase in the number of dendritic spines (Kellner et al., under review). In addition, the transitory stabilization of the actin cytoskeleton after Nogo-A inhibition may support the new insertion of AMPARs probably via the regulation of ADF/cofilin, resulting in higher synaptic potentiation (Delekate et al., 2011). The stable actin fraction is related to the spine head width (Honkura et al., 2008) which has been shown to be correlated to synaptic strength: larger synaptic efficiency are accompanied with an increase in F-actin and bigger spine heads (Fischer et al., 1998; Huber et al., 2004; Kasai, 2003; Kopec et al., 2006; Okamoto et al., 2004). Indeed, Nogo-A neutralisation increases the stable actin fraction, still the spines head width is not altered. It must be pointed out that changes in

spine neck width can regulate the biochemical and electrical compartmentalization of the spine which is important for the diffusional coupling between the spine head and the dendritic shaft (Bloodgood and Sabatini, 2005; Tønnesen et al., 2014; Yuste, 2013). The spine neck contains long branched and linear longitudinal arranged actin filaments (Korobova and Svitkina, 2010). Interesting, myosin II induces contractility which could further regulate spine morphology and synaptic strength by controlling the spine neck width (Hotulainen and Hoogenraad, 2010; Ryu et al., 2006). Interestingly, the spine neck length is inversely correlated to the amplitude at the soma of an uncaged evoked potential, suggesting that the spine neck has a filter function for membrane potentials (Araya et al., 2006). The elongation of the spine neck might electrically isolates the synapse from the dendrites preventing large conductance changes in dendrites and could help the neuron integrate and independently modulate the strength of large numbers of synaptic inputs (Yuste, 2013). Certainly, Nogo-A neutralisation leads to an increase in the number of spines, to an increase in AMPARs clusters (Kellner et al., under review) and to a higher LTP (Delekate et al., 2011). Thus, the stabilization of the actin cytoskeleton may lead to an elongation of the spine and resulting in the electrical isolation of spines from the dendrite to compensate the consequences of an increasing number of synaptic inputs (Yuste, 2013) upon Nogo-A neutralisation. All in all, interfering with Nogo-A signalling pathway might transitory increase the actin cytoskeleton stability of mature dendritic spines resulting finally in longer spines.

5.1.5 Nogo-A exerts a biphasic action in regulating memory acquisition and retention

The strengthening of synaptic connections between neurons is widely considered to be essential for learning and memory formation in the CNS (Bailey and Kandel, 1993; Martin et al., 2000). Interestingly, changes in synaptic strength have been shown to accompany motor skill acquisition (Rioult-Pedotti et al., 1998, 2000) and Nogo-A down-regulation results in higher LTP in the motor cortex (Tews et al., 2013). Recent studies have delivered evidence that learning involves gain and loss of synapses leading to the formation of memory traces that influence behaviour (Caroni et al., 2012). Learning of motor skills leads to dendritic spine growth in the motor cortex (Xu et al., 2009; Yang et al., 2009a; Zemmar et al., 2014, under review) or in the dentate gyrus (O'Malley et al., 2000) and increase in dendritic spine number is correlated to learning processes and memory formation. Nogo receptor 1 signalling (Kleene and Schachner, 2004) was shown to control learning and memory formation as well as experience dependent structural plasticity in the cortex in two independent learning paradigms (Akbik et al., 2013; Karlén et al., 2009). Therefore I explored the possibility whether Nogo-A might be involved in

processes of spatial learning and memory retention in the Morris water maze by regulating structural plasticity at spines of CA3 hippocampal neurons. First my data confirm previous results from Willi and colleagues (2009) showing that *nogo-a* KO and WT mice learn equally well to locate the hidden platform (Willi et al., 2009). Second I identified a crucial role for Nogo-A in the early phase of memory formation. Performing a probe trial at the end of the training period (day 9) revealed no difference in reference memory, in contrast during the early acquisition phase (day 3) *nogo-a* KO mice form a reference memory significantly faster than WT mice. This initial and transient advantage of *nogo-a* KO mice in forming a reference memory in the Morris water maze supports the role of Nogo-A in regulating the initial phase of memory acquisition. In the rat hippocampus the expression of Nogo-A or the Nogo receptor 1 are induced with age-related cognitive decline and correlate with deficits of spatial learning and memory (VanGuilder Starkey et al., 2013a, 2013b; Vanguilder et al., 2012). The lack of an effect for *nogo-a* KO mice on the performance during training in the Morris water maze could be due to a generally mild phenotype in the *nogo-a* KO mice. Interestingly, the neutralisation of Nogo-A or NgR1 function by blocking antibodies has been shown to be significantly more efficient in promoting axonal regeneration upon injury than the genetic deletion of the respective genes (Schwab and Strittmatter, 2014; Teng and Tang, 2005). Also the dendritic and axonal architecture of CA3 pyramidal neurons as well as dendritic spine density and dynamics (observation Zagrebelsky, unpublished data) are altered upon a neutralisation of Nogo-A but not in *nogo-a* KO hippocampal cultures (Zagrebelsky et al., 2010). Indeed, in the *nogo-a* KO mice other inhibitory factors like NogoB and MAG, Ephrin/Eph and Semaphorin/Plexin are up-regulated and may compensate the lack of Nogo-A (Kempf et al., 2013).

It has been shown that learning of a new task or experiencing novel sensory stimulations are correlated with a phase of synaptic remodelling due to the rapid formation of new spines followed by the selective elimination of previously existing spines (Yu and Zuo, 2011). These results, together with the observation that increased spine turnover or formation correlates with the performance upon motor learning suggest that spine plasticity plays an important role in the formation and maintenance of motor memories (Xu et al., 2009; Yang et al., 2009a). I showed that the initial advantage of *nogo-a* KO mice in forming a spatial reference memory in the Morris water maze is associated to an increase in dendritic spine density for CA3 pyramidal neurons already after 3 days of training. Interestingly, the delayed formation of a reference memory in WT mice correlates with a significant increase in dendritic spine density after 9 days of water maze training. Finally, the reference memory at probe trial of day 9 was comparable between the two genotypes and was correlated to similar spine density values due to a slight decrease in spine

density of *nogo-a* KO mice. This observation suggests that the new spines added during the learning processes are not maintained or that pre-existing spines are eliminated later on during training. Indeed, both spine gain and elimination processes are associated with motor learning and long-lasting synaptic reorganisation to stabilize neuronal connections (Caroni et al., 2012; Xu et al., 2009). Previous studies reported an activity-dependent down-regulation of Nogo-A and NgR1, and transgenic mice overexpressing NgR1 show impaired long-term spatial memory (Karlén et al., 2009 Mingorance et al., 2004). The activity-dependent down regulation of Nogo-A mRNA was shown for the dentate gyrus but not in the CA1 or CA3 region of the hippocampus (Karlsson et al., 2013; Mingorance et al., 2004). WT mice trained for 3 days in the Morris water maze showed a transitory significant increase in Nogo-A expression levels in the hippocampus which was not maintained up on day 9. The increase in Nogo-A expression levels in trained WT mice correlate with the delay in spine density increase in in the CA3 pyramidal neurons and in reference memory acquisition in WT mice when compared to *nogo-a* KO. Taken together, the data open the possibility that Nogo-A signalling restricts structural plasticity and provides a biphasic control of learning and memory processes at the acquisition and at the consolidation phase of hippocampus-dependent memory storage.

5.2 The BDNF effects on neuronal architecture depend on the maturation stage and the neuronal activity

5.2.1 BDNF/TrkB signalling regulates the architecture of mature hippocampal neurons

While in the first part of my thesis I examined the role of Nogo-A in restricting structural plasticity in the second part of my work I analysed the role of BDNF as a positive regulator in maintaining the mature architecture of CNS neurons. The results obtained in my study are in line with previous work showing a surprising selectivity in the brain areas requiring BDNF-signalling for their post-natal development (Minichiello et al., 1999; Rauskolb et al., 2010; Zakharenko et al., 2003). While a global lack of BDNF throughout the CNS impairs the proper post-natal growth of striatal medium spiny neurons, BDNF deprivation fails to cause major alteration in the structure of mature CA1 pyramidal neurons in the hippocampus. Yet, the dendritic spine type distribution is significantly shifted towards more immature types (Rauskolb et al., 2010). These results suggest a crucial but rather limited and specific effect of BDNF in maintaining the mature phenotype of dendritic spines without affecting the general architecture of hippocampal neurons. My observations *in vitro* show a similar effect upon the application of two loss-of-function

approaches for BDNF to hippocampal primary cultures (function blocking BDNF antibodies and TrkB receptor bodies) confirming a physiological role of the endogenous BDNF. Nevertheless, my experiment fail to reproduce previously published data showing a highly significant increase in dendritic spine density and alterations in spine morphology upon the application of exogenous BDNF to mature hippocampal primary neurons (Ji et al., 2005, 2010) or to hippocampal slice cultures (Tyler and Pozzo-miller, 2003, 2001). The discrepancy between the data presented here and other previously published data regarding the role of exogenous BDNF in regulating the architecture of mature hippocampal neurons may have different reasons. One possible explanation is the different animal species used for the experiment. While studies showing an effect of a BDNF loss-of-function either *in vivo* (Rauskolb et al., 2010) or *in vitro* (my study: Kellner et al., 2014) were performed in mouse derived cultures, most of the previous *in vitro* work describing an effect for a BDNF gain-of-function was done using rat hippocampal neurons (Tyler and Pozzo-Miller, 2001, 2003; Ji et al., 2005, 2010) suggesting a possible difference in the sensitivity to BDNF signalling in the two different species. In addition, different level of BDNF release from neurons into the medium could change the initial BDNF content and by this also the sensitivity to BDNF for the gain-of-function experiment. It is noteworthy that my gain-of-function experiments didn't show any alterations of the spine density or morphology in primary rat hippocampal cultures performed in collaboration with the group S. Halpain (UCSD; Kellner, 2010). Implying that not the two different species but rather different culture conditions, may be responsible for this discrepancy. Indeed, culture conditions have been shown to possibly influence the expression levels as well as the cellular response to BDNF (Chapleau et al., 2008). Here I show that the levels of neuronal activity in the cultures determine the responsiveness to the exogenous or the endogenous BDNF. Low levels of neuronal activity during the cultivation period result in lower spine density values and an increased responsiveness of hippocampal neurons to the applications of exogenous BDNF (Figure 32). Indeed, the synthesis and secretion of BDNF have been shown to be directly correlated to neuronal activity (Gärtner and Staiger, 2002; Thoenen, 1991). Control neurons in previous publications showing a strong effect upon an exogenous BDNF application (Ji et al., 2005, 2010) had a spine density which is about 10 times lower than the one measured here or described *in vivo* (De Simoni et al., 2003) and 5 times smaller than the one described for a more complex *in vitro* system like the organotypic slice cultures (De Simoni et al., 2003; Rauskolb et al., 2010). It should also be noted that in the culture system used here the levels of neuronal activity as well as the cellular responsiveness to BDNF were tested in different ways. It was tested by quantifying the changes in TrkB phosphorylation as well as the activation of the IEG c-fos, two critical events known to occur upon the acute

activation of BDNF signalling (Ji et al., 2005, 2010; Marty et al., 1996). Both immunohistochemistry of the primary neurons showed a clear response upon BDNF treatment. In line with previous studies the application of exogenous BDNF led to a response of the neuronal network via a transient raise of the intracellular calcium concentration (Berninger et al., 1993; Lang et al., 2007). In contrast, blocking intrinsic BDNF signalling was shown to reduce the frequency of spontaneously occurring calcium signals in developing rat hippocampal neurons (Lang et al., 2007). Overall, my observation indicated that mature primary hippocampal neurons under normal culture conditions (1.5 mM Mg^{2+}) were responsive to application of exogenous BDNF even if they lack morphological effects observed in previous *in vitro* studies (Ji et al., 2005, 2010).

5.2.2 Endogenous BDNF regulates dendritic spine morphology

One important open question concerns the functional consequences of the observed structural changes at spines regulated by BDNF signalling. Interestingly, the dendritic spines morphology is associated to their compartmentalisation features and the respective functions in synaptic transmission (Matsuzaki et al., 2004b; Yuste et al., 2000). My results upon a BDNF loss-of-function confirm the structural alterations at spines observed already *in vivo* (Rauskolb et al., 2010). Specifically, the BDNF deprivation in mature primary neurons results in a decrease in dendritic spine density accompanied by a decrease in spine head width and an increase in spine length (Figure 32). The loss of the mature spines phenotype possibly results in a decrease and a weakening of synaptic connections under these conditions. Indeed, an increase in dendritic spines length has been shown in association with increased spine motility (Zito et al., 2004) and the spine head width is correlated with the size of the post-synaptic density and the number of AMPA receptors (Holtmaat and Svoboda, 2009). A shrinking of the spine head width has been correlated to the synaptic weakening occurring upon long-term depression induction (Zhou et al., 2004). Moreover, the spine neck has been suggested to act as a diffusion barrier regulating the biochemical and electrical compartmentalization in the spine head (Holthoff et al., 2010; Sjöström et al., 2008; Tønnesen et al., 2014; Yuste, 2013). Indeed, spines with long necks have been shown to be electrically silent at the soma, although their heads are activated by an uncaging event (Araya et al., 2006) and a BDNF-dependent shortening of the spine neck was observed upon inducing long-term potentiation at single spines (Tanaka et al., 2008). It has been show that upon maturation the proportion of mushroom spines increases while the one of thin long spines decreases (De Simoni et al., 2003). It will be important to explore the possibility that the structural changes of dendritic spines upon blocking intrinsic BDNF signalling may be accompanied by a weakening of synaptic strength and, a reduction of neuronal activity. It should also be noted that the

dendritic spine density and head width is lower in primary neurons 16 DIV in comparison to 23 DIV whereas the spine length is increased suggesting that dendritic spine maturation occurs between this time points. Indeed, it has been shown that primary young neurons change their morphology during the maturation process to a mature spine phenotype (Papa and Segal, 1996; Papa et al., 1995). Interestingly, the effects exerted by blocking BDNF signalling are in young primary neurons not as pronounced as in mature suggesting, that endogenous BDNF signalling plays a crucial role in maintaining the mature architecture of dendritic spines in excitatory neurons.

5.2.3 Activity-dependent structural plasticity

Increasing the strength of synaptic connections by inducing LTP in the CA3-CA1 hippocampal pathway depends on the NMDAR activation and is correlated to an increase of spine head width, as well as the formation of new spines (Engert and Bonhoeffer, 1999; Maletic-Savatic, 1999; Matsuzaki et al., 2004a). The secretion and local synthesis of BDNF is activity-dependent, and transgenic mice with impaired activity-dependent release or synthesis of BDNF exhibit defects in both LTP and memory (An et al., 2008; Chen et al., 2006; Ninan et al., 2010). Here calcium imaging was used to test the effects of increasing the magnesium concentration in the culture medium on neuronal activity. So, I could confirm that manipulating magnesium concentration in the medium results in a long lasting reduction in neuronal excitability and network activity of primary hippocampal cultures (Dribben et al., 2010). While this reduction in neuronal activity does not influence dendritic morphology and complexity, it is accompanied by a significant decrease in dendritic spine density as well as by an increased cellular sensitivity to the application of exogenous BDNF (Figure 32). Whether the increased neuronal responsiveness to BDNF is due to an activity-dependent decrease in BDNF release from neurons or, as recently described from microglia (Parkhurst et al., 2013) will be very interesting to address. Indeed, changes in magnesium concentration have also been shown to possibly influence ATP release (Li et al., 1997) and could thereby indirectly influence BDNF release from microglia (Parkhurst et al., 2013; Trang et al., 2009). Moreover, it will be crucial to explore the possibility that different amounts of microglia may influence the BDNF levels in the primary hippocampal cultures and thereby their responsiveness to a BDNF exogenous application. My results show that reducing neuronal activity during the application of exogenous BDNF prevents morphological changes at dendritic spines pointing to an activity-dependent effect of BDNF on dendritic spines (Figure 32). This result is consistent with previous work showing that during the early development of cortical pyramidal neurons in ferrets, BDNF regulates dendritic architecture in an activity-dependent manner (McAllister et al., 1996).

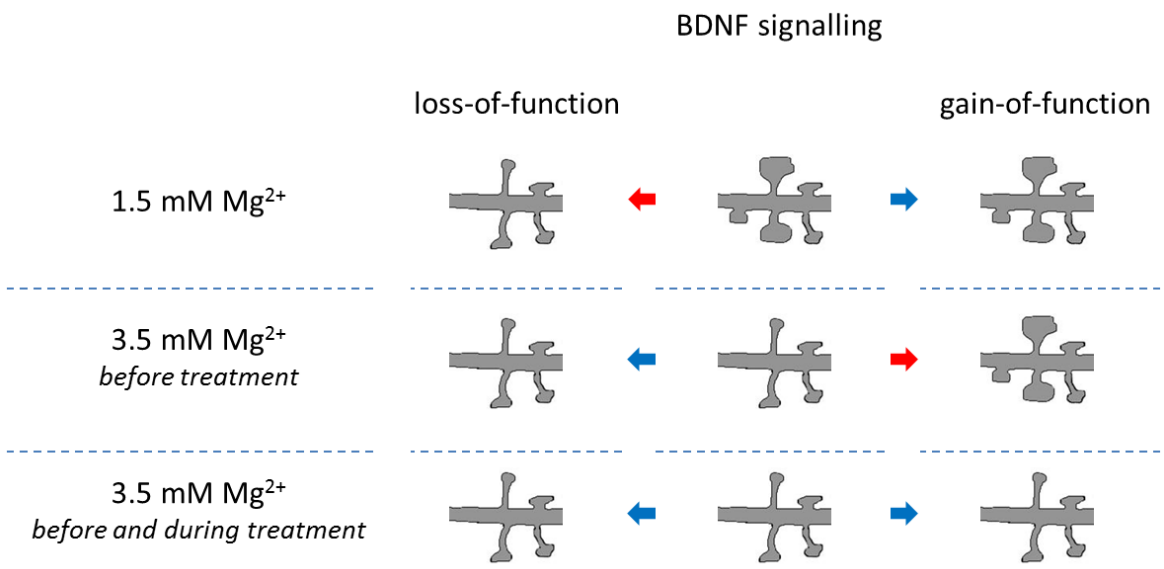

Figure 32: BDNF signalling regulates structural plasticity of dendritic spines in an activity-dependent manner. Scheme showing the effects of the gain- and loss-of-function of BDNF signalling on dendritic spines under three different neuronal excitability conditions. 1) basal neuronal excitability (1.5 mM Mg^{2+}), 2) low neuronal excitability (3.5 mM Mg^{2+}) before the treatment and 3) low neuronal excitability (3.5 mM Mg^{2+}) before and during treatment. Arrows: in red indicate structural changes, in blue no changes.

Moreover, in cerebellar cultures, BDNF increases the spine density of Purkinje cells only in the presence of granule cells suggesting a crucial role of neuronal activity in mediating this BDNF effect (Shimada et al., 1998). In line with these observations are the results from Tanaka et al. (2008) showing that indeed the dependence of BDNF in regulating structural changes at dendritic spines is activity-dependent in mature hippocampal neurons.

5.2.4 The actin cytoskeletal a targets of BDNF/TrkB signalling

Finally, I could show that endogenous BDNF modulates the actin cytoskeleton within dendritic spines in parallel to regulating their morphology. Filamentous actin is highly abundant and the main cytoskeleton component within dendritic spines (Fifková and Delay, 1982; Matus et al., 1982). Moreover, activity-dependent as well as spontaneous structural changes of dendritic spines are dependent on the modulation of actin dynamics within spines (Cingolani and Goda, 2008; Fukazawa et al., 2003; Krucker et al., 2000; Lin et al., 2005). Noteworthy in this context is the observation that BDNF modulates actin regulatory binding proteins which control the turnover of the actin cytoskeleton as well as cytoskeleton-associated proteins like Arc, LIMK1 and Homer (Bramham, 2008; Messaoudi et al., 2002, 2007; Rex et al., 2007; Schratt et al., 2004). Remarkably, these proteins are known to promote actin polymerization required for spine head maturation (Meng et al., 2002; Sala et al., 2001) and LTP consolidation (Bramham and Wells, 2007). Furthermore, the actin binding protein cortactin was shown to be involved in the maintenance of

dendritic spines (Hering and Sheng, 2003) and, interestingly, its localization at postsynaptic sites seems to be BDNF dependent (Iki et al., 2005). While the gain-of-function approach performed in this study did not affect the F-actin content within dendritic spines, the loss-of-function experiment resulted in a significant decrease in the F-actin content. The results of Rex et al. (2007) showed that exogenous application of BDNF to rat hippocampal slices increased the number of F-actin labelled spines only when theta burst stimulation was applied. Moreover, the effect of theta burst stimulation on F-actin was completely abolished by a BDNF scavenger (TrkB-Fc; Rex et al., 2007) suggesting a role for the TrkB receptor in this context. On the other hand, BDNF might also modulate actin dynamics via the $p75^{NTR}$. In a series of gain- and loss-of-function experiments it was previously shown that $p75^{NTR}$ negatively modulates dendritic spine density and morphology (Zagrebelsky et al., 2005), in addition to its effect on long-term depression (Rösch et al., 2005; Woo et al., 2005). It has been shown that signalling via the $p75^{NTR}$ controls the activity of the small GTPase RhoA, thereby regulating the actin cytoskeleton (Gehler et al., 2004; Yamashita and Tohyama, 2003; Yamashita et al., 1999) and possibly preparing it for processes of negative synaptic plasticity (spine loss and shrinkage). A recent study showed that BDNF signalling is required for the enlargement of the spine head mediated via Rac1 by a direct interaction between phosphorylated TrkB and Tiam1 (Lai et al., 2012). Suggesting that BDNF signalling might regulate the actin cytoskeleton via the Rac1 or RhoA pathway dependent on the respective receptor activation and by this BDNF may modulate synaptic plasticity.

5.2.5 Crosstalk between BDNF and Nogo-A signalling

BDNF as a member of the neurotrophin family is known to be a growth-promoting factor in the developing CNS, leading to growth cone expansion and neurite elongation (Gehler et al., 2004; McAllister et al., 1996, 1995, 1999). On the other hand, Nogo-A is well-known as myelin-associated growth suppressor leading to growth cone collapse and neurite retraction (Chen et al., 2000; Niederöst et al., 2002; Oertle et al., 2003). These opposing effects can be explained by the different regulation of the actin cytoskeleton within the growth cone. As described above Nogo-A signalling is transmitted to RhoA and further downstream to ADF/cofilin leading to a destabilization of the actin cytoskeleton (Hsieh et al., 2006; Montani et al., 2009). Whereas BDNF stabilizes the actin cytoskeleton by reducing the phosphorylation of ADF/cofilin (Gehler et al., 2004). Interestingly, also an opposing regulation of neurite growth specific proteins and transcription factors was reported, as BDNF promotes the phosphorylation of CREB (Mayr and Montminy, 2001) while Nogo-A signalling decreases CREB phosphorylation (Joset et al., 2010; Schwab, 2010). In the adult CNS BDNF levels are up-regulated by an increase of neural activity or

exercise (Vaynman and Gomez-Pinilla, 2005), conversely Nogo-A as well as the NgR1 are down regulated (Griesbach et al., 2009; Josephson et al., 2003). This is also reflected by their action during LTP, where BDNF promotes and Nogo-A restricts synaptic plasticity (for reviews see: Gottmann et al., 2009; Kempf and Schwab, 2013; Park and Poo, 2012; Schwab, 2010; Zagrebelsky and Korte, 2013). It is noteworthy that the NgR1 and the $p75^{NTR}$ build a receptor complex which could antagonize the activation of the BDNF-TrkB signalling in a 'yin and yang' like mechanism (Boyd and Gordon, 2001; Schwab, 2010). BDNF signalling increases cyclic AMP (cAMP) while the NgR1-$p75^{NTR}$ complex reduces via a G-protein the cAMP levels (Filbin, 2003; Gao et al., 2003; Joset et al., 2010). This antagonistic regulation of cAMP regulate the protein kinase A (PKA) which can control the RhoA-ROCK pathway as well as gene transcription, necessary to mediate long-term synaptic plasticity (Filbin, 2003; Lu et al., 2005). Further evidence for a crosstalk in the adult CNS between Nogo-A and BDNF signalling pathways derive from studies showing that a pre-incubation with BDNF reduces the response of primary neurons to myelin inhibitors like Nogo-A (Gao et al., 2003; Raiker et al., 2010). Furthermore, after an injury BDNF application antagonizes the lesion-induced up-regulation of Nogo-A in the hippocampus (Chytrova et al., 2008). In the *ngr1* KO mice Raiker et al. (2010) showed a constitutively elevated MAP kinase signalling (p-ERK) in the neocortex and hippocampus. The activation of the MAP kinase signalling can also be seen upon exogenous BDNF application in primary neurons (Ji et al., 2010) and is prevented by an application of Nogo-A (Raiker et al., 2010). On the other hand, Nogo-A and BDNF may interact in a cooperative manner: Karlén and colleagues (2009) hypothesise that the loss of the Nogo-A signalling together with cell adhesion molecules (Kleene and Schachner, 2004) play an important role in regulating functional and structural plasticity through restriction. After neutralisation of plasticity restricting proteins like Nogo-A axonal boutons and dendritic spines become temporarily unstable and capable of rearrangements in response to plasticity promoting factor like local increased of BDNF levels. (Lu, 2003; Karlén et al., 2009). Overall, the antagonistic relationship between the BDNF/TrkB and Nogo-A signalling pathway and function suggests a coordinated and highly regulated interaction; where BDNF signalling may suppresses Nogo-A action (or vice versa) and thereby maintain synaptic stability and plasticity.

5.3 Conclusions and outlook

In the present study, I started by correlating changes in actin dynamics within dendritic spines mediated by Nogo-A and their receptors with structural changes in their morphology. I could show that Nogo-A signalling rapidly modulates the spine actin cytoskeleton to control structural plasticity at dendritic spines of CA3 hippocampal pyramidal cells. Moreover, my data show that Nogo-A restricts the early reference memory formation during spatial learning as tested in the Morris water maze and negatively regulates structural plasticity at spine density of hippocampal neurons in this context. Taken together, this study indicates a crucial physiological function for Nogo-A in regulating the balance between stability and plasticity of mature neuronal networks in the adult hippocampus. By this activity, Nogo-A is possibly contributing to the maintenance of the spatial and temporal specificity of structural plasticity needed during learning processes.

The actin cytoskeleton was shown to be controlled by diverse signalling pathways to determine spine number, morphology and synaptic strength (Cingolani and Goda, 2008; Hotulainen and Hoogenraad, 2010; Matus, 2000; Okamoto et al., 2009). Actin, with its ability to transit between dynamic and stable states, is a prime candidate for mediating synaptic plasticity to ensure memory acquisition and consolidation (Lamprecht and LeDoux, 2004; Matus, 2000). Nogo-A signalling has been shown to modulate functional and structural plasticity in the adult CNS (Akbik et al., 2013; Delekate et al., 2011; Djurisic et al., 2013; Kempf et al., 2014; Lee et al., 2008; Mironova and Giger, 2013; Raiker et al., 2010). However, the intracellular pathways downstream of Nogo-A signalling in mature neurons and their synapses still need to be elucidated. In this thesis I could show that blocking Nogo-A signalling restricts actin cytoskeleton dynamic within single mature dendritic spines. On the other hand, the FRAP method does not allow imaging simultaneously several dendritic spines before and after interfering with the Nogo-A signalling. To gain further inside into how the different spine types react and also to study changes in the equilibrium between G- and F-actin a fluorescent energy transfer (FRET) actin imaging technique could be used (Okamoto and Hayashi, 2006; Okamoto et al., 2004). Moreover, single molecule detection techniques could be applied like Fluorescence correlation spectroscopy (FCS) or two-photon-FCS (2P-FCS) which belong to a class of non-invasive and extremely sensitive imaging techniques (Kim and Schwille, 2003; Kim et al., 2007). 2P-FCS provides access to the diffusion time, particle numbers and brightness of eGFP-actin in real time and allows fast temporal and high spatial resolution analysis of small F-actin filaments within dendritic spines (Chen and Kellner et al., under review). To combine these imaging techniques with the inhibition of the Nogo-A signalling would allow

to describe in detail its role in regulating the dynamics of actin filaments within dendritic spines and possibly to obtain some information about the signalling pathways mediating these effects. Indeed, to elucidate the intracellular pathways mediating the role of Nogo-A signalling in regulating actin dynamics within dendritic spines is crucial for understanding how Nogo-A restrict synaptic plasticity. Here I showed that ROCK inhibition mimics the effects seen after Nogo-A neutralisation on actin dynamics within spines pointing to a contribution of an actin cytoskeleton regulatory pathway involving the modulation via the RhoA/ROCK pathway and maybe the activation of cofilin via LIMK as recently shown from Bosch et al. (2014). To test whether Nogo-A signalling regulates the actin cytoskeleton via the above pathway, biochemical assays or the described imaging techniques could be used in combination with an acute blocking of RhoA with C3 transferase (Borasio et al., 1989; Niederöst et al., 2002), LIMK with the inhibitor 1-16-peptide (Bosch et al., 2014) and cofilin with S3-peptide (Aizawa et al., 2001). Neutralising Nogo-A signalling induces an increase in dendritic spine density (Kellner et al., under review) and an increase of the stable actin fraction has which been shown to be sufficient to induce spinogenesis (Zito et al., 2004). The here observed stabilization of the actin cytoskeleton within preexisting spines up Nogo-A blocking cannot directly be correlated to the gain of new spines (Kellner et al., under review). It would be interesting to further examine how Nogo-A signalling regulates spinogenesis and whether the actin cytoskeleton is involved. In addition, an increased F-actin stabilization is sufficient to promote spine elongation (Zito et al., 2004). Here a significant positive correlation between the amount of stable actin and the change in length could be observed only for elongating spines. This indicates that Nogo-A acutely modulates dendritic spine shape by stabilizing the spine actin cytoskeleton in a rapid and transitory manner. Time-lapse imaging experiments monitoring the spine morphology and actin dynamics (e.g. with 2P-FCS) in parallel are necessary to further clarify this issue.

In all experiments performed in this thesis Nogo-A signalling was blocked via a bath application of the respective antibodies or blockers resulting in a global loss-of-function for the entire network. Using this experimental design it is not possible to distinguish if the effect observed on dendritic spines of CA3 hippocampal neurons is due to a local action on individual synapse or is secondary to changes at the network level. To address this question, local applications by puffing Nogo-Ab blocking antibodies on defined dendritic stretches could be used. Furthermore, this approach will provide a precise temporal control on the Nogo-A neutralisation. Recent data show that Nogo-A neutralisation in primary hippocampal neurons results in the fast insertion of AMPA receptors at synaptic sites (Kellner et al., under review). To test the hypothesis of whether the changes in spine morphology and actin dynamics upon Nogo-A neutralisation are secondary to changes in network activity a pre-treatment with tetrodotoxin could be used to block neuronal activity.

Further time-lapse imaging and FRAP experiments comparing different levels in neuronal activity are necessary to test this hypothesis. Moreover, to test for a role of Nogo-A in regulating activity-dependent structural plasticity at spines, its neutralisation could be combined with the chemical induction of LTP. Several studies showed that Nogo-A and their receptors influence Hebbian forms of synaptic plasticity (Delekate et al., 2011; Kempf et al., 2014; Lee et al., 2008; Raiker et al., 2010). Nevertheless, it is not clear whether and how Nogo-A signalling is regulated in an activity-dependent manner. A local regulatory mechanism such as activity-dependent insertion, internalisation or cleavage at synaptic sites of Nogo-A or its receptors, may be achieved rapidly and with high temporal and spatial specificity allowing or restricting changes at individual synapses (Mironova and Giger, 2013). To address this question, an approach is required allowing to detect the movement of Nogo-A or its receptors at a single molecule level over time by simultaneously altering neuronal activity. 2P-FCS or photoactivation might be used at single synapses in cells expressing Nogo-A, NgR1 or S1P2R tagged either with eGFP or with a photoactivatable eGFP. To avoid unspecific effects due to the overexpression, the expression of the tagged molecules should be controlled by the correspondent endogenous promoter.

Activity and experience-dependent changes in the shape and number of dendritic spines have been correlated to learning processes and memory formation (Holtmaat and Svoboda, 2009; O'Malley et al., 2000; Xu et al., 2009; Yang et al., 2009a). Whether the changes in spine density occurring upon Nogo-A neutralisation (Kellner et al., under review) might be correlated to an improvement in spatial learning was tested in the Morris water maze. In line with my observation, previous studies showed that *nogo-a* KO and WT mice learned equally well to locate the hidden platform during the Morris water maze test (Willi et al., 2008). Also the over expression of the Nogo receptor 1 revealed similar results but a probe trail performed after 39 days showed a clear impairment in long-term memory consolidation (Karlén et al., 2009). Finally, the early and transient advantage of *nogo-a* KO mice in forming a reference memory tested in the probe trail at day 3 indicates a role for Nogo-A in restricting the initial acquisition phase. To draw a conclusion about whether Nogo-A is needed for long-term memory consolidation a later 3rd probe trial beyond day 9 should be performed.

In the second topic addressed in this thesis, I could elucidate the essential physiological functions of endogenous BDNF in maintaining dendritic spine density and a mature spine morphology in excitatory hippocampal neurons. Additionally I could confirm that BDNF is required for the activity-dependent structural plasticity of dendritic spines. In addition, results presented here shed some light on why published *in vivo* and *in vitro* results

concerning morphological effects of BDNF are often contradictory: while previous *in vivo* work showed a specific selectivity in the brain areas requiring BDNF-signalling for their post-natal development (Minichiello et al., 1999; Rauskolb et al., 2010; Zakharenko et al., 2003), most of the *in vitro* work describes a strong effect for a BDNF gain-of-function (Tyler and Pozzo-Miller, 2001, 2003; Ji et al., 2005, 2010). My observations here suggest rather that different culture conditions and also different levels of neuronal activity are responsible for this discrepancy (Kellner et al., 2014). However, to finally demonstrate that the role of BDNF signalling on structural plasticity at spines is activity-dependent regulated, further experiments with electrical or chemical induced LTP combined with gain-or loss-of-function experiments are necessary. Microglia are myeloid cells that occupy all regions of the CNS and although their role has been extensively studied, their contribution to normal CNS function remains unclear. In a recent study Parkhurst et al., (2013) show that microglia promote learning-induced formation of synapses and that this effect is mediated by microglial BDNF. As a consequence, it is necessary to determine the quantity of microglia in the culture system to clarify if the discrepancies aforementioned are due to the content of microglia BDNF. Furthermore under high magnesium concentration (with low neuronal activity conditions) I observed an increased neuronal responsiveness to BDNF. Whether this effect is due to an activity-dependent decrease in BDNF release from neurons or, from microglia will be very interesting to address.

The effects of endogenous BDNF in modulating the architecture of neurons seem to be depending on their developmental stage and for dendritic spines also on the brain region as well as the cell-type (Rauskolb et al., 2010; Zagrebelsky and Korte, 2013). Here, I focus only at excitatory hippocampal neurons. To clarify the cell type specificity of BDNF, it is required to analyse the effects of endogenous BDNF *in vivo* on excitatory and inhibitory neurons within the same brain regions. In my study I used fixed time points after the gain- and loss-of-function experiments. Consequently only the time point of fixation could be examined. Live imaging experiments would help to analyse fast events and provide more details about what kind of spines change their morphology and their temporal characteristics upon an alteration of BDNF signalling. Tanaka and colleague (2008) showed indeed with time-lapse imaging that the activity of BDNF in regulating structural changes at dendritic spines depends on activity. They artificially supplied the neurons with the cytoskeletal protein β-actin to observe activity-dependent spine head enlargements. Therefore it remains an open issue whether BDNF signalling contributes to acute structural changes under physiological conditions and whether the actin cytoskeleton in spines is a denominator on which BDNF signalling controls spine morphology. Furthermore, it is interesting to investigate how BDNF regulates actin

dynamics at individual dendritic spines by combing gain- and loss-of-function experiments for BDNF with FRAP experiments.

Finally, BDNF and Nogo-A may interact in a cooperative manner to modulate the spatial and temporal specificity of functional and structural plasticity by promoting or restricting plasticity, respectively (Karlén et al., 2009). In this context it is interesting to do further experiments combining specific gain- and loss-of-function experiments for both BDNF and Nogo-A signalling pathways to further elucidate the fascinating mechanisms modulating synaptic plasticity *versus* synaptic stability in correlation to learning and memory processes.

6 References

Ackermann, M., and Matus, A. (2003). Activity-induced targeting of profilin and stabilization of dendritic spine morphology. Nat. Neurosci. *6*, 1194–1200.

Aizawa, H., Wakatsuki, S., Ishii, A., Moriyama, K., Sasaki, Y., Ohashi, K., Sekine-Aizawa, Y., Sehara-Fujisawa, A., Mizuno, K., Goshima, Y., et al. (2001). Phosphorylation of cofilin by LIM-kinase is necessary for semaphorin 3A-induced growth cone collapse. Nat. Neurosci. *4*, 367–373.

Akbik, F. V, Bhagat, S.M., Patel, P.R., Cafferty, W.B.J., and Strittmatter, S.M. (2013). Anatomical plasticity of adult brain is titrated by Nogo Receptor 1. Neuron *77*, 859–866.

Allison, D.W., Gelfand, V.I., Spector, I., and Craig, A.M. (1998). Role of actin in anchoring postsynaptic receptors in cultured hippocampal neurons: differential attachment of NMDA versus AMPA receptors. J. Neurosci. *18*, 2423–2436.

Aloy, E.M., Weinmann, O., Pot, C., Kasper, H., Dodd, D.A., Rülicke, T., Rossi, F., and Schwab, M.E. (2006). Synaptic destabilization by neuronal Nogo-A. Brain Cell Biol. *35*, 137–156.

Alvarez, P., Zola-Morgan, S., and Squire, L.R. (1994). The animal model of human amnesia: long-term memory impaired and short-term memory intact. Proc. Natl. Acad. Sci. U. S. A. *91*, 5637–5641.

An, J.J., Gharami, K., Liao, G.-Y., Woo, N.H., Lau, A.G., Vanevski, F., Torre, E.R., Jones, K.R., Feng, Y., Lu, B., et al. (2008). Distinct role of long 3' UTR BDNF mRNA in spine morphology and synaptic plasticity in hippocampal neurons. Cell *134*, 175–187.

Andersen, P., Bliss, T. V, and Skrede, K.K. (1971). Lamellar organization of hippocampal pathways. Exp. Brain Res. *13*, 222–238.

Andrianantoandro, E., and Pollard, T.D. (2006). Mechanism of actin filament turnover by severing and nucleation at different concentrations of ADF/cofilin. Mol. Cell *24*, 13–23.

Araya, R., Jiang, J., Eisenthal, K.B., and Yuste, R. (2006). The spine neck filters membrane potentials. Proc. Natl. Acad. Sci. U. S. A. *103*, 17961–17966.

Arber, S., Barbayannis, F.A., Hanser, H., Schneider, C., Stanyon, C.A., Bernard, O., and Caroni, P. (1998). Regulation of actin dynamics through phosphorylation of cofilin by LIM-kinase. Nature *393*, 805–809.

Atwal, J.K., Pinkston-Gosse, J., Syken, J., Stawicki, S., Wu, Y., Shatz, C., and Tessier-Lavigne, M. (2008). PirB is a functional receptor for myelin inhibitors of axonal regeneration. Science *322*, 967–970.

Bailey, C.H., and Kandel, E.R. (1993). Structural changes accompanying memory storage. Annu. Rev. Physiol. *55*, 397–426.

Bamburg, J.R., and Bernstein, B.W. (2010). Roles of ADF/cofilin in actin polymerization and beyond. F1000 Biol. Rep. *2*, 62.

Bamburg, J.R., Harris, H.E., and Weeds, A.G. (1980). Partial purification and characterization of an actin depolymerizing factor from brain. FEBS Lett. *121*, 178–182.

Bandtlow, C.E., Schmidt, M.F., Hassinger, T.D., Schwab, M.E., and Kater, S.B. (1993). Role of intracellular calcium in NI-35-evoked collapse of neuronal growth cones. Science *259*, 80–83.

Baquet, Z.C., Gorski, J. a, and Jones, K.R. (2004). Early striatal dendrite deficits followed by neuron loss with advanced age in the absence of anterograde cortical brain-derived neurotrophic factor. J. Neurosci. *24*, 4250–4258.

Bareyre, F.M., Haudenschild, B., and Schwab, M.E. (2002). Long-lasting sprouting and gene expression changes induced by the monoclonal antibody IN-1 in the adult spinal cord. J. Neurosci. *22*, 7097–7110.

Berninger, B., García, D.E., Inagaki, N., Hahnel, C., and Lindholm, D. (1993). BDNF and NT-3 induce intracellular Ca2+ elevation in hippocampal neurones. Neuroreport *4*, 1303–1306.

Bibel, M. (2000). Neurotrophins: key regulators of cell fate and cell shape in the vertebrate nervous system. Genes Dev. *14*, 2919–2937.

Bliss, T. V, and Collingridge, G.L. (1993). A synaptic model of memory: long-term potentiation in the hippocampus. Nature *361*, 31–39.

Bliss, T. V, and Lomo, T. (1973). Long-lasting potentiation of synaptic transmission in the dentate area of the anaesthetized rabbit following stimulation of the perforant path. J. Physiol. *232*, 331–356.

Bloodgood, B.L., and Sabatini, B.L. (2005). Neuronal activity regulates diffusion across the neck of dendritic spines. Science *310*, 866–869.

Blum, R., and Konnerth, A. (2005). Neurotrophin-mediated rapid signaling in the central nervous system: mechanisms and functions. Physiology (Bethesda). *20*, 70–78.

Von Bohlen und Halbach, O. (2010). Involvement of BDNF in age-dependent alterations in the hippocampus. Front. Aging Neurosci. *2*.

Bonhoeffer, T., and Yuste, R. (2002). Spine motility. Phenomenology, mechanisms, and function. Neuron *35*, 1019–1027.

Borasio, G.D., John, J., Wittinghofer, A., Barde, Y.A., Sendtner, M., and Heumann, R. (1989). ras p21 protein promotes survival and fiber outgrowth of cultured embryonic neurons. Neuron *2*, 1087–1096.

Bosch, M., Castro, J., Saneyoshi, T., Matsuno, H., Sur, M., and Hayashi, Y. (2014). Structural and Molecular Remodeling of Dendritic Spine Substructures during Long-Term Potentiation. Neuron *82*, 444–459.

Bourne, J.N., Chirillo, M. a, and Harris, K.M. (2013). Presynaptic ultrastructural plasticity along CA3→CA1 axons during long-term potentiation in mature hippocampus. J. Comp. Neurol. *521*, 3898–3912.

Boyd, J.G., and Gordon, T. (2001). The neurotrophin receptors, trkB and p75, differentially regulate motor axonal regeneration. J. Neurobiol. *49*, 314–325.

Boyer, C., Schikorski, T., and Stevens, C.F. (1998). Comparison of hippocampal dendritic spines in culture and in brain. J. Neurosci. *18*, 5294–5300.

Bramham, C.R. (2008). Local protein synthesis, actin dynamics, and LTP consolidation. Curr. Opin. Neurobiol. *18*, 524–531.

Bramham, C.R., and Wells, D.G. (2007). Dendritic mRNA: transport, translation and function. Nat. Rev. Neurosci. *8*, 776–789.

Bridgman, P.C. (2004). Myosin-dependent transport in neurons. J. Neurobiol. *58*, 164–174.

Brody, D.L., and Holtzman, D.M. (2006). Morris water maze search strategy analysis in PDAPP mice before and after experimental traumatic brain injury. Exp. Neurol. *197*, 330–340.

Bubb, M.R., Senderowicz, A.M., Sausville, E.A., Duncan, K.L., and Korn, E.D. (1994). Jasplakinolide, a cytotoxic natural product, induces actin polymerization and competitively inhibits the binding of phalloidin to F-actin. J. Biol. Chem. *269*, 14869–14871.

Burgess, N., Maguire, E.A., and O'Keefe, J. (2002). The Human Hippocampus and Spatial and Episodic Memory. Neuron *35*, 625–641.

Cajal, R. y (1899). Textura del Sistema Nervioso del Hombre y de los Vertebrados.

Canossa, M., Griesbeck, O., Berninger, B., Campana, G., Kolbeck, R., and Thoenen, H. (1997). Neurotrophin release by neurotrophins: implications for activity-dependent neuronal plasticity. Proc. Natl. Acad. Sci. U. S. A. *94*, 13279–13286.

Carlier, M.F., Laurent, V., Santolini, J., Melki, R., Didry, D., Xia, G.X., Hong, Y., Chua, N.H., and Pantaloni, D. (1997). Actin depolymerizing factor (ADF/cofilin) enhances the rate of filament turnover: implication in actin-based motility. J. Cell Biol. *136*, 1307–1322.

Caroni, P., Donato, F., and Muller, D. (2012). Structural plasticity upon learning: regulation and functions. Nat. Rev. Neurosci. *13*, 478–490.

Carretón, O., Giralt, A., Torres-Peraza, J.F., Brito, V., Lucas, J.J., Ginés, S., Canals, J.M., and Alberch, J. (2012). Age-dependent decline of motor neocortex but not hippocampal performance in heterozygous BDNF mice correlates with a decrease of cortical PSD-95 but an increase of hippocampal TrkB levels. Exp. Neurol. *237*, 335–345.

Chan, J.R., Jolicoeur, C., Yamauchi, J., Elliott, J., Fawcett, J.P., Ng, B.K., and Cayouette, M. (2006). The polarity protein Par-3 directly interacts with p75NTR to regulate myelination. Science *314*, 832–836.

Chao, M. V (2003). Neurotrophins and their receptors: a convergence point for many signalling pathways. Nat. Rev. Neurosci. *4*, 299–309.

Chapleau, C.A., Carlo, M.E., Larimore, J.L., and Pozzo-Miller, L. (2008). The actions of BDNF on dendritic spine density and morphology in organotypic slice cultures depend on the presence of serum in culture media. J. Neurosci. Methods *169*, 182–190.

Chen, G., Kolbeck, R., Barde, Y. a, Bonhoeffer, T., and Kossel, a (1999). Relative contribution of endogenous neurotrophins in hippocampal long-term potentiation. J. Neurosci. *19*, 7983–7990.

Chen, M.S., Huber, A.B., van der Haar, M.E., Frank, M., Schnell, L., Spillmann, A.A., Christ, F., and Schwab, M.E. (2000). Nogo-A is a myelin-associated neurite outgrowth inhibitor and an antigen for monoclonal antibody IN-1. Nature *403*, 434–439.

Chen, Z.-Y., Jing, D., Bath, K.G., Ieraci, A., Khan, T., Siao, C.-J., Herrera, D.G., Toth, M., Yang, C., McEwen, B.S., et al. (2006). Genetic variant BDNF (Val66Met) polymorphism alters anxiety-related behavior. Science *314*, 140–143.

Chytrova, G., Ying, Z., and Gomez-Pinilla, F. (2008). Exercise normalizes levels of MAG and Nogo-A growth inhibitors after brain trauma. Eur. J. Neurosci. *27*, 1–11.

Cingolani, L. a, and Goda, Y. (2008). Actin in action: the interplay between the actin cytoskeleton and synaptic efficacy. Nat. Rev. Neurosci. *9*, 344–356.

Citri, A., and Malenka, R.C. (2008). Synaptic plasticity: multiple forms, functions, and mechanisms. Neuropsychopharmacology *33*, 18–41.

Cohen, S., Levi-Montalcini, R., and Hamburger, V. (1954). A NERVE GROWTH-STIMULATING FACTOR ISOLATED FROM SARCOM AS 37 AND 180. Proc. Natl. Acad. Sci. U. S. A. *40*, 1014–1018.

Conde, C., and Cáceres, A. (2009). Microtubule assembly, organization and dynamics in axons and dendrites. Nat. Rev. Neurosci. *10*, 319–332.

Cooper, J. a (1987). Effects of cytochalasin and phalloidin on actin. J. Cell Biol. *105*, 1473–1478.

Craveiro, L.M., Hakkoum, D., Weinmann, O., Montani, L., Stoppini, L., and Schwab, M.E. (2008). Neutralization of the membrane protein Nogo-A enhances growth and reactive sprouting in established organotypic hippocampal slice cultures. Eur. J. Neurosci. *28*, 1808–1824.

Crick, F. (1982). Do dendritic spines twitch? Trends Neurosci. *5*, 44–46.

Dailey, M.E., and Smith, S.J. (1996). The dynamics of dendritic structure in developing hippocampal slices. J. Neurosci. *16*, 2983–2994.

Danzer, S.C., Pan, E., Nef, S., Parada, L.F., and McNamara, J.O. (2004). Altered regulation of brain-derived neurotrophic factor protein in hippocampus following slice preparation. Neuroscience *126*, 859–869.

Delekate, A., Zagrebelsky, M., Kramer, S., Schwab, M.E., and Korte, M. (2011). NogoA restricts synaptic plasticity in the adult hippocampus on a fast time scale. Proc. Natl. Acad. Sci. U. S. A. *108*, 2569–2574.

Derkach, V.A., Oh, M.C., Guire, E.S., and Soderling, T.R. (2007). Regulatory mechanisms of AMPA receptors in synaptic plasticity. Nat. Rev. Neurosci. *8*, 101–113.

Dieni, S., Matsumoto, T., Dekkers, M., Rauskolb, S., Ionescu, M.S., Deogracias, R., Gundelfinger, E.D., Kojima, M., Nestel, S., Frotscher, M., et al. (2012). BDNF and its pro-peptide are stored in presynaptic dense core vesicles in brain neurons. J. Cell Biol. *196*, 775–788.

Dillon, C., and Goda, Y. (2005). The actin cytoskeleton: integrating form and function at the synapse. Annu. Rev. Neurosci. *28*, 25–55.

Dimou, L., Schnell, L., Montani, L., Duncan, C., Simonen, M., Schneider, R., Liebscher, T., Gullo, M., and Schwab, M.E. (2006). Nogo-A-deficient mice reveal strain-dependent differences in axonal regeneration. J. Neurosci. *26*, 5591–5603.

Djurisic, M., Vidal, G.S., Mann, M., Aharon, A., Kim, T., Ferrao Santos, A., Zuo, Y., Hübener, M., and Shatz, C.J. (2013). PirB regulates a structural substrate for cortical plasticity. Proc. Natl. Acad. Sci. U. S. A. *110*, 20771–20776.

Dodd, D.A., Niederoest, B., Bloechlinger, S., Dupuis, L., Loeffler, J.P., and Schwab, M.E. (2005a). Nogo-A, -B, and -C are found on the cell surface and interact together in many different cell types. J.Biol.Chem. *280*, 12494–12502.

Domeniconi, M., Cao, Z., Spencer, T., Sivasankaran, R., Wang, K., Nikulina, E., Kimura, N., Cai, H., Deng, K., Gao, Y., et al. (2002). Myelin-associated glycoprotein interacts with the Nogo66 receptor to inhibit neurite outgrowth. Neuron *35*, 283–290.

Dribben, W.H., Eisenman, L.N., and Mennerick, S. (2010). Magnesium induces neuronal apoptosis by suppressing excitability. Cell Death Dis. *1*, e63.

Edwards, F.A. (1998). Dancing dendrites. Nature *394*, 129–130.

Eichenbaum, H. (2004). Hippocampus: cognitive processes and neural representations that underlie declarative memory. Neuron *44*, 109–120.

Engert, F., and Bonhoeffer, T. (1999). Dendritic spine changes associated with hippocampal long-term synaptic plasticity. Nature *399*, 66–70.

Erickson, K.I., Voss, M.W., Prakash, R.S., Basak, C., Szabo, A., Chaddock, L., Kim, J.S., Heo, S., Alves, H., White, S.M., et al. (2011). Exercise training increases size of hippocampus and improves memory. Proc. Natl. Acad. Sci. U. S. A. *108*, 3017–3022.

Fifková, E., and Delay, R.J. (1982). Cytoplasmic actin in neuronal processes as a possible mediator of synaptic plasticity. J. Cell Biol. *95*, 345–350.

Filbin, M.T. (2003). Myelin-associated inhibitors of axonal regeneration in the adult mammalian CNS. Nat. Rev. Neurosci. *4*, 703–713.

Finkbeiner, S., Tavazoie, S.F., Maloratsky, A., Jacobs, K.M., Harris, K.M., and Greenberg, M.E. (1997). CREB: A Major Mediator of Neuronal Neurotrophin Responses. Neuron *19*, 1031–1047.

Fischer, M., Kaech, S., Knutti, D., and Matus, A. (1998). Rapid actin-based plasticity in dendritic spines. Neuron *20*, 847–854.

Fournier, A.E., GrandPre, T., and Strittmatter, S.M. (2001). Identification of a receptor mediating Nogo-66 inhibition of axonal regeneration. Nature *409*, 341–346.

Fukazawa, Y., Saitoh, Y., Ozawa, F., Ohta, Y., Mizuno, K., and Inokuchi, K. (2003). Hippocampal LTP is accompanied by enhanced F-actin content within the dendritic spine that is essential for late LTP maintenance in vivo. Neuron *38*, 447–460.

Gao, Y., Nikulina, E., Mellado, W., and Filbin, M.T. (2003). Neurotrophins elevate cAMP to reach a threshold required to overcome inhibition by MAG through extracellular signal-regulated kinase-dependent inhibition of phosphodiesterase. J. Neurosci. *23*, 11770–11777.

Garthe, A., and Kempermann, G. (2013). An old test for new neurons: refining the Morris water maze to study the functional relevance of adult hippocampal neurogenesis. Front. Neurosci. *7*, 63.

Garthe, A., Behr, J., and Kempermann, G. (2009). Adult-generated hippocampal neurons allow the flexible use of spatially precise learning strategies. PLoS One *4*, e5464.

Gärtner, A., and Staiger, V. (2002). Neurotrophin secretion from hippocampal neurons evoked by long-term-potentiation-inducing electrical stimulation patterns. Proc. Natl. Acad. Sci. U. S. A. *99*, 6386–6391.

Gascon, E., Vutskits, L., Zhang, H., Barral-Moran, M.J., Kiss, P.J., Mas, C., and Kiss, J.Z. (2005). Sequential activation of p75 and TrkB is involved in dendritic development of subventricular zone-derived neuronal progenitors in vitro. Eur. J. Neurosci. *21*, 69–80.

Gehler, S., Shaw, A.E., Sarmiere, P.D., Bamburg, J.R., and Letourneau, P.C. (2004). Brain-derived neurotrophic factor regulation of retinal growth cone filopodial dynamics is mediated through actin depolymerizing factor/cofilin. J. Neurosci. *24*, 10741–10749.

Genoud, C., Knott, G.W., Sakata, K., Lu, B., and Welker, E. (2004). Altered synapse formation in the adult somatosensory cortex of brain-derived neurotrophic factor heterozygote mice. J. Neurosci. *24*, 2394–2400.

Gödecke, N. (2012). Neurotrophin Evolution – Funktionelle Analyse des Neurotrophins BDNF aus Danio rerio und Mammalia. Masterarbeit.

Goldschmidt-Clermont, P.J., Furman, M.I., Wachsstock, D., Safer, D., Nachmias, V.T., and Pollard, T.D. (1992). The control of actin nucleotide exchange by thymosin beta 4 and profilin. A potential regulatory mechanism for actin polymerization in cells. Mol. Biol. Cell *3*, 1015–1024.

Gonzales, R.B., DeLeon Galvan, C.J., Rangel, Y.M., and Claiborne, B.J. (2001). Distribution of thorny excrescences on CA3 pyramidal neurons in the rat hippocampus. J. Comp. Neurol. *430*, 357–368.

Gordon, J.A., and Stryker, M.P. (1996). Experience-dependent plasticity of binocular responses in the primary visual cortex of the mouse. J. Neurosci. *16*, 3274–3286.

Gorski, J.A., Balogh, S.A., Wehner, J.M., and Jones, K.R. (2003). Learning deficits in forebrain-restricted brain-derived neurotrophic factor mutant mice. Neuroscience *121*, 341–354.

Gottmann, K., Mittmann, T., and Lessmann, V. (2009). BDNF signaling in the formation, maturation and plasticity of glutamatergic and GABAergic synapses. Exp. Brain Res. *199*, 203–234.

GrandPré, T., Nakamura, F., Vartanian, T., and Strittmatter, S.M. (2000). Identification of the Nogo inhibitor of axon regeneration as a Reticulon protein. Nature *403*, 439–444.

Griesbach, G.S., Hovda, D.A., and Gomez-Pinilla, F. (2009). Exercise-induced improvement in cognitive performance after traumatic brain injury in rats is dependent on BDNF activation. Brain Res. *1288*, 105–115.

Gu, J., Lee, C.W., Fan, Y., Komlos, D., Tang, X., Sun, C., Yu, K., Hartzell, H.C., Chen, G., Bamburg, J.R., et al. (2010). ADF/cofilin-mediated actin dynamics regulate AMPA receptor trafficking during synaptic plasticity. Nat. Neurosci. *13*, 1208–1215.

Harris, K.M., and Stevens, J.K. (1989). Dendritic spines of CA 1 pyramidal cells in the rat hippocampus: serial electron microscopy with reference to their biophysical characteristics. J. Neurosci. *9*, 2982–2997.

He, X.-P., Kotloski, R., Nef, S., Luikart, B.W., Parada, L.F., and McNamara, J.O. (2004). Conditional deletion of TrkB but not BDNF prevents epileptogenesis in the kindling model. Neuron *43*, 31–42.

Hebb, D.O. (1949). The Organization of Behavior: A Neuropsychological Theory (Wiley).

Hering, H., and Sheng, M. (2001). Dendritic spines: structure, dynamics and regulation. Nat. Rev. Neurosci. *2*, 880–888.

Hering, H., and Sheng, M. (2003). Activity-dependent redistribution and essential role of cortactin in dendritic spine morphogenesis. J. Neurosci. *23*, 11759–11769.

Hofer, S.B., Mrsic-Flogel, T.D., Bonhoeffer, T., and Hübener, M. (2009). Experience leaves a lasting structural trace in cortical circuits. Nature *457*, 313–317.

Holthoff, K., Zecevic, D., and Konnerth, A. (2010). Rapid time course of action potentials in spines and remote dendrites of mouse visual cortex neurons. J. Physiol. *588*, 1085–1096.

Holtmaat, A., and Svoboda, K. (2009). Experience-dependent structural synaptic plasticity in the mammalian brain. Nat. Rev. Neurosci. *10*, 647–658.

Holtmaat, A., Wilbrecht, L., Knott, G.W., Welker, E., and Svoboda, K. (2006). Experience-dependent and cell-type-specific spine growth in the neocortex. Nature *441*, 979–983.

Hong, E.J., McCord, A.E., and Greenberg, M.E. (2008). A biological function for the neuronal activity-dependent component of Bdnf transcription in the development of cortical inhibition. Neuron *60*, 610–624.

Honkura, N., Matsuzaki, M., Noguchi, J., Ellis-Davies, G.C.R., and Kasai, H. (2008). The subspine organization of actin fibers regulates the structure and plasticity of dendritic spines. Neuron *57*, 719–729.

Horch, H.W., Krüttgen, a, Portbury, S.D., and Katz, L.C. (1999). Destabilization of cortical dendrites and spines by BDNF. Neuron *23*, 353–364.

Hotulainen, P., and Hoogenraad, C.C. (2010). Actin in dendritic spines: connecting dynamics to function. J. Cell Biol. *189*, 619–629.

Hotulainen, P., Llano, O., Smirnov, S., Tanhuanpää, K., Faix, J., Rivera, C., and Lappalainen, P. (2009). Defining mechanisms of actin polymerization and depolymerization during dendritic spine morphogenesis. J. Cell Biol. *185*, 323–339.

Hsieh, S.H.-K., Ferraro, G.B., and Fournier, A.E. (2006). Myelin-associated inhibitors regulate cofilin phosphorylation and neuronal inhibition through LIM kinase and Slingshot phosphatase. J. Neurosci. *26*, 1006–1015.

Huang, E.J., and Reichardt, L.F. (2001). Neurotrophins: roles in neuronal development and function. Annu. Rev. Neurosci. *24*, 677–736.

Hubel, D.H., and Wiesel, T.N. (1962). Receptive fields, binocular interaction and functional architecture in the cat's visual cortex. J. Physiol. *160*, 106–154.

Huber, A.B., Weinmann, O., Brösamle, C., Oertle, T., and Schwab, M.E. (2002). Patterns of Nogo mRNA and protein expression in the developing and adult rat and after CNS lesions. J. Neurosci. *22*, 3553–3567.

Huber, L., Menzel, R., Matsuzaki, M., Honkura, N., and Ellis-Davies, G. (2004). Structural basis of long-term potentiation in single dendritic spines. Nature *429*.

Hunt, D., Mason, M.R.J., Campbell, G., Coffin, R., and Anderson, P.N. (2002). Nogo receptor mRNA expression in intact and regenerating CNS neurons. Mol. Cell. Neurosci. *20*, 537–552.

Iki, J., Inoue, A., Bito, H., and Okabe, S. (2005). Bi-directional regulation of postsynaptic cortactin distribution by BDNF and NMDA receptor activity. Eur. J. Neurosci. *22*, 2985–2994.

Imagama, S., Sakamoto, K., Tauchi, R., Shinjo, R., Ohgomori, T., Ito, Z., Zhang, H., Nishida, Y., Asami, N., Takeshita, S., et al. (2011). Keratan Sulfate Restricts Neural Plasticity after Spinal Cord Injury. J. Neurosci. *31*, 17091–17102.

Ishizuka, N., Weber, J., and Amaral, D.G. (1990). Organization of intrahippocampal projections originating from CA3 pyramidal cells in the rat. J. Comp. Neurol. *295*, 580–623.

Ishizuka, N., Cowan, W.M., and Amaral, D.G. (1995). A quantitative analysis of the dendritic organization of pyramidal cells in the rat hippocampus. J. Comp. Neurol. *362*, 17–45.

Izeddin, I., Specht, C.G., Lelek, M., Darzacq, X., Triller, A., Zimmer, C., and Dahan, M. (2011). Super-resolution dynamic imaging of dendritic spines using a low-affinity photoconvertible actin probe. PLoS One *6*, e15611.

Ji, Y., Pang, P.T., Feng, L., and Lu, B. (2005). Cyclic AMP controls BDNF-induced TrkB phosphorylation and dendritic spine formation in mature hippocampal neurons. Nat. Neurosci. *8*, 164–172.

Ji, Y., Lu, Y., Yang, F., Shen, W., Tang, T.T.-T., Feng, L., Duan, S., and Lu, B. (2010). Acute and gradual increases in BDNF concentration elicit distinct signaling and functions in neurons. Nat. Neurosci. *13*, 302–309.

Josephson, A., Trifunovski, A., Schéele, C., Widenfalk, J., Wahlestedt, C., Brené, S., Olson, L., and Spenger, C. (2003). Activity-induced and developmental downregulation of the Nogo receptor. Cell Tissue Res. *311*, 333–342.

Joset, A., Dodd, D. a, Halegoua, S., and Schwab, M.E. (2010). Pincher-generated Nogo-A endosomes mediate growth cone collapse and retrograde signaling. J. Cell Biol. *188*, 271–285.

Kandel, E.R. (2001). The molecular biology of memory storage: a dialogue between genes and synapses. Science *294*, 1030–1038.

Kang, M.-G., Guo, Y., and Huganir, R.L. (2009). AMPA receptor and GEF-H1/Lfc complex regulates dendritic spine development through RhoA signaling cascade. Proc. Natl. Acad. Sci. U. S. A. *106*, 3549–3554.

Karlén, A., Karlsson, T.E., Mattsson, A., Lundstro, K., Codeluppi, S., Pham, T.M., Åberg, E., Hoffman, A.F., Sherling, M.A., Lupica, C.R., et al. (2009). Nogo receptor 1 regulates formation of lasting memories. Proc. Natl. Acad. Sci. U. S. A. *106*, 20476–20481.

Karlsson, T.E., Koczy, J., Brené, S., Olson, L., and Josephson, A. (2013). Differential conserted activity induced regulation of Nogo receptors (1-3), LOTUS and Nogo mRNA in mouse brain. PLoS One *8*, e60892.

Kasai, H. (2003). Structure–stability–function relationships of dendritic spines. Trends Neurosci. *26*, 360–368.

Kasai, H., Fukuda, M., Watanabe, S., Hayashi-Takagi, A., and Noguchi, J. (2010). Structural dynamics of dendritic spines in memory and cognition. Trends Neurosci. *33*, 121–129.

Kelley, K.W. (2008). NIH public access policy. Brain. Behav. Immun. *22*, 629.

Kellner, Y. (2010). Die Rolle des BDNF-TrkB Signalweges in synaptischen Strukturen hippocampaler Neurone Master of Science.

Kellner, Y., Gödecke, N., Dierkes, T., Thieme, N., Zagrebelsky, M., and Korte, M. (2014). The BDNF effects on dendritic spines of mature hippocampal neurons depend on neuronal activity. Front. Synaptic Neurosci. *6*.

Kempf, A., and Schwab, M.E. (2013). Nogo-a represses anatomical and synaptic plasticity in the central nervous system. Physiology (Bethesda). *28*, 151–163.

Kempf, A., Montani, L., Petrinovic, M.M., Schroeter, A., Weinmann, O., Patrignani, A., and Schwab, M.E. (2013). Upregulation of axon guidance molecules in the adult central nervous system of Nogo-A knockout mice restricts neuronal growth and regeneration. Eur. J. Neurosci. 1–13.

Kempf, A., Tews, B., Arzt, M.E., Weinmann, O., Obermair, F.J., Pernet, V., Zagrebelsky, M., Delekate, A., Iobbi, C., Zemmar, A., et al. (2014). The Sphingolipid Receptor S1PR2 Is a Receptor for Nogo-A Repressing Synaptic Plasticity. PLoS Biol. *12*, e1001763.

Kennedy, M.B., Beale, H.C., Carlisle, H.J., and Washburn, L.R. (2005). Integration of biochemical signalling in spines. Nat. Rev. Neurosci. *6*, 423–434.

Kesner, R.P. (2007). Behavioral functions of the CA3 subregion of the hippocampus. Learn. Mem. *14*, 771–781.

Kessels, H.W., and Malinow, R. (2009). Synaptic AMPA receptor plasticity and behavior. Neuron *61*, 340–350.

Kim, C.H., and Lisman, J.E. (1999). A role of actin filament in synaptic transmission and long-term potentiation. J. Neurosci. *19*, 4314–4324.

Kim, S.A., and Schwille, P. (2003). Intracellular applications of fluorescence correlation spectroscopy: prospects for neuroscience. Curr. Opin. Neurobiol. *13*, 583–590.

Kim, I.H., Racz, B., Wang, H., Burianek, L., Weinberg, R., Yasuda, R., Wetsel, W.C., and Soderling, S.H. (2013). Disruption of Arp2/3 results in asymmetric structural plasticity of dendritic spines and progressive synaptic and behavioral abnormalities. J. Neurosci. *33*, 6081–6092.

Kim, S.A., Heinze, K.G., and Schwille, P. (2007). Fluorescence correlation spectroscopy in living cells. Nat. Methods *4*, 963–973.

Kinases, R., Medicine, F., and Discovery, D. (2000). Pharmacological Properties of Y-27632 , a Specific Inhibitor of. 976–983.

Kleene, R., and Schachner, M. (2004). Glycans and neural cell interactions. Nat. Rev. Neurosci. *5*, 195–208.

Klein, R., Conway, D., Parada, L.F., and Barbacid, M. (1990). The trkB tyrosine protein kinase gene codes for a second neurogenic receptor that lacks the catalytic kinase domain. Cell *61*, 647–656.

Kneussel, M., and Wagner, W. (2013). Myosin motors at neuronal synapses: drivers of membrane transport and actin dynamics. Nat. Rev. Neurosci. *14*, 233–247.

Knierim, J.J., Lee, I., and Hargreaves, E.L. (2006). Hippocampal place cells: parallel input streams, subregional processing, and implications for episodic memory. Hippocampus *16*, 755–764.

Kopec, C.D., Li, B., Wei, W., Boehm, J., and Malinow, R. (2006). Glutamate receptor exocytosis and spine enlargement during chemically induced long-term potentiation. J. Neurosci. *26*, 2000–2009.

Korkotian, E., and Segal, M. (1999). Release of calcium from stores alters the morphology of dendritic spines in cultured hippocampal neurons. Proc. Natl. Acad. Sci. U. S. A. *96*, 12068–12072.

Korkotian, E., and Segal, M. (2001). Regulation of dendritic spine motility in cultured hippocampal neurons. J. Neurosci. *21*, 6115–6124.

Korobova, F., and Svitkina, T. (2010). Molecular Architecture of Synaptic Actin Cytoskeleton in Hippocampal Neurons Reveals a Mechanism of Dendritic Spine Morphogenesis Farida Korobova and Tatyana Svitkina. Mol. Biol. Cell *21*, 165–176.

Korte, M., Carroll, P., Wolf, E., Brem, G., Thoenen, H., and Bonhoeffer, T. (1995). Hippocampal long-term potentiation is impaired in mice lacking brain-derived neurotrophic factor. Proc. Natl. Acad. Sci. U. S. A. *92*, 8856–8860.

Korte, M., Griesbeck, O., Gravel, C., Carroll, P., Staiger, V., Thoenen, H., and Bonhoeffer, T. (1996). Virus-mediated gene transfer into hippocampal CA1 region restores long-term potentiation in brain-derived neurotrophic factor mutant mice. Proc. Natl. Acad. Sci. U. S. A. *93*, 12547–12552.

Kovar, D.R., Harris, E.S., Mahaffy, R., Higgs, H.N., and Pollard, T.D. (2006). Control of the assembly of ATP- and ADP-actin by formins and profilin. Cell *124*, 423–435.

Kramer, S. (2013). ROLE OF NOGO-A IN SYNAPSE FORMATION AND SYNAPTIC PLASTICITY Chapter 1- Introduction Chapter 2- Nogo-A restricts synapse formation in dissociated hippocampal neurons.

Krucker, T., Siggins, G.R., and Halpain, S. (2000). Dynamic actin filaments are required for stable long-term potentiation (LTP) in area CA1 of the hippocampus. Proc. Natl. Acad. Sci. U. S. A. *97*, 6856–6861.

Kuhlman, P.A., Hughes, C.A., Bennett, V., and Fowler, V.M. (1996). A new function for adducin: Calcium/calmodulin-regulated capping of the barbed ends of actin filaments. J. Biol. Chem. *271*, 7986–7991.

Kwon, H.-B., and Sabatini, B.L. (2011). Glutamate induces de novo growth of functional spines in developing cortex. Nature *474*, 100–104.

Lai, K.-O., Wong, A.S.L., Cheung, M.-C., Xu, P., Liang, Z., Lok, K.-C., Xie, H., Palko, M.E., Yung, W.-H., Tessarollo, L., et al. (2012). TrkB phosphorylation by Cdk5 is required for activity-dependent structural plasticity and spatial memory. Nat. Neurosci. *15*, 1506–1515.

Lamprecht, R. (2014). The actin cytoskeleton in memory formation. Prog. Neurobiol.

Lamprecht, R., and LeDoux, J. (2004). Structural plasticity and memory. Nat. Rev. Neurosci. *5*, 45–54.

Lang, S.B., Bonhoeffer, T., and Lohmann, C. (2006). Simultaneous imaging of morphological plasticity and calcium dynamics in dendrites. Nat. Protoc. *1*, 1859–1864.

Lang, S.B., Stein, V., Bonhoeffer, T., and Lohmann, C. (2007). Endogenous brain-derived neurotrophic factor triggers fast calcium transients at synapses in developing dendrites. J. Neurosci. *27*, 1097–1105.

Lee, H., Raiker, S.J., Venkatesh, K., Geary, R., Robak, L. a, Zhang, Y., Yeh, H.H., Shrager, P., and Giger, R.J. (2008). Synaptic function for the Nogo-66 receptor NgR1: regulation of dendritic spine morphology and activity-dependent synaptic strength. J. Neurosci. *28*, 2753–2765.

Levi-Montalcini, R. (1987). The Nerve Growth Factor: thirty-five years later. EMBO J. *6*, 2856.

Li, C., Peoples, R.W., and Weight, F.F. (1997). Mg2+ inhibition of ATP-activated current in rat nodose ganglion neurons: evidence that Mg2+ decreases the agonist affinity of the receptor. J. Neurophysiol. *77*, 3391–3395.

Li, X.G., Somogyi, P., Ylinen, A., and Buzsáki, G. (1994). The hippocampal CA3 network: an in vivo intracellular labeling study. J. Comp. Neurol. *339*, 181–208.

Liebscher, T., Schnell, L., Schnell, D., Scholl, J., Schneider, R., Gullo, M., Fouad, K., Mir, A., Rausch, M., Kindler, D., et al. (2005). Nogo-A antibody improves regeneration and locomotion of spinal cord-injured rats. Ann. Neurol. *58*, 706–719.

Lin, B., Kramár, E. a, Bi, X., Brucher, F. a, Gall, C.M., and Lynch, G. (2005). Theta stimulation polymerizes actin in dendritic spines of hippocampus. J. Neurosci. *25*, 2062–2069.

Lisman, J.E., and Zhabotinsky, A.M. (2001). A model of synaptic memory: a CaMKII/PP1 switch that potentiates transmission by organizing an AMPA receptor anchoring assembly. Neuron *31*, 191–201.

Liu, Y.Y., Jin, W.L., Liu, H.L., and Ju, G. (2003). Electron microscopic localization of Nogo-A at the postsynaptic active zone of the rat. Neurosci. Lett. *346*, 153–156.

Lohmann, C. (2009). Calcium signaling and the development of specific neuronal connections. Prog. Brain Res. *175*, 443–452.

Lu, B. (2003). BDNF and activity-dependent synaptic modulation. Learn. Mem. *10*, 86–98.

Lu, B., Pang, P.T., and Woo, N.H. (2005). The yin and yang of neurotrophin action. Nat. Rev. Neurosci. *6*, 603–614.

Lu, B., Nagappan, G., Guan, X., Nathan, P.J., and Wren, P. (2013). BDNF-based synaptic repair as a disease-modifying strategy for neurodegenerative diseases. Nat. Rev. Neurosci. *14*, 401–416.

Lu, W., Man, H., Ju, W., Trimble, W.S., MacDonald, J.F., and Wang, Y.T. (2001). Activation of synaptic NMDA receptors induces membrane insertion of new AMPA receptors and LTP in cultured hippocampal neurons. Neuron *29*, 243–254.

Luikart, B.W., Nef, S., Virmani, T., Lush, M.E., Liu, Y., Kavalali, E.T., and Parada, L.F. (2005). TrkB has a cell-autonomous role in the establishment of hippocampal Schaffer collateral synapses. J. Neurosci. *25*, 3774–3786.

Maier, I.C., Ichiyama, R.M., Courtine, G., Schnell, L., Lavrov, I., Edgerton, V.R., and Schwab, M.E. (2009). Differential effects of anti-Nogo-A antibody treatment and treadmill training in rats with incomplete spinal cord injury. Brain *132*, 1426–1440.

Malenka, R.C., and Bear, M.F. (2004). LTP and LTD: an embarrassment of riches. Neuron *44*, 5–21.

Maletic-Savatic, M. (1999). Rapid Dendritic Morphogenesis in CA1 Hippocampal Dendrites Induced by Synaptic Activity. Science (80-.). *283*, 1923–1927.

Maletic-Savatic, M., Malinow, R., and Svoboda, K. (1999). Rapid dendritic morphogenesis in CA1 hippocampal dendrites induced by synaptic activity. Science *283*, 1923–1927.

Manns, J.R., and Eichenbaum, H. (2006). Evolution of declarative memory. Hippocampus *16*, 795–808.

Martin, S.J., Grimwood, P.D., and Morris, R.G. (2000). Synaptic plasticity and memory: an evaluation of the hypothesis. Annu. Rev. Neurosci. *23*, 649–711.

Marty, S., Castr, E., and Martinsried, D.- (1996). Brain-Derived Neurotrophic Factor Various Hippocampal Nbnpyramidal Cells , in Organotypic Promotes the Differentiation Neurons , Including Slice Cultures. Control *76*, 675–687.

Matsumoto, T., Rauskolb, S., Polack, M., Klose, J., Kolbeck, R., Korte, M., and Barde, Y.-A. (2008). Biosynthesis and processing of endogenous BDNF: CNS neurons store and secrete BDNF, not pro-BDNF. Nat. Neurosci. *11*, 131–133.

Matsuzaki, M., Honkura, N., Ellis-Davies, G.C.R., and Kasai, H. (2004a). Structural basis of long-term potentiation in single dendritic spines. Nature *429*, 761–766.

Matsuzaki, M., Honkura, N., Ellis-Davies, G.C.R., and Kasai, H. (2004b). Structural basis of long-term potentiation in single dendritic spines. Nature *429*, 761–766.

Matus, a. (2000). Actin-Based Plasticity in Dendritic Spines. Science (80-.). *290*, 754–758.

Matus, a, Ackermann, M., Pehling, G., Byers, H.R., and Fujiwara, K. (1982). High actin concentrations in brain dendritic spines and postsynaptic densities. Proc. Natl. Acad. Sci. U. S. A. *79*, 7590–7594.

Mayer, M.L., and Westbrook, G.L. (1987). Permeation and block of N-methyl-D-aspartic acid receptor channels by divalent cations in mouse cultured central neurones. J. Physiol. *394*, 501–527.

Mayr, B., and Montminy, M. (2001). Transcriptional regulation by the phosphorylation-dependent factor CREB. Nat. Rev. Mol. Cell Biol. *2*, 599–609.

Mcallister, a (1995). Neurotrophins regulate dendritic growth in developing visual cortex. Neuron *15*, 791–803.

McAllister, a K., Katz, L.C., and Lo, D.C. (1996). Neurotrophin regulation of cortical dendritic growth requires activity. Neuron *17*, 1057–1064.

McAllister, A.K., Lo, D.C., and Katz, L.C. (1995). Neurotrophins regulate dendritic growth in developing visual cortex. Neuron *15*, 791–803.

McAllister, A.K., Katz, L.C., and Lo, D.C. (1999). Neurotrophins and synaptic plasticity. Annu. Rev. Neurosci. *22*, 295–318.

McGee, A.W., Yang, Y., Fischer, Q.S., Daw, N.W., and Strittmatter, S.M. (2005). Experience-driven plasticity of visual cortex limited by myelin and Nogo receptor. Science *309*, 2222–2226.

Medeiros, N.A., Burnette, D.T., and Forscher, P. (2006). Myosin II functions in actin-bundle turnover in neuronal growth cones. Nat. Cell Biol. *8*, 215–226.

Meier, S., Bräuer, A.U., Heimrich, B., Schwab, M.E., Nitsch, R., and Savaskan, N.E. (2003). Molecular analysis of Nogo expression in the hippocampus during development and following lesion and seizure. FASEB J. *17*, 1153–1155.

Meijering, E., Jacob, M., Sarria, J.-C.F., Steiner, P., Hirling, H., and Unser, M. (2004). Design and validation of a tool for neurite tracing and analysis in fluorescence microscopy images. Cytometry. A *58*, 167–176.

Meng, Y., Zhang, Y., Tregoubov, V., Janus, C., Cruz, L., Jackson, M., Lu, W.Y., MacDonald, J.F., Wang, J.Y., Falls, D.L., et al. (2002). Abnormal spine morphology and enhanced LTP in LIMK-1 knockout mice. Neuron *35*, 121–133.

Menna, E., Zambetti, S., Morini, R., Donzelli, A., Disanza, A., Calvigioni, D., Braida, D., Nicolini, C., Orlando, M., Fossati, G., et al. (2013). Eps8 controls dendritic spine density and synaptic plasticity through its actin-capping activity. EMBO J. *32*, 1730–1744.

Messaoudi, E., Ying, S.-W., Kanhema, T., Croll, S.D., and Bramham, C.R. (2002). Brain-derived neurotrophic factor triggers transcription-dependent, late phase long-term potentiation in vivo. J. Neurosci. *22*, 7453–7461.

Messaoudi, E., Kanhema, T., Soulé, J., Tiron, A., Dagyte, G., da Silva, B., and Bramham, C.R. (2007). Sustained Arc/Arg3.1 synthesis controls long-term potentiation consolidation through regulation of local actin polymerization in the dentate gyrus in vivo. J. Neurosci. *27*, 10445–10455.

Mi, S., Lee, X., Shao, Z., Thill, G., Ji, B., Relton, J., Levesque, M., Allaire, N., Perrin, S., Sands, B., et al. (2004). LINGO-1 is a component of the Nogo-66 receptor/p75 signaling complex. Nat. Neurosci. *7*, 221–228.

Michaelsen, K., Murk, K., Zagrebelsky, M., Dreznjak, A., Jockusch, B.M., Rothkegel, M., and Korte, M. (2010). Fine-tuning of neuronal architecture requires two profilin isoforms. Proc. Natl. Acad. Sci. U. S. A. *107*, 15780–15785.

Michaelsen-Preusse, K., Kellner, Y., Korte, M., and Zagrebelsky, M. (2014). Analysis of Actin Turnover and Spine Dynamics in Hippocampal Slice Cultures. In Laser Scanning Microscopy and Quantitative Image Analysis of Neuronal Tissue Neuromethods Volume 87, L. Bakota, and R. Brandt, eds. (New York, NY: Springer New York), pp. 189–217.

Mingorance, A., Fontana, X., Solé, M., Burgaya, F., Ureña, J.M., Teng, F.Y.H., Tang, B.L., Hunt, D., Anderson, P.N., Bethea, J.R., et al. (2004). Regulation of Nogo and Nogo receptor during the development of the entorhino-hippocampal pathway and after adult hippocampal lesions. Mol. Cell. Neurosci. *26*, 34–49.

Minichiello, L. (2009). TrkB signalling pathways in LTP and learning. Nat. Rev. Neurosci. *10*, 850–860.

Minichiello, L., Korte, M., Wolfer, D., Ku, R., Unsicker, K., Cestari, V., Rossi-arnaud, C., Lipp, H., Bonhoeffer, T., Zu, C.-, et al. (1999). Essential Role for TrkB Receptors in Hippocampus-Mediated Learning University of Heidelberg. *24*, 401–414.

Mironova, Y. a, and Giger, R.J. (2013). Where no synapses go: gatekeepers of circuit remodeling and synaptic strength. Trends Neurosci. *66*, 1–11.

Mogilner, A., and Oster, G. (1996). Cell motility driven by actin polymerization. Biophys. J. *71*, 3030–3045.

Montani, L., Gerrits, B., Gehrig, P., Kempf, A., Dimou, L., Wollscheid, B., and Schwab, M.E. (2009). Neuronal Nogo-A modulates growth cone motility via Rho-GTP/LIMK1/cofilin in the unlesioned adult nervous system. J. Biol. Chem. *284*, 10793–10807.

Monteggia, L.M., Luikart, B., Barrot, M., Theobold, D., Malkovska, I., Nef, S., Parada, L.F., and Nestler, E.J. (2007). Brain-derived neurotrophic factor conditional knockouts show gender differences in depression-related behaviors. Biol. Psychiatry *61*, 187–197.

Morales, M., and Fifková, E. (1989). In situ localization of myosin and actin in dendritic spines with the immunogold technique. J. Comp. Neurol. *279*, 666–674.

Morris, R. (1984). Developments of a water-maze procedure for studying spatial learning in the rat. J. Neurosci. Methods *11*, 47–60.

Morris, R.G.M. (1981). Spatial localization does not require the presence of local cues. Learn. Motiv. *12*, 239–260.

Morris, R.G.M., Garrud, P., Rawlins, J.N.P., and O'Keefe, J. (1982). Place navigation impaired in rats with hippocampal lesions. Nature *297*, 681–683.

Mullins, R.D., Heuser, J.A., and Pollard, T.D. (1998). The interaction of Arp2/3 complex with actin: nucleation, high affinity pointed end capping, and formation of branching networks of filaments. Proc. Natl. Acad. Sci. U. S. A. *95*, 6181–6186.

Murakoshi, H., Wang, H., and Yasuda, R. (2011). Local, persistent activation of Rho GTPases during plasticity of single dendritic spines. Nature *472*, 100–104.

Nägerl, U.V., Eberhorn, N., Cambridge, S.B., and Bonhoeffer, T. (2004). Bidirectional activity-dependent morphological plasticity in hippocampal neurons. Neuron *44*, 759–767.

Nash, M., Pribiag, H., Fournier, A.E., and Jacobson, C. (2009). Central nervous system regeneration inhibitors and their intracellular substrates. Mol. Neurobiol. *40*, 224–235.

Niederöst, B., Oertle, T., Fritsche, J., McKinney, R.A., and Bandtlow, C.E. (2002). Nogo-A and myelin-associated glycoprotein mediate neurite growth inhibition by antagonistic regulation of RhoA and Rac1. J. Neurosci. *22*, 10368–10376.

Ninan, I., Bath, K.G., Dagar, K., Perez-Castro, R., Plummer, M.R., Lee, F.S., and Chao, M. V (2010). The BDNF Val66Met polymorphism impairs NMDA receptor-dependent synaptic plasticity in the hippocampus. J. Neurosci. *30*, 8866–8870.

Nusser, Z., LUJAN, R., LAUBE, G., ROBERTS, J., MOLNAR, E., and SOMOGYI, P. (1998). Cell Type and Pathway Dependence of Synaptic AMPA Receptor Number and Variability in the Hippocampus. Neuron *21*, 545–559.

O'Brien, R.J., Kamboj, S., Ehlers, M.D., Rosen, K.R., Fischbach, G.D., and Huganir, R.L. (1998). Activity-Dependent Modulation of Synaptic AMPA Receptor Accumulation. Neuron *21*, 1067–1078.

O'Malley, a, O'Connell, C., Murphy, K.J., and Regan, C.M. (2000). Transient spine density increases in the mid-molecular layer of hippocampal dentate gyrus accompany consolidation of a spatial learning task in the rodent. Neuroscience *99*, 229–232.

Oertle, T., and Schwab, M.E. (2003). Nogo and its paRTNers. Trends Cell Biol. *13*, 187–194.

Oertle, T., van der Haar, M.E., Bandtlow, C.E., Robeva, A., Burfeind, P., Buss, A., Huber, A.B., Simonen, M., Schnell, L., Brosamle, C., et al. (2003a). Nogo-A Inhibits Neurite Outgrowth and Cell Spreading with Three Discrete Regions. J. Neurosci. *23*, 5393–5406.

Oertle, T., van der Haar, M.E., Bandtlow, C.E., Robeva, A., Burfeind, P., Buss, A., Huber, A.B., Simonen, M., Schnell, L., Brösamle, C., et al. (2003b). Nogo-A inhibits neurite outgrowth and cell spreading with three discrete regions. J. Neurosci. *23*, 5393–5406.

Oertle, T., Huber, C., van der Putten, H., and Schwab, M.E. (2003c). Genomic structure and functional characterisation of the promoters of human and mouse nogo/rtn4. J. Mol. Biol. *325*, 299–323.

Oertner, T.G., and Matus, A. (2005). Calcium regulation of actin dynamics in dendritic spines. Cell Calcium *37*, 477–482.

Okamoto, K., and Hayashi, Y. (2006). Visualization of F-actin and G-actin equilibrium using fluorescence resonance energy transfer (FRET) in cultured cells and neurons in slices. Nat. Protoc. *1*, 911–919.

Okamoto, K., Bosch, M., and Hayashi, Y. (2009). The roles of CaMKII and F-actin in the structural plasticity of dendritic spines: a potential molecular identity of a synaptic tag? Physiology (Bethesda). *24*, 357–366.

Okamoto, K.-I., Nagai, T., Miyawaki, A., and Hayashi, Y. (2004). Rapid and persistent modulation of actin dynamics regulates postsynaptic reorganization underlying bidirectional plasticity. Nat. Neurosci. *7*, 1104–1112.

Okamura, K., Tanaka, H., Yagita, Y., Saeki, Y., Taguchi, A., Hiraoka, Y., Zeng, L.-H., Colman, D.R., and Miki, N. (2004). Cadherin activity is required for activity-induced spine remodeling. J. Cell Biol. *167*, 961–972.

Papa, M., and Segal, M. (1996). Morphological plasticity in dendritic spines of cultured hippocampal neurons. Neuroscience *71*, 1005–1011.

Papa, M., Bundman, M.C., Greenberger, V., and Segal, M. (1995). Morphological analysis of dendritic spine development in primary cultures of hippocampal neurons. J. Neurosci. *15*, 1–11.

Park, H., and Poo, M. (2012). Neurotrophin regulation of neural circuit development and function. Nat. Rev. Neurosci. *14*, 7–23.

Park, J.B., Yiu, G., Kaneko, S., Wang, J., Chang, J., He, X.L., Garcia, K.C., and He, Z. (2005). A TNF receptor family member, TROY, is a coreceptor with Nogo receptor in mediating the inhibitory activity of myelin inhibitors. Neuron *45*, 345–351.

Parkhurst, C.N., Yang, G., Ninan, I., Savas, J.N., Yates, J.R., Lafaille, J.J., Hempstead, B.L., Littman, D.R., and Gan, W.-B. (2013). Microglia promote learning-dependent synapse formation through brain-derived neurotrophic factor. Cell *155*, 1596–1609.

Peters, A., and Kaiserman-Abramof, I.R. (1969). The small pyramidal neuron of the rat cerebral cortex. The synapses upon dendritic spines. Z. Zellforsch. Mikrosk. Anat. *100*, 487–506.

Peters, A., and Kaiserman-Abramof, I.R. (1970). The small pyramidal neuron of the rat cerebral cortex. The perikaryon, dendrites and spines. Am. J. Anat. *127*, 321–355.

Petrinovic, M.M., Duncan, C.S., Bourikas, D., Weinman, O., Montani, L., Schroeter, A., Maerki, D., Sommer, L., Stoeckli, E.T., and Schwab, M.E. (2010). Neuronal Nogo-A regulates neurite fasciculation, branching and extension in the developing nervous system. Development *137*, 2539–2550.

Petrinovic, M.M., Hourez, R., Aloy, E.M., Dewarrat, G., Gall, D., Weinmann, O., Gaudias, J., Bachmann, L.C., Schiffmann, S.N., Vogt, K.E., et al. (2013). Neuronal Nogo-A negatively regulates dendritic morphology and synaptic transmission in the cerebellum. Proc. Natl. Acad. Sci. U. S. A. *110*, 1083–1088.

Phair, R.D., Gorski, S. a, and Misteli, T. (2004). Measurement of dynamic protein binding to chromatin in vivo, using photobleaching microscopy. Methods Enzymol. *375*, 393–414.

Pickard, L., Noël, J., Duckworth, J.K., Fitzjohn, S.M., Henley, J.M., Collingridge, G.L., and Molnar, E. (2001). Transient synaptic activation of NMDA receptors leads to the insertion of native AMPA receptors at hippocampal neuronal plasma membranes. Neuropharmacology *41*, 700–713.

Pilo Boyl, P., Di Nardo, A., Mulle, C., Sassoè-Pognetto, M., Panzanelli, P., Mele, A., Kneussel, M., Costantini, V., Perlas, E., Massimi, M., et al. (2007). Profilin2 contributes to synaptic vesicle exocytosis, neuronal excitability, and novelty-seeking behavior. EMBO J. *26*, 2991–3002.

Pollard, T.D., and Borisy, G.G. (2003). Cellular motility driven by assembly and disassembly of actin filaments. Cell *112*, 453–465.

Pollard, T.D., Blanchoin, L., and Mullins, R.D. (2000). Molecular mechanisms controlling actin filament dynamics in nonmuscle cells. Annu. Rev. Biophys. Biomol. Struct. *29*, 545–576.

Pradhan, a D., Case, a M., Farrer, R.G., Tsai, S.Y., Cheatwood, J.L., Martin, J.L., and Kartje, G.L. (2010). Dendritic spine alterations in neocortical pyramidal neurons following postnatal neuronal Nogo-A knockdown. Dev. Neurosci. *32*, 313–320.

Prinjha, R., Moore, S.E., Vinson, M., Blake, S., Morrow, R., Christie, G., Michalovich, D., Simmons, D.L., and Walsh, F.S. (2000). Inhibitor of neurite outgrowth in humans. Nature *403*, 383–384.

Psotta, L., Lessmann, V., and Endres, T. (2013). Impaired fear extinction learning in adult heterozygous BDNF knock-out mice. Neurobiol. Learn. Mem. *103*, 34–38.

Rácz, B., and Weinberg, R.J. (2013). Microdomains in forebrain spines: an ultrastructural perspective. Mol. Neurobiol. *47*, 77–89.

Raiker, S.J., Lee, H., Baldwin, K.T., Duan, Y., Shrager, P., and Giger, R.J. (2010). Oligodendrocyte-myelin glycoprotein and Nogo negatively regulate activity-dependent synaptic plasticity. J. Neurosci. *30*, 12432–12445.

Rapizzi, E., Donati, C., Cencetti, F., Pinton, P., Rizzuto, R., and Bruni, P. (2007). Sphingosine 1-phosphate receptors modulate intracellular Ca2+ homeostasis. Biochem. Biophys. Res. Commun. *353*, 268–274.

Rauskolb, S., Zagrebelsky, M., Dreznjak, A., Deogracias, R., Matsumoto, T., Wiese, S., Erne, B., Sendtner, M., Schaeren-Wiemers, N., Korte, M., et al. (2010). Global deprivation of brain-derived neurotrophic factor in the CNS reveals an area-specific requirement for dendritic growth. J. Neurosci. *30*, 1739–1749.

Rex, C.S., Lin, C.-Y., Kramár, E. a, Chen, L.Y., Gall, C.M., and Lynch, G. (2007). Brain-derived neurotrophic factor promotes long-term potentiation-related cytoskeletal changes in adult hippocampus. J. Neurosci. *27*, 3017–3029.

Rex, C.S., Chen, L.Y., Sharma, A., Liu, J., Babayan, A.H., Gall, C.M., and Lynch, G. (2009). Different Rho GTPase-dependent signaling pathways initiate sequential steps in the consolidation of long-term potentiation. J. Cell Biol. *186*, 85–97.

Rex, C.S., Gavin, C.F., Rubio, M.D., Kramar, E.A., Chen, L.Y., Jia, Y., Huganir, R.L., Muzyczka, N., Gall, C.M., Miller, C.A., et al. (2010). Myosin IIb regulates actin dynamics during synaptic plasticity and memory formation. Neuron *67*, 603–617.

Richard, M., Giannetti, N., Saucier, D., Sacquet, J., Jourdan, F., and Pellier-Monnin, V. (2005). Neuronal expression of Nogo-A mRNA and protein during neurite outgrowth in the developing rat olfactory system. Eur. J. Neurosci. *22*, 2145–2158.

Riedl, J., Crevenna, A.H., Kessenbrock, K., Yu, J.H., Neukirchen, D., Bradke, F., Jenne, D., Holak, T.A., Werb, Z., Sixt, M., et al. (2008). Lifeact : a versatile marker to visualize F-actin. Nat. Methods *5*, 605–607.

Riedl, J., Flynn, K.C., Raducanu, A., Gärtner, F., Beck, G., Bösl, M., Bradke, F., Massberg, S., Aszodi, A., Sixt, M., et al. (2010). Lifeact mice for studying F-actin dynamics. Nat. Methods *7*, 168–169.

Rios, M., Fan, G., Fekete, C., Kelly, J., Bates, B., Kuehn, R., Lechan, R.M., and Jaenisch, R. (2001). Conditional deletion of brain-derived neurotrophic factor in the postnatal brain leads to obesity and hyperactivity. Mol. Endocrinol. *15*, 1748–1757.

Rösch, H., Schweigreiter, R., Bonhoeffer, T., Barde, Y.-A., and Korte, M. (2005). The neurotrophin receptor p75NTR modulates long-term depression and regulates the expression of AMPA receptor subunits in the hippocampus. Proc. Natl. Acad. Sci. U. S. A. *102*, 7362–7367.

Rust, M.B., Gurniak, C.B., Renner, M., Vara, H., Morando, L., Görlich, A., Sassoè-Pognetto, M., Banchaabouchi, M. Al, Giustetto, M., Triller, A., et al. (2010). Learning, AMPA receptor mobility and synaptic plasticity depend on n-cofilin-mediated actin dynamics. EMBO J. *29*, 1889–1902.

Ryu, J., Liu, L., Wong, T.P., Wu, D.C., Burette, A., Weinberg, R., Wang, Y.T., and Sheng, M. (2006). A critical role for myosin IIb in dendritic spine morphology and synaptic function. Neuron *49*, 175–182.

Sala, C., and Segal, M. (2014). Dendritic spines: the locus of structural and functional plasticity. Physiol. Rev. *94*, 141–188.

Sala, C., Piëch, V., Wilson, N.R., Passafaro, M., Liu, G., and Sheng, M. (2001). Regulation of dendritic spine morphology and synaptic function by Shank and Homer. Neuron *31*, 115–130.

Schikorski, T., and Stevens, C.F. (1999). Quantitative fine-structural analysis of olfactory cortical synapses. Proc. Natl. Acad. Sci. U. S. A. *96*, 4107–4112.

Schratt, G.M., Nigh, E.A., Chen, W.G., Hu, L., and Greenberg, M.E. (2004). BDNF regulates the translation of a select group of mRNAs by a mammalian target of rapamycin-phosphatidylinositol 3-kinase-dependent pathway during neuronal development. J. Neurosci. *24*, 7366–7377.

Schubert, V., and Dotti, C.G. (2007). Transmitting on actin: synaptic control of dendritic architecture. J. Cell Sci. *120*, 205–212.

Schwab, M.E. (2010). Functions of Nogo proteins and their receptors in the nervous system. Nat. Rev. Neurosci. *3*, 1–13.

Schwab, M.E., and Strittmatter, S.M. (2014). Nogo limits neural plasticity and recovery from injury. Curr. Opin. Neurobiol. *27C*, 53–60.

Scoville, W.B., and Milner, B. (1957). Loss of recent memory after bilateral hippocampal lesions. J. Neurol. Neurosurg. Psychiatry *20*, 11–21.

Scoville, W.B., and Milner, B. (2000). Loss of recent memory after bilateral hippocampal lesions. 1957. J. Neuropsychiatry Clin. Neurosci. *12*, 103–113.

Segal, P. (1996). Morphological plasticity in dendritic spi9nes of cultured Hippocampal Neurons. Neuroscience *71*, 1005–1011.

Segal, R.A., and Greenberg, M.E. (1996). Intracellular signaling pathways activated by neurotrophic factors. Annu. Rev. Neurosci. *19*, 463–489.

Sekino, Y., Kojima, N., and Shirao, T. (2007). Role of actin cytoskeleton in dendritic spine morphogenesis. Neurochem. Int. *51*, 92–104.

Sellers, J.R. (2000). Myosins: a diverse superfamily. Biochim. Biophys. Acta *1496*, 3–22.

Shao, Z., Browning, J.L., Lee, X., Scott, M.L., Shulga-Morskaya, S., Allaire, N., Thill, G., Levesque, M., Sah, D., McCoy, J.M., et al. (2005). TAJ/TROY, an orphan TNF receptor family member, binds Nogo-66 receptor 1 and regulates axonal regeneration. Neuron *45*, 353–359.

Shen, K., and Cowan, C.W. (2010). Guidance molecules in synapse formation and plasticity. Cold Spring Harb. Perspect. Biol. *2*, a001842.

Shepherd, G.M. (1996). The dendritic spine: a multifunctional integrative unit. J. Neurophysiol. *75*, 2197–2210.

Shi, S.H., Hayashi, Y., Petralia, R.S., Zaman, S.H., Wenthold, R.J., Svoboda, K., and Malinow, R. (1999). Rapid spine delivery and redistribution of AMPA receptors after synaptic NMDA receptor activation. Science *284*, 1811–1816.

Shimada, A., Mason, C.A., and Morrison, M.E. (1998). TrkB Signaling Modulates Spine Density and Morphology Purkinje Cells. Cell *18*, 8559–8570.

Sholl, D.A. (1953). Dendritic organization in the neurons of the visual and motor cortices of the cat. J. Anat. *87*, 387–406.

Silver, J., and Miller, J.H. (2004). Regeneration beyond the glial scar. Nat. Rev. Neurosci. *5*, 146–156.

Simonen, M., Pedersen, V., Weinmann, O., Schnell, L., Buss, A., Ledermann, B., Christ, F., Sansig, G., van der, P.H., and Schwab, M.E. (2003). Systemic deletion of the myelin-associated

outgrowth inhibitor Nogo-A improves regenerative and plastic responses after spinal cord injury. Neuron *38*, 201–211.

De Simoni, A., Griesinger, C.B., and Edwards, F.A. (2003). Development of rat CA1 neurones in acute versus organotypic slices: role of experience in synaptic morphology and activity. J. Physiol. *550*, 135–147.

Singh, I.N., and Hall, E.D. (2008). Multifaceted roles of sphingosine-1-phosphate: how does this bioactive sphingolipid fit with acute neurological injury? J. Neurosci. Res. *86*, 1419–1433.

Sjöström, P.J., Rancz, E.A., Roth, A., and Häusser, M. (2008). Dendritic excitability and synaptic plasticity. Physiol. Rev. *88*, 769–840.

Spiegel, S., and Milstien, S. (2003). Sphingosine-1-phosphate: an enigmatic signalling lipid. Nat. Rev. Mol. Cell Biol. *4*, 397–407.

Squire, L.R., Stark, C.E.L., and Clark, R.E. (2004). The medial temporal lobe. Annu. Rev. Neurosci. *27*, 279–306.

Stamatakou, E., Marzo, A., Gibb, A., and Salinas, P.C. (2013). Activity-dependent spine morphogenesis: a role for the actin-capping protein Eps8. J. Neurosci. *33*, 2661–2670.

Star, E.N., Kwiatkowski, D.J., and Murthy, V.N. (2002). Rapid turnover of actin in dendritic spines and its regulation by activity. Nat. Neurosci. *5*, 239–246.

Stoppini, L., Buchs, P. a, and Muller, D. (1991). A simple method for organotypic cultures of nervous tissue. J. Neurosci. Methods *37*, 173–182.

Stranahan, A.M. (2011). Physiological variability in brain-derived neurotrophic factor expression predicts dendritic spine density in the mouse dentate gyrus. Neurosci. Lett. *495*, 60–62.

Suzuki, W.A., Miller, E.K., and Desimone, R. (1997). Object and place memory in the macaque entorhinal cortex. J. Neurophysiol. *78*, 1062–1081.

Syken, J., Grandpre, T., Kanold, P.O., and Shatz, C.J. (2006). PirB restricts ocular-dominance plasticity in visual cortex. Science *313*, 1795–1800.

Tada, T., and Sheng, M. (2006). Molecular mechanisms of dendritic spine morphogenesis. Curr. Opin. Neurobiol. *16*, 95–101.

Takumi, Y., Ramírez-León, V., Laake, P., Rinvik, E., and Ottersen, O.P. (1999). Different modes of expression of AMPA and NMDA receptors in hippocampal synapses. Nat. Neurosci. *2*, 618–624.

Tanaka, J.-I., Horiike, Y., Matsuzaki, M., Miyazaki, T., Ellis-Davies, G.C.R., and Kasai, H. (2008). Protein synthesis and neurotrophin-dependent structural plasticity of single dendritic spines. Science *319*, 1683–1687.

Tashiro, A., Minden, A., and Yuste, R. (2000). Regulation of dendritic spine morphology by the rho family of small GTPases: antagonistic roles of Rac and Rho. Cereb. Cortex *10*, 927–938.

Tatavarty, V., Kim, E.-J., Rodionov, V., and Yu, J. (2009). Investigating sub-spine actin dynamics in rat hippocampal neurons with super-resolution optical imaging. PLoS One *4*, e7724.

Teng, F.Y.H., and Tang, B.L. (2005). Why do Nogo/Nogo-66 receptor gene knockouts result in inferior regeneration compared to treatment with neutralizing agents? J. Neurochem. *94*, 865–874.

Teng, H.K., Teng, K.K., Lee, R., Wright, S., Tevar, S., Almeida, R.D., Kermani, P., Torkin, R., Chen, Z.-Y., Lee, F.S., et al. (2005). ProBDNF induces neuronal apoptosis via activation of a receptor complex of p75NTR and sortilin. J. Neurosci. *25*, 5455–5463.

Tews, B., Schönig, K., Arzt, M.E., Clementi, S., Rioult-Pedotti, M.-S., Zemmar, A., Berger, S.M., Schneider, M., Enkel, T., Weinmann, O., et al. (2013). Synthetic microRNA-mediated downregulation of Nogo-A in transgenic rats reveals its role as regulator of synaptic plasticity and cognitive function. Proc. Natl. Acad. Sci. U. S. A. *110*, 6583–6588.

Thieme, N. (2011). Die Rolle des BDNF-TrkB Signalwegs auf die dendritische Architektur von hippocampalen Neuronen. Bachelorarbeit.

Thoenen, H. (1991). The changing scene of neurotrophic factors. Trends Neurosci. *14*, 165–170.

Toman, R.E., Payne, S.G., Watterson, K.R., Maceyka, M., Lee, N.H., Milstien, S., Bigbee, J.W., and Spiegel, S. (2004). Differential transactivation of sphingosine-1-phosphate receptors modulates NGF-induced neurite extension. J. Cell Biol. *166*, 381–392.

Toni, N., Buchs, P.A., Nikonenko, I., Bron, C.R., and Muller, D. (1999). LTP promotes formation of multiple spine synapses between a single axon terminal and a dendrite. Nature *402*, 421–425.

Tønnesen, J., Katona, G., Rózsa, B., and Nägerl, U.V. (2014). Spine neck plasticity regulates compartmentalization of synapses. Nat. Neurosci.

Trang, T., Beggs, S., Wan, X., and Salter, M.W. (2009). P2X4-receptor-mediated synthesis and release of brain-derived neurotrophic factor in microglia is dependent on calcium and p38-mitogen-activated protein kinase activation. J. Neurosci. *29*, 3518–3528.

Van Troys, M., Huyck, L., Leyman, S., Dhaese, S., Vandekerkhove, J., and Ampe, C. (2008). Ins and outs of ADF/cofilin activity and regulation. Eur. J. Cell Biol. *87*, 649–667.

Tyler, W.J., and Pozzo-miller, L. (2003). Miniature synaptic transmission and BDNF modulate dendritic spine growth and form in rat CA1 neurones. Neurobiology 497–509.

Tyler, W.J., and Pozzo-miller, L.D. (2001). BDNF Enhances Quantal Neurotransmitter Release and Increases Hippocampal Excitatory Synapses. Abacus A J. Account. Financ. Bus. Stud. *21*, 4249–4258.

Unger, T.J., Calderon, G.A., Bradley, L.C., Sena-Esteves, M., and Rios, M. (2007). Selective deletion of Bdnf in the ventromedial and dorsomedial hypothalamus of adult mice results in hyperphagic behavior and obesity. J. Neurosci. *27*, 14265–14274.

Uruno, T., Liu, J., Zhang, P., Fan Yx, Egile, C., Li, R., Mueller, S.C., and Zhan, X. (2001). Activation of Arp2/3 complex-mediated actin polymerization by cortactin. Nat. Cell Biol. *3*, 259–266.

Vanguilder, H.D., Bixler, G. V, Sonntag, W.E., and Freeman, W.M. (2012). Hippocampal expression of myelin-associated inhibitors is induced with age-related cognitive decline and correlates with deficits of spatial learning and memory. J. Neurochem. *121*, 77–98.

VanGuilder Starkey, H.D., Bixler, G. V, Sonntag, W.E., and Freeman, W.M. (2013a). Expression of NgR1-antagonizing proteins decreases with aging and cognitive decline in rat hippocampus. Cell. Mol. Neurobiol. *33*, 483–488.

VanGuilder Starkey, H.D., Sonntag, W.E., and Freeman, W.M. (2013b). Increased hippocampal NgR1 signaling machinery in aged rats with deficits of spatial cognition. Eur. J. Neurosci. *37*, 1643–1658.

Venkatesh, K., Chivatakarn, O., Lee, H., Joshi, P.S., Kantor, D.B., Newman, B.A., Mage, R., Rader, C., and Giger, R.J. (2005). The Nogo-66 receptor homolog NgR2 is a sialic acid-dependent receptor selective for myelin-associated glycoprotein. J. Neurosci. *25*, 808–822.

Vorhees, C. V, and Williams, M.T. (2006). Morris water maze: procedures for assessing spatial and related forms of learning and memory. Nat. Protoc. *1*, 848–858.

Wang, K.C., Koprivica, V., Kim, J.A., Sivasankaran, R., Guo, Y., Neve, R.L., and He, Z. (2002a). Oligodendrocyte-myelin glycoprotein is a Nogo receptor ligand that inhibits neurite outgrowth. Nature *417*, 941–944.

Wang, X., Chun, S.-J., Treloar, H., Vartanian, T., Greer, C. a, and Strittmatter, S.M. (2002b). Localization of Nogo-A and Nogo-66 receptor proteins at sites of axon-myelin and synaptic contact. J. Neurosci. *22*, 5505–5515.

Weaver, A.M., Karginov, A. V, Kinley, A.W., Weed, S.A., Li, Y., Parsons, J.T., and Cooper, J.A. (2001). Cortactin promotes and stabilizes Arp2/3-induced actin filament network formation. Curr. Biol. *11*, 370–374.

Welch, M.D., Rosenblatt, J., Skoble, J., Portnoy, D.A., and Mitchison, T.J. (1998). Interaction of human Arp2/3 complex and the Listeria monocytogenes ActA protein in actin filament nucleation. Science *281*, 105–108.

Wiessner, C., Bareyre, F.M., Allegrini, P.R., Mir, A.K., Frentzel, S., Zurini, M., Schnell, L., Oertle, T., and Schwab, M.E. (2003). Anti-Nogo-A antibody infusion 24 hours after experimental stroke improved behavioral outcome and corticospinal plasticity in normotensive and spontaneously hypertensive rats. J. Cereb. Blood Flow Metab. *23*, 154–165.

Willi, R., Aloy, E.M., Yee, B.K., Feldon, J., and Schwab, M.E. (2009). Behavioral characterization of mice lacking the neurite outgrowth inhibitor Nogo-A. Genes. Brain. Behav. *8*, 181–192.

Wills, Z.P., Mandel-Brehm, C., Mardinly, A.R., McCord, A.E., Giger, R.J., and Greenberg, M.E. (2012). The Nogo Receptor Family Restricts Synapse Number in the Developing Hippocampus. Neuron *73*, 466–481.

Wolfer, D.P., Madani, R., Valenti, P., and Lipp, H.-P. (2001). Extended analysis of path data from mutant mice using the public domain software Wintrack. Physiol. Behav. *73*, 745–753.

Woo, N.H., Teng, H.K., Siao, C., Chiaruttini, C., Pang, P.T., Milner, T.A., Hempstead, B.L., and Lu, B. (2005). Activation of p75 NTR by proBDNF facilitates hippocampal long-term depression. Nat. Neurosci. *8*, 1069–1077.

Xu, T., Yu, X., Perlik, A.J., Tobin, W.F., Zweig, J.A., Tennant, K., Jones, T., and Zuo, Y. (2009). Rapid formation and selective stabilization of synapses for enduring motor memories. Nature *462*, 915–919.

Yamashita, T., and Tohyama, M. (2003). The p75 receptor acts as a displacement factor that releases Rho from Rho-GDI. Nat. Neurosci. *6*, 461–467.

Yamashita, T., Tucker, K.L., and Barde, Y. (1999). Neurotrophin Binding to the p75 Receptor Modulates Rho Activity and Axonal Outgrowth. Receptor *24*, 585–593.

Yang, G., Pan, F., and Gan, W.-B. (2009a). Stably maintained dendritic spines are associated with lifelong memories. Nature *462*, 920–924.

Yang, J., Siao, C., Nagappan, G., Marinic, T., Jing, D., Mcgrath, K., Chen, Z., Mark, W., Tessarollo, L., Lee, F.S., et al. (2009b). Neuronal release of proBDNF. Nature *12*, 2008–2010.

Yasuda, R., Harvey, C.D., Zhong, H., Sobczyk, A., van Aelst, L., and Svoboda, K. (2006). Supersensitive Ras activation in dendrites and spines revealed by two-photon fluorescence lifetime imaging. Nat. Neurosci. *9*, 283–291.

Yiu, G., and He, Z. (2006). Glial inhibition of CNS axon regeneration. Nat. Rev. Neurosci. *7*, 617–627.

Yoshii, A., and Constantine-paton, M. (2007). BDNF induces transport of PSD-95 to dendrites through PI3K-AKT signaling after NMDA receptor activation. Online *10*, 702–711.

Yu, X., and Zuo, Y. (2011). Spine plasticity in the motor cortex. Curr. Opin. Neurobiol. *21*, 169–174.

Yuste, R. (2011). Dendritic Spines and Distributed Circuits. Neuron *71*, 772–781.

Yuste, R. (2013). Electrical compartmentalization in dendritic spines. Annu. Rev. Neurosci. *36*, 429–449.

Yuste, R., and Bonhoeffer, T. (2001). Morphological changes in dendritic spines associated with long-term synaptic plasticity. Annu. Rev. Neurosci. *24*, 1071–1089.

Yuste, R., Majewska, a, and Holthoff, K. (2000). From form to function: calcium compartmentalization in dendritic spines. Nat. Neurosci. *3*, 653–659.

Zafra, F., Hengerer, B., Leibrock, J., Thoenen, H., and Lindholm, D. (1990). Activity dependent regulation of BDNF and NGF mRNAs in the rat hippocampus is mediated by non-NMDA glutamate receptors. EMBO J. *9*, 3545–3550.

Zagrebelsky, M., and Korte, M. (2013). Form follows function: BDNF and its involvement in sculpting the function and structure of synapses. Neuropharmacology.

Zagrebelsky, M., Buffo, A., Skerra, A., Schwab, M.E., Strata, P., and Rossi, F. (1998). Retrograde regulation of growth-associated gene expression in adult rat Purkinje cells by myelin-associated neurite growth inhibitory proteins. J. Neurosci. *18*, 7912–7929.

Zagrebelsky, M., Holz, A., Dechant, G., Barde, Y.-A., Bonhoeffer, T., and Korte, M. (2005). The p75 neurotrophin receptor negatively modulates dendrite complexity and spine density in hippocampal neurons. J. Neurosci. *25*, 9989–9999.

Zagrebelsky, M., Schweigreiter, R., Bandtlow, C.E., Schwab, M.E., and Korte, M. (2010). Nogo-A stabilizes the architecture of hippocampal neurons. J. Neurosci. *30*, 13220.

Zakharenko, S.S., Patterson, S.L., Dragatsis, I., Zeitlin, S.O., Siegelbaum, S.A., Kandel, E.R., and Morozov, A. (2003). Presynaptic BDNF Required for a Presynaptic but Not Postsynaptic Component of LTP at Hippocampal CA1-CA3 Synapses. Neuron *39*, 975–990.

Zhou, Q., Homma, K.J., and Poo, M. (2004). Shrinkage of dendritic spines associated with long-term depression of hippocampal synapses. Neuron *44*, 749–757.

Zito, K., Knott, G., Shepherd, G.M.G., Shenolikar, S., and Svoboda, K. (2004). Induction of spine growth and synapse formation by regulation of the spine actin cytoskeleton. Neuron *44*, 321–334.

7 Supplement

7.1 Supplementary data

Table S1: Summary of FRAP experiments addressing the role of Nogo-A in regulating actin dynamics. The table reports the values for the turnover time, dynamic-, stable- and monomeric- actin fraction treated neurons for the experiments described in **Fig. 11-16.**

Figure 11-16.				
Treatment Cells/spines	**turnover time [sec]**	**dynamic actin fraction [%]**	**stable actin fraction [%]**	**monomeric actin fraction [%]**
Control BrdU 20 min 27 spines / 8 cells	18.37 ± 0.90	70.25 ± 1.80	15.5 ± 1.64	14.26 ± 1.00
Control BrdU 180 min 22 spines / 7 cells	20.09 ± 1.39	70.94 ± 2.44	15.21 ± 2.2	13.85 ± 1.71
Nogo-A Abs (11c7) 20 min 29 spines / 8 cells	34.69 ± 2.62	64.63 ± 2.19	21.87 ± 2.36	13.5 ± 1.11
Nogo-A Abs (11c7) 180 min 29 spines / 8 cells	32.07 ± 4.04	73.86 ± 2.73	14.97 ± 2.74	11.17 ± 1.00
NgR1 Abs 20 min 30 spines / 12 cells	35.14 ± 4.90	63.19 ± 2.08	24.96 ± 1.95	11.85 ± 1.37
NgR1 Abs 20 min 27 spines / 11 cells	30.24 ± 2.54	68.03 ± 2.14	20.52 ± 2.21	11.45 ± 0.95
Control DMSO20 min 15 spines / 7 cells	20.67 ± 2.99	70.93 ± 2.88	13.25 ± 2.58	15.84 ± 1.70
Control DMSO 180 min 21 spines / 7 cells	20.00 ± 1.47	70.34 ± 1.96	14.02 ± 1.63	15.64 ± 1.66
S1P2R Abs (JTE-013) 20 min 20 spines / 9 cells	29.75 ± 3.62	61.89 ± 2.41	23.01 ± 2.43	15.11 ± 1.50
S1P2R Abs (JTE-013) 180 min 22 spines / 8 cells	30.45 ± 4.72	62.15 ± 2.86	23.58 ± 3.06	14.27 ± 1.40
Control BSA before 28 spines / 14 cells	23.64 ± 2.00	69.60 ± 2.26	15.17 ± 2.20	15.23 ± 1.35
Nogo-A-Δ20 5 min 11 / 14	17.14 ± 1.70	76.75 ± 3.36	8.71 ± 1.72	14.54 ± 2.31
Nogo-A-Δ20 20 min 25 spines / 14 cells	25.84 ± 2.37	62.94 ± 1.79	24.36 ± 2.17	12.70 ± 1.46
Control 20 min 35 spines / 17 cells	23.09 ± 2.25	70.52 ± 2.42	16.30 ± 2.01	13.19 ± 1.19

Control 180 min 25 spines / 11 cells	22.08 ± 2.21	66.91± 2.01	15.75 ± 1.91	17.34 ± 1.72
ROCK inhibitor (Y27632) 20 min 21 spines / 9 cells	20.95 ± 1.96	62.34 ± 2.05	22.62 ± 2.09	15.04 ± 1.16
ROCK inhibitor (Y27632) 180 min 27 spines / 8 cells	24.00 ± 2.39	67.49 ± 2.12	19.90 ± 2.12	12.61 ± 1.22

Table S2: Summary of behaviour experiments addressing the role of Nogo-A in regulating learning and memory acquisition in the Morris water maze. The table reports the values for the escape latencies and the probe trails at day 3 and 9 for the experiments described in **Fig. 17.**

Figure 17.								
Genotype	**day 1**	**day 2**	**day 3**	**day 4**	**day 5**	**day 6**	**day 7**	**day 8**
WT time in [s] n= 16 mice	36.65 ± 4.61	28.72 ± 3.81	21.89 ± 3.31	21.15 ± 2.63	15.96 ± 3.63	14.81 ± 3.59	10.03 ± 2.09	6.58 ± 1.03
nogo-a KO time in [s] n= 14 mice	28.53 ± 4.30	23.76 ± 3.30	21.83 ± 5.17	19.99 ± 4.11	16.61 ± 2.80	12.67 ± 2.42	9.29 ± 1.97	6.59 ± 2.02

Genotype	**NE time [%]**	**SE time [%]**	**SW time [%]**	**NW time [%]**	**# of platform crossings**
WT PT day3 n=19 mice	21.97 ± 3.09	21.70 ± 3.62	26.28 ± 3.73	30.04 ± 3.31	1.21 ± 0.28
KO PT day3 n=15 mice	22.87 ± 2.31	14.21 ± 2.02	23.96 ± 1.70	38.95 ± 2.75	1.87 ± 0.32
WT PT day9 n=16 mice	18.37 ± 3.29	12.80 ± 2.77	21.04 ± 2.71	47.79 ± 4.39	3.19 ± 0.58
KO PT day9 n=14 mice	13.76 ± 2.80	4.73 ± 1.52	21.39 ± 3.18	60.12 ± 3.93	3.86 ± 0.58

Table S3: Summary of the behaviour experiments addressing the role of Nogo-A in regulating searching strategies in the Morris water maze. The table reports the values for the hippocampus-dependent and -independent search strategies (day 1-8) for WT and *nogo-a* KO mice described in **Fig. 18** and the dendritic spine density before and after 3 and 9 days of training described in **Fig. 19**.

Figure 18 and 19.								
Figure 18.	**day 1**	**day 2**	**day 3**	**day 4**	**day 5**	**day 6**	**day 7**	**day 8**
WT hippocampus - indep. [%] n= 16 mice	78.13 ± 7.17	81.25 ± 4.84	71.88 ± 7.17	67.19 ± 5.92	65.63 ± 5.98	51.56 ± 7.02	54.69 ± 7.98	37.50 ± 7.22
***nogo-a* KO hippocampus-indep. [%] n= 14 mice**	85.71 ± 4.32	78.57 ± 5.78	57.14 ± 5.52	58.93 ± 6.74	67.86 ± 6.11	48.21 ± 8.06	39.29 ± 6.26	33.93 ± 8.12
WT hippocampus-dep. [%] n= 16 mice	21.88 ± 7.17	18.75 ± 4.84	28.13 ± 7.17	32.81 ± 5.92	34.38 ± 5.98	48.44 ± 7.02	45.31 ± 7.98	62.50 ± 7.22
***nogo-a* KO hippocampus-dep. [%] n= 14 mice**	14.29 ± 4.32	21.43 ± 5.78	42.86 ± 5.52	41.07 ± 6.74	32.14 ± 6.11	51.79 ± 8.06	60.71 ± 6.26	66.07 ± 8.12

Figure 19. Genotype	**not-trained**	**3 days training**	**9 days training**
WT C57Bl/6 cells	1.41 ± 0.06 n= 19	1.36 ± 0.07 n= 16	1.63 ± 0.05 n= 17
***nogo-a* KO cells**	1.50 ± 0.09 n= 12	1.70 ± 0.06 n= 13	1.55 ± 0.05 n= 21
WT C57Bl/6 normalized Nogo-A levels	1 ± 0.08 n= 4	1.57 ± 0.01 n= 3	1.12 ± 0.17 n= 3

Table S4: The table reports the values for spine density, head width and length as well as the total number of dendritic intersections for control, BDNF and BDNF-Abs treated neurons for the experiments described in **Fig. 20-22** (above and middle). The values for the normalized mean intensity for Lifeact of control, BDNF and BDNF-Abs treated neurons for the experiments described in **Fig. 23** are given in the lower part.

Figure 20 and 21.	**Control**	**BDNF**	**BDNF-Abs**
C. # of spines / µm	0.98 ± 0.04 (n=19)	0.96 ± 0.03 (n=22)	0.77 ± 0.03 (n=23)
D. spine head width [µm]	0.49 ± 0.02 (n=19)	0.48 ± 0.01 (n=21)	0.43 ± 0.01 (n=18)
E. spine length [µm]	1.14 ± 0.03 (n=19)	1.12 ± 0.03 (n=21)	1.33 ± 0.05 (n=18)
Fig. 21 C. total # of intersections	240.08 ± 38.51 (n=13)	205.25 ± 23.20 (n=20)	238.50 ± 26.81 (n=18)
Figure 22.	**Control**	**BDNF**	**BDNF-Abs**
B. # of spines /µm	0.84 ± 0.02 (n=25)	0.80 ± 0.05 (n=22)	0.59 ± 0.02 (n=23)
C. spine head width [µm]	0.45 ± 0.01 (n=20)	0.47 ± 0.01 (n=19)	0.44 ± 0.02 (n=19)
D. spine length [µm]	1.14 ± 0.03 (n=20)	1.18 ± 0.03 (n=19)	1.57 ± 0.06 (n=19)
G'. total # of intersections	155.93 ± 7.51 (n=14)	196.15 ± 18.44 (n=14)	166.29 ± 21.82 (n=13)
Figure 23	**Control**	**BDNF**	**BDNF-Abs**
C. 23 DIV normalized mean intensity [%]	100.00 ± 4.46 (n=20)	104.16 ± 5.08 (n=19)	76.93 ± 3.16 (n=20)
D.16 DIV normalized mean intensity [%]	100.00 ± 4.63 (n=20)	94.91 ± 5.34 (n=22)	69.97 ± 2.74 (n=20)

Table S5: The table reports the values relative to the experiments described in **Fig. 24-26**. Specifically, the normalized intensity for the phospho-TrkB immunohistochemistry and the number in percent of phospho-TrkB positive cells for control and BDNF treated neurons; the values for the normalized frequency of global calcium transients for control and BDNF treatments as well as the normalized mean intensity and the number of c-fos positive cells for control and BDNF treated neurons. The numbers in brackets indicate respectively the number of experiments.

Figure 24-26.		**Control**	**BDNF**
Fig. 24 C. normalized intensity		1.00 ± 0.03 (n=7)	1.61 ± 0.08 (n=7)
Fig. 24 D. # of +P TrkB positive cells [%]		0.68 ± 0.04 (n=7)	0.85 ± 0.04 (n=7)
Fig. 25 C. normalized frequency of global calcium transients	**2 min after BDNF**	0.82 ± 0.1(n=6)	1.26 ± 0.15 (n=7)
	10 min after washout	0.83 ± 0.05 (n=5)	0.91 ± 0.16 (n=7)
Fig. 26 C. normalized mean intensity		1.00 ± 0.06 (n=26)	1.46 ± 0.13 (n=21)
Fig. 26 D. # of c-fos positive cells [%]		4.92 ± 1.43 (n=26)	20.93 ± 2.63 (n=21)

Table S6: The values for total neurite length, the number of primary neurites and the number of branching points at neurites are shown for control, BDNF, BDNF-Abs, TrkB-Fc and TrkB-Fc + BDNF treated neurons for the experiments described in **Fig. 27**. The numbers in brackets indicate the number of cells analysed.

Figure 27.	**Control**	**BDNF**	**BDNF-Abs**	**TrkB-Fc**	**TrkB-Fc + BDNF**
C. total neurite length [µm]	167.73 ± 5.72 (n=80)	341.43 ± 10.34 (n=73)	193.56 ± 22.81 (n=21)	175.71 ± 4.24 (n=80)	168.51 ± 15.50 (n=13)
D. # of primary neurites	4.56 ± 0.12 (n=80)	5.29 ± 0.14 (n=73)	5.14 ± 0.37 (n=21)	4.36 ± 0.15 (n=80)	4.15 ± 0.25 (n=13)
E. # of branch points	1.64 ± 0.14 (n=80)	4.00 ± 0.25 (n=73)	1.57 ± 0.26 (n=21)	2.15 ± 0.18 (n=80)	1.69 ± 0.35 (n=13)

Table S7: The table reports the values of the frequency of global calcium transients per second and the total number of intersections for control 1.5 mM Mg^{2+} and control 3.5 mM Mg^{2+} neurons shown in **Fig.6.** Spine density, the mean values for the spine head width and for spine length are shown for control neurons in 1.5 mM Mg^{2+}, control, BDNF and TrkB-Fc treated neurons in 3.5 mM Mg^{2+} for the experiments are described in **Fig. 28 -30**.

Figure 28 and 29.	**Control 1.5 mM Mg^{2+}**	**control 3.5 mM Mg^{2+}**	**BDNF 3.5 mM Mg^{2+}**	**TrkB-Fc 3.5 mM Mg^{2+}**
Fig. 28 B. frequency of global calcium transients / sec	0.18 ± 0.01 (n=16)	0.13 ± 0.01 (n=16)		
Fig. 28 C. amplitude $\Delta F/F_0$ [%]	20.16 ± 1.26 (n=16)	22.51 ± 0.99 (n=16)		
Fig. 28 D'. total # of intersections	292.92 ± 26.28 (n=13)	324.46 ± 22.05 (n=13)		
Fig. 29 B # of spines / µm	0.68 ± 0.03 (n=23)	0.47 ± 0.02 (n=22)	0.52 ± 0.03 (n=23)	0.53 ± 0.03 (n=26)
Fig. 29 C spine head width [µm]		0.45 ± 0.02 (n=22)	0.50 ± 0.02 (n=21)	0.48 ± 0.02 (n=22)
Fig. 29 D spine length [µm]		1.20 ± 0.05 (n=22)	1.1 ± 0.07 (n=21)	1.17 ± 0.06 (n=22)
Figure 30.	**Control 1.5 mM Mg^{2+}**	**Control 3.5 mM Mg^{2+}**	**BDNF 3.5 mM Mg^{2+}**	**TrkB-Fc 3.5 mM Mg^{2+}**
B. # of spines / µm	0.68 ± 0.03 (n=23)	0.54 ± 0.04 (n=19)	0.53 ± 0.03 (n=20)	0.43 ± 0.03 (n=16)
C. spine head width [µm]		0.44 ± 0.01 (n=15)	0.46 ± 0.02 (n=16)	0.42 ± 0.01 (n=10)
D. spine length [µm]		1.13 ± 0.05 (n=15)	1.20 ± 0.05 (n=16)	1.16 ± 0.05 (n=10)

7.2 Abbreviations

Abs	antibodies
ACSF	artificial cerebrospinal fluid
BDNF	Brain-derived neurotrophic factor
AMPA(R)	α-amino-3-hydroxy-5-methyl-4-isoxazole propionic acid (receptor)
ANOVA	analysis of variance
BrdU	Bromdesoxyuridin
BSA	bovine serum albumin
CA	cornu ammonis
CaMKII	$Ca^{2+/}$calmodulin-dependent protein kinase II
CNS	central nervous system
CREB	cyclic AMP response element binding protein
DAPI	4',6-diamidino-2-phenylindole
DIV	days *in vitro* (post transplantation)
DMSO	Dimethylsulfoxid
EGFP	enhanced green fluorescent protein
FRAP	fluorescence recovery after photobleaching
GBSS	Gey's balanced salt solution
IEG	immediate early gene
KO	Knockout
LIMK	LIM kinase
LTD	long-term depression
LTP	long-term potentiation
MAP2	microtubule-associated protein 2
MWM	Morris water maze
NgR	Nogo-66 receptor
PBS	phosphate buffered saline
PSD	postsynaptic density
$p75^{NTR}$	pan neurotrophin receptor p75
RFP	red fluorescent protein
RhoA	small Rho A GTPases
ROCK	Rho kinase
ROI	region of intres
S1PR2	sphingosine 1-phosphate receptor 2
TrkB	tropomyosin-related kinase receptor B
vs	*versus*
WT	Wild type

7.3 Acknowledgements

Mein größter Dank gilt meinem Doktorvater Professor Dr. Martin Korte für die großartige Möglichkeit während meiner Promotion an diesen höchst interessanten und breit gefächerten Projekten arbeiten zu dürfen. Ich bin ihm dankbar für die immerwährende Unterstützung und die Möglichkeiten auch den internationalen Wissenschaftsbereich kennen gelernt zu haben. Ich danke Herrn Prof. Dr. Reinhard Köster für die freundliche Übernahme des Koreferates und Herrn Prof. Dr. Peter J. Walla für den Vorsitz der Promotionskommission, sowie die zahlreichen Diskussionen in unserer Kooperation.
Ebenso gilt mein ganz besonderen Dank Dr. Marta Zagrebelsky für die außerordentliche Unterstützung, die direkte Hilfe bei all meinen Anliegen und Fragen. Ich danke ihr für die unzähligen Stunden der Diskussion, ihre konstruktiv kritischen Fragen und Anregungen haben mich stets gefordert und meine wissenschaftliche Sichtweise geprägt.

Im Rahmen des Nogo-A Projekts kooperierten wir mit dem Labor von Prof. Dr. Martin Schwab. Ihm danke ich für die Bereitstellung verschiedenster Antikörper und Peptide. Ebenfalls danke ich Dr. Stella Kramer für ihre Hilfe und zahlreichen Gespräche über Nogo-A Signalwege und das Leben als Wissenschaftler. In diesem Zusammenhang möchte ich Niklas Lonnemann und Dr. Kristin Michaelsen-Preusse für ihre Unterstützung und Hilfe beim MWM danken und ganz besonders Diane Mundil, die Expertin rund um die Zellkultur. Hervorragende fachmännische Unterstützung bekam ich von Steffen Fricke, Carmen Wucherpfennig und Tanja Meßerschmidt bei der Proteinanalyse, sowie dem Fachmann des Aktincytoskelettes Dr. Martin Rothkegel. Den BDNF Experten Tobias Dierkes, Nina Gödecke und Nils Thime danke ich für die Unterstützung und die zahlreichen Stunden des Auswertens.
Vielen lieben Dank an Stefanie Schweinhuber und Sabine Zessin für die tolle Zeit, eure immer fortwährende und ansteckende gute Laune (ohne Schreib-Stress) ist großartig. Die Pausen und die Zeit mit euch waren ein Lichtblick im Laboralltag und ich Danke euch auch für die Unterstützung im gemeinsamen Endspurt auf unseren Zielgeraden.
Weiterhin gilt ein großer Dank der gesamten Arbeitsgruppe für die tolle Atmosphäre, es macht Spaß und Freude mit euch zu arbeiten oder auch den Abend ausklingen zu lassen. Danke: Dr. Anita Remus, Melissa O'Brien, Jan Kleveman, Franziska Scharkowski, Ulrike Herrmann, Susann Ludewig, Marianna Weller, Cristina Iobbi, Dr. Sheeja Navakkode, Dr. Sredharan Sajikumar, Qin Li, Dr. Jian-Hua Chen, Dr. Ajmal Zemmar, Dr. Franziska Neuser, Dr. Andrea Delekate, Dr. Martin Polack und natürlich Reinhard Huwe für die schöne Zeit.

Von ganzen Herzen danke ich meinen Eltern und meinem Bruder, für den Rückhalt und die großartige Unterstützung während meiner gesamten Promotion.